Port Hedland
Zone 5 Channel Bypass Project

Modelling of Hydrodynamics, Waves and Dredging Spill

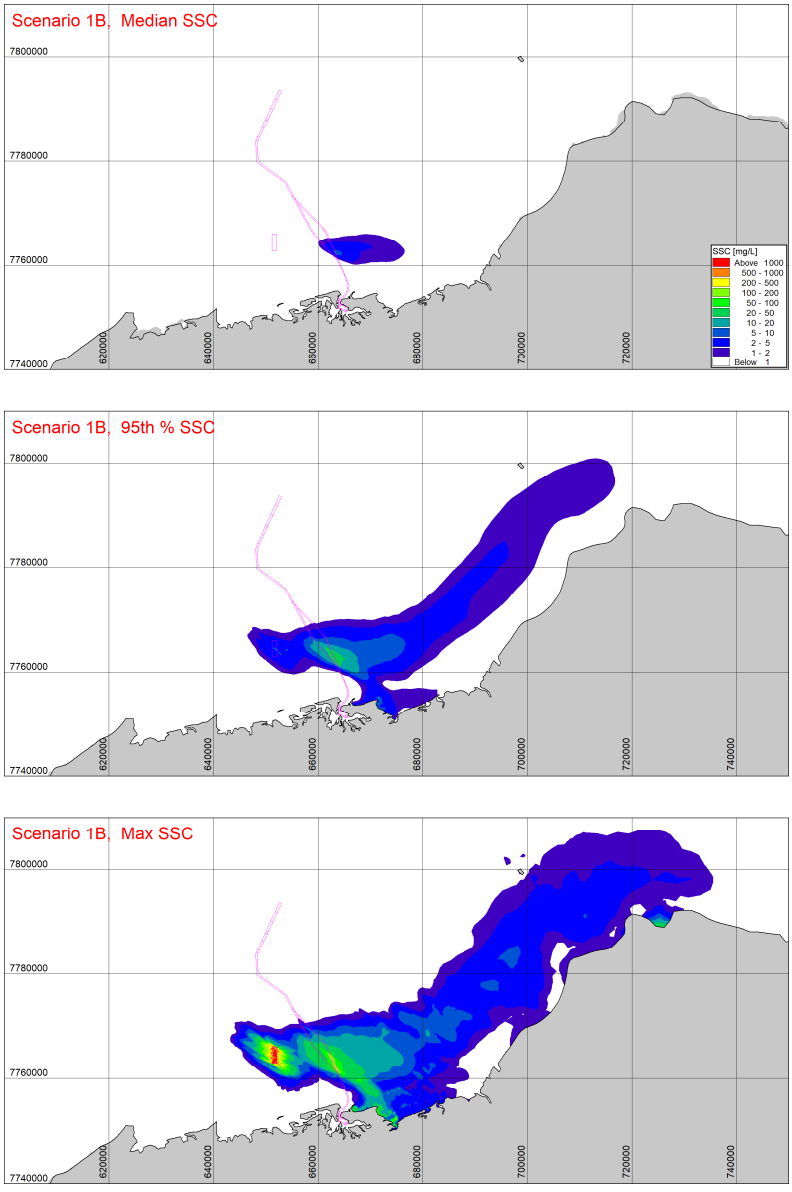

MScience for Pilbara Ports

Final Report

March 2026

Port Hedland
Zone 5 Channel Bypass Project

Modelling of Hydrodynamics, Waves and Dredging Spill

Prepared for	MScience on behalf of Pilbara Ports
Represented by	Mr. Iain Posnett

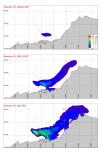

Author	Andrew Driscoll
Project Manager	Jason Antenucci

Project number	43804930
Approval date	30 March 2026
Revision	Final 2.2
Classification	**Confidential:** This document is only accessible to the project team members and sharing it outside the project team is subject to the client's prior approval.

CONTENTS

FIGURES

TABLES

Nomenclature

Abbreviations	
AHO	Australian Hydrographic Office
ASB	Above seabed
AWAC	Nortek Acoustic Wave and Current Profiler
BARRA	Bureau's Atmospheric High-resolution Regional Reanalysis for Australia
CD	Chart Datum
CEP	Channel Entry Project
CFSR	Climate Forecast System Reanalysis (global meteorological fields)
CROP	Channel Risk and Optimization Project
CSD	Cutter-Suction Dredger
CTW	Coastal Trapped Waves
FM	Flexible mesh (unstructured model domain)
GA	Geosciences Australia
GEBCO	General Bathymetric Chart of the Oceans
GWM	Global Wave Model
HD	Abbreviated reference to Hydrodynamic engine of MIKE21/MIKE3 FM Model
Hm0	Spectral definition of the significant wave height
LAT	Lowest Astronomical Tide
LIDAR	Light Detection and Ranging
LOA	Length overall (of vessel)
MIKE21	DHI's Flexible Mesh 2D model system
MIKE3	DHI's Flexible Mesh 3D model system
MSL	Metres above Mean Sea Level
MT	Abbreviated reference to Mud Transport engine of MIKE21/MIKE3 FM Model
MWD	Mean wave direction
PSD	Particle Size Distribution
RMSE	Root Mean Square Error
SC7C	Spoilground 7C
SSC	Suspended Sediment Concentration
SW	Abbreviated reference to Spectral Wave engine of MIKE21 FM Model
TG	Tide Gauge
Tp	Peak wave period
TSHD	Trailing Suction Hopper Dredger
UTC	Coordinated Universal Time (Universal Time Coordinated)
WAMSI	Western Australian Marine Science Institution
WRB	Waverider Buoy

1 Introduction

DHI Water & Environment (DHI) has been commissioned by MScience (Client) on behalf of Pilbara Ports to provide numerical modelling of dredging spill associated with the construction of the Zone 5 Bypass channel. The Zone 5 Bypass has been proposed to manage commercial and safety risk associated with potential blockage of the main channel at Port Hedland, whereby a second channel in Zone 5 (Figure 1-1) will be cut to allow vessel bypass.

Development of the channel bypass requires dredging of approximately 800,000 m^3 of *in situ* material as well as the associated disposal of the dredged material. The present work has been performed under the assumptions that the work will be performed by either a trailing suction hopper dredger (TSHD) in isolation, or via a combination of a cutter-suction dredger (CSD) to pre-cut the hardest material then followed by a TSHD. All works are assumed to occur outside of the cyclone season.

Pilbara Ports requires an EPA environmental referral package and sea dumping permit application to be prepared for the project, which will be provided by MScience. The dredge plume modelling reported here will be a key input to the permitting effort. The objective of the DHI scope is thus to provide the dredge plume modelling and reporting for the project, suitable for EPA referral.

The dredge spill modelling system established in support of the Zone 5 Bypass integrates hydrodynamic, wave and sediment transport models. Rev 2 of this report has been updated to incorporate project-specific geotech information as well as a significantly revised dredging plan.

1.1 Report Structure

The remainder of the report is structured as follows:

- Section 2 presents the Zone 5 project and provides a high-level site characterisation.
- Section 3 describes the establishment and execution of 2D/3D hydrodynamic models in support of the dredging spill simulations.
- Section 4 describes the establishment and execution of basin-scale, regional and local wave models in support of the dredging spill simulations.
- Section 5 describes an assessment of dredging spillage associated with Zone 5 construction activities
- Section 6 lists references cited

The report also incorporates four appendices which hold additional graphics. Figure references numbers beginning with a letter (Figure B-2) point to the respective appendix while those beginning with a number (Figure 3-2) are located within the main body of the report.

1.2 Conventions

Unless otherwise stated, the following conventions prevail within the report:

- Horizontal positioning is provided in the MGA-50 projection system.
- Models are necessarily constructed relative to mean sea level (MSL), and model bathymetries are presented as such. However, given the dredging focus of the work, most vertical references within the report are provided relative to chart datum (CD). Reference tidal planes are provided in Table 2-2.
- Wind and wave directions are reported as "from", while currents are “toward”
- Time references denote UTC.

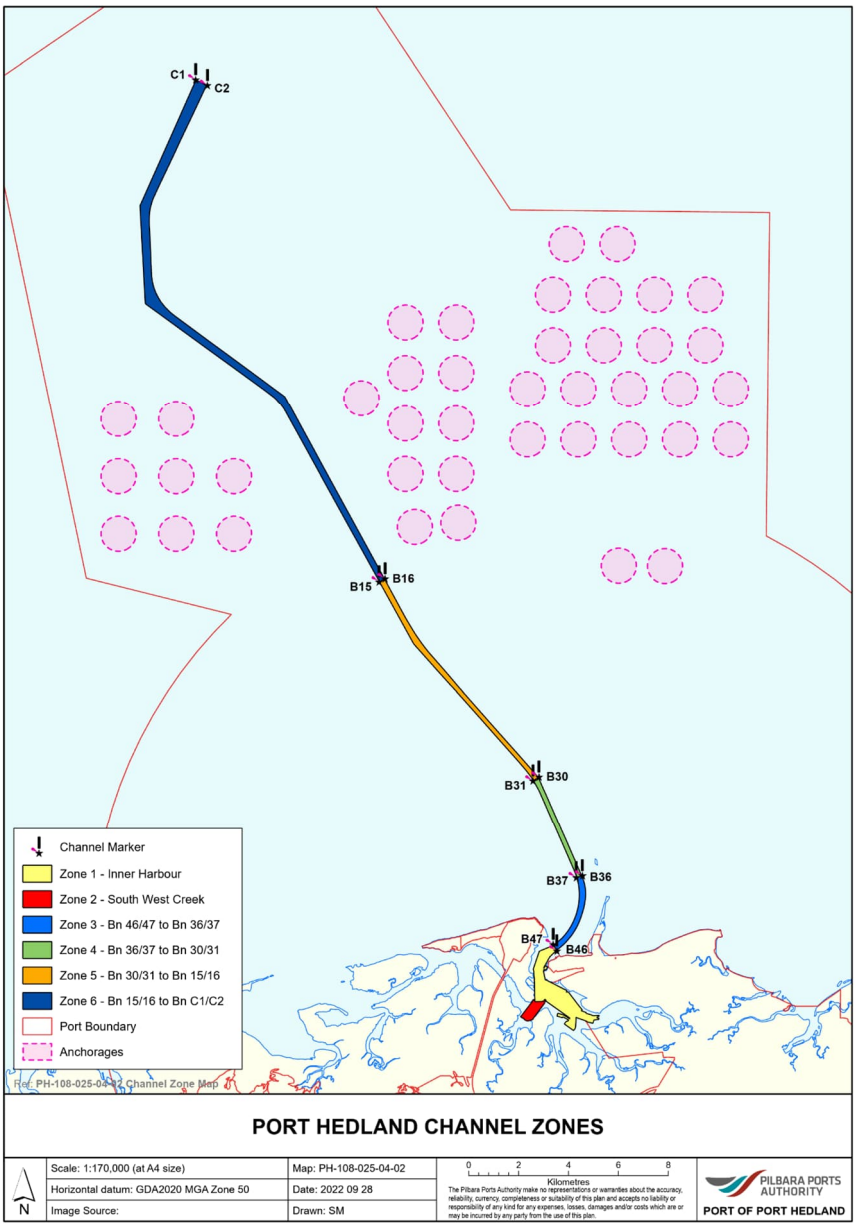

Figure 1-1 Zonation of Port Hedland access channel, indicating the reach of Zone 5 along which the bypass channel is proposed.

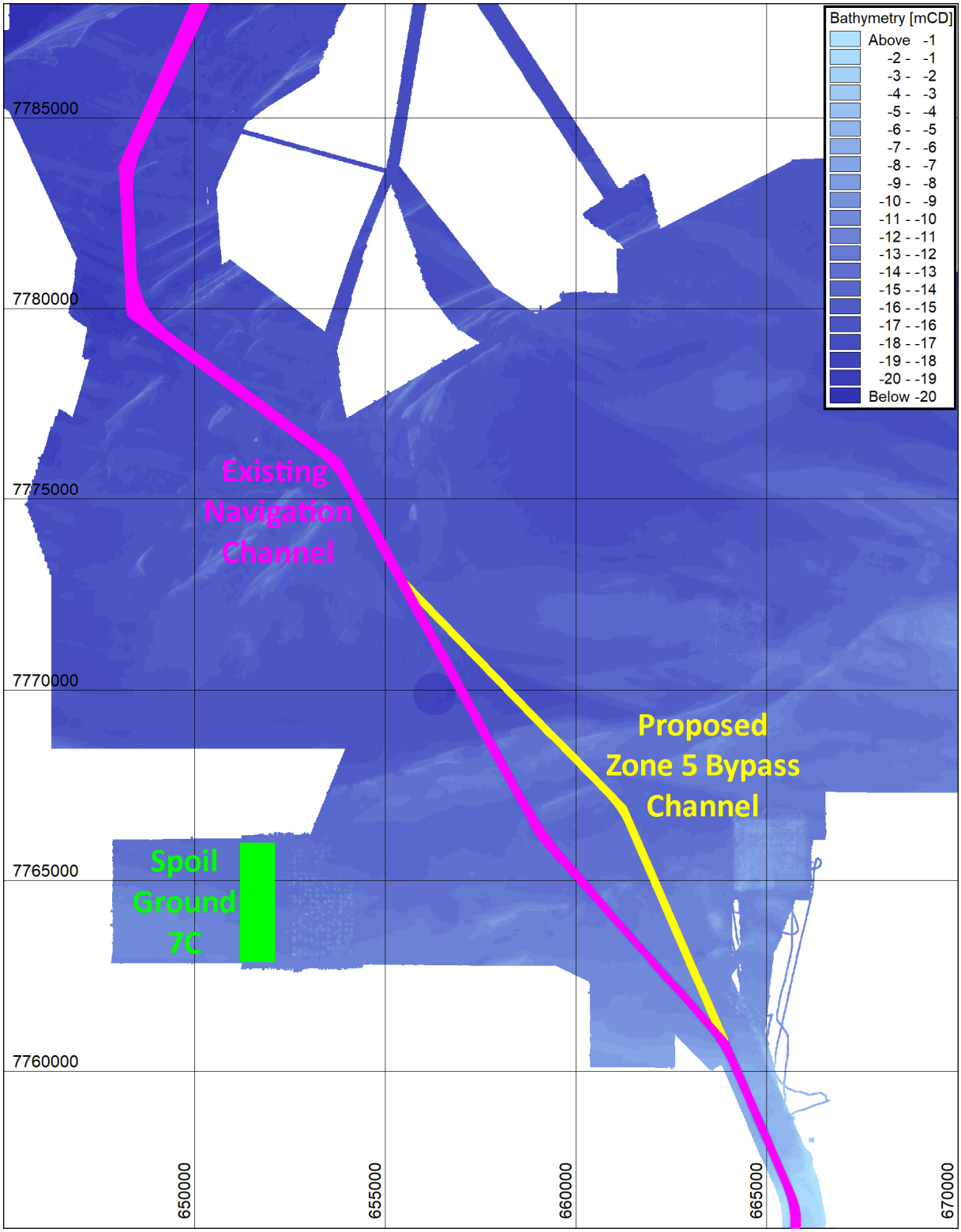

Figure 1-2 Geospatial data as provided by Pilbara Ports, including shapefiles of the existing navigation channel, proposed Zone 5 bypass and Spoilground 7C (SG7C), all overlaying 1m gridded bathymetric survey data.

2 Project Description and Site Characterisation

2.1 Zone 5 Bypass Project Description

The proposed Zone 5 Bypass channel is indicated in Figure 1-2, and is proposed to be deepened to -11.5m CD. The total *in situ* dredged volume removed from the seabed in association with these works is approximately 800,000 m^3.

The majority of the area indicated in yellow in Figure 1-2 is already below -12.1m CD, with only some 25% of the footprint requiring deepening. Per Figure 5-1, the resulting dredging operations are focussed upon the southernmost portion of the designated channel. The mean dredging thickness is slightly less than 1m. The shallowest portions of the pre-dredged seabed lie immediately adjacent to the southern intersection with the main navigation channel. The maximum dredging thickness of 3.6m occurs in this area.

Zone 5 Bypass construction operations are planned to occur in the second half of 2026 prior to the onset of the cyclone season on 01 November. (Pilbara Ports, 2025). The construction is anticipated to be performed by one of two work methods:

- Scenario 1: a jumbo trailing suction hopper dredger (TSHD) performs the full campaign in isolation
- Scenario 2: a mega CSD pre-cuts the harder portions of the dredging area, with cut materials subsequently dredged by a similar jumbo TSHD.

Disposal of dredged material is planned as TSHD bottom dumping within Spoilground 7C (SG7C) as indicated in Figure 1-2.

The formal overdredging allowance for the project is 1.0m. This value accommodates seabed disturbance to -12.5m during CSD pre-cutting operations in Scenario 2, though not all pre-cut material will be removed. In the present context of dredging spill permitting, the full channel is assumed to ultimately be lowered to -12.1m CD, for an effective overdredging of 0.6m. The cited total *in situ* volume removal of 800,000 m^3 aligns with 0.6m of overdredging.

2.2 Site Characterisation

2.2.1 Physiography

The Port Hedland region is characterised as a limestone barrier system, with the nearshore seabed character described as “dominated by sandy plains, interspersed with a series of hard substrate ridgelines which run parallel to the coastline in water depths of greater than 10 m chart datum” (Smith et al, 2015). The substrate ridgelines are clearly visible in Figure 1-2 and Figure 2-1. Sediments between the ridgelines are typically coarse-grained.

The bathymetric profile is gently sloping, with the -20m CD contour lying some 40km from the mouth of the port. This has necessitated extensive capital and maintenance dredging works to maintain deep-draft vessel access. Spoilgrounds have been established both east and west of the access channel (also visible in Figure 1-2 and Figure 2-1), most recently Spoilground 7 on the western side of the channel in connection with the Channel Risk and Optimization Project (CROP) and Channel Entry Project (CEP). SG7C is a westward expansion to this existing spoilground.

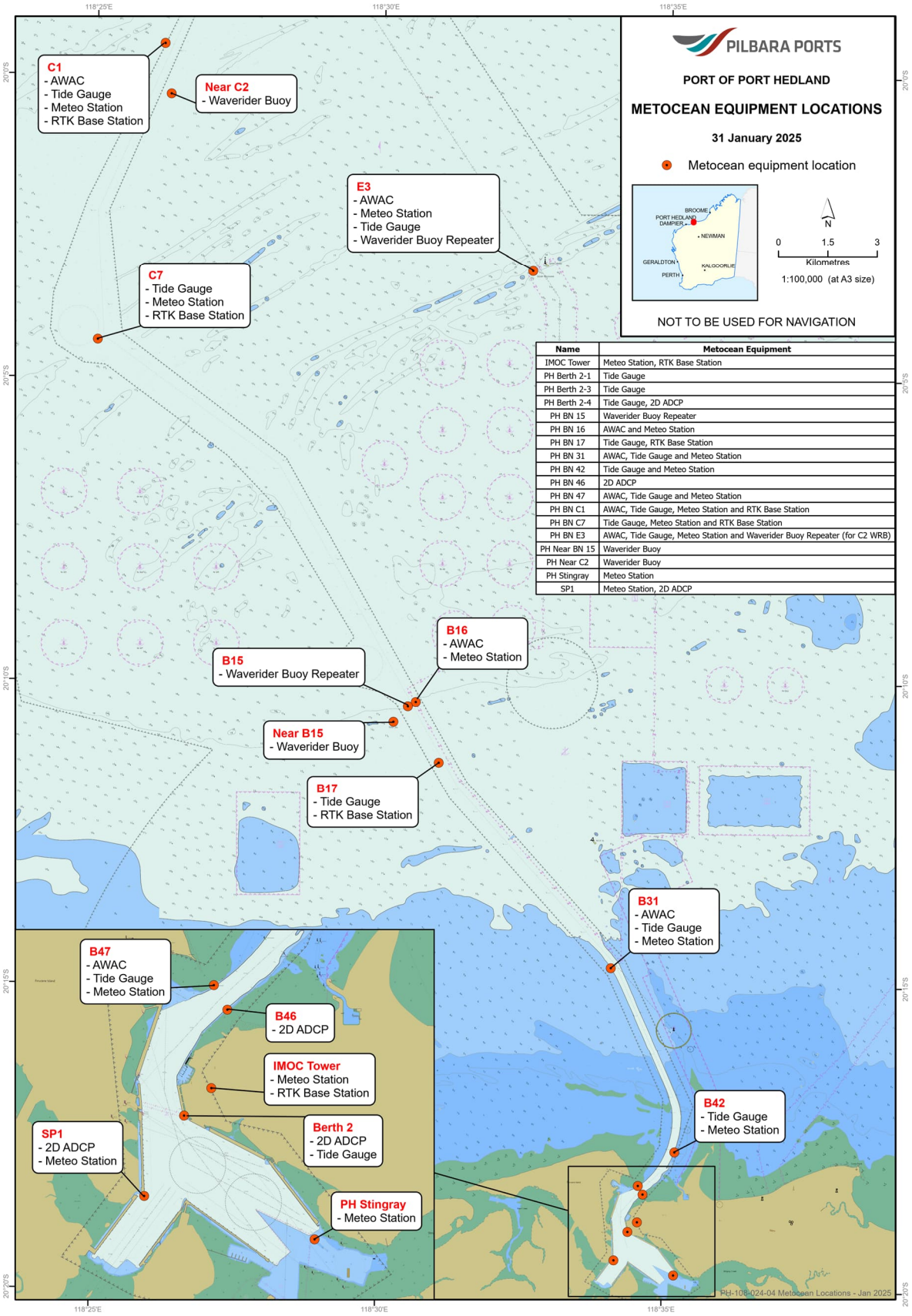

Name	Metocean Equipment
IMOC Tower	Meteo Station, RTK Base Station
PH Berth 2-1	Tide Gauge
PH Berth 2-3	Tide Gauge
PH Berth 2-4	Tide Gauge, 2D ADCP
PH BN 15	Waverider Buoy Repeater
PH BN 16	AWAC and Meteo Station
PH BN 17	Tide Gauge, RTK Base Station
PH BN 31	AWAC, Tide Gauge and Meteo Station
PH BN 42	Tide Gauge and Meteo Station
PH BN 46	2D ADCP
PH BN 47	AWAC, Tide Gauge and Meteo Station
PH BN C1	AWAC, Tide Gauge, Meteo Station and RTK Base Station
PH BN C7	Tide Gauge, Meteo Station and RTK Base Station
PH BN E3	AWAC, Tide Gauge, Meteo Station and Waverider Buoy Repeater (for C2 WRB)
PH Near BN 15	Waverider Buoy
PH Near C2	Waverider Buoy
PH Stingray	Meteo Station
SP1	Meteo Station, 2D ADCP

Figure 2-1 Metocean instrumentation maintained by Pilbara Ports.

2.2.2 Metocean Datasets

The site characterisation has the benefit of relying upon the extensive array of metocean instrumentation maintained by Pilbara Ports, as shown in Figure 2-1. Following a review of data availability and quality, the present work has relied primarily upon the stations listed in Table 2-1.

Table 2-1 Primary sources of Pilbara Ports metocean data as applied in present work.

Station	MGA50 E	MGA50 N	Instruments Utilised*
C1	650246	7788808	TG
Near C2	650430	7787277	WRB
E3	661412	7781870	AWAC, TG
Near B15	657164	7768146	WRB
B16	657843	7768745	AWAC
B17	658540	7766906	TG
B31	663765	7760638	AWAC, TG
Berth 2-1	664269	7751342	TG

*AWAC = Nortek Acoustic Wave and Current Profiler, TG = tide gauge

2.2.3 Water Levels

Water levels in the vicinity of Port Hedland are dominated by tidal forcing. The local tidal regime can be classified according to the amplitude ratio of the primary diurnal and semidiurnal constituents according to the tidal "form factor" F (Pugh, 1987) as:

$$F = \left(\frac{A_{K1} + A_{O1}}{A_{M2} + A_{S2}}\right) = \left(\frac{0.242 + 0.149}{1.701 + 1.030}\right) = 0.14$$

F = 0 to 0.25 semidiurnal form
F = 0.25 to 1.50 mixed, mainly semidiurnal
F = 1.50 to 3.00 mixed, mainly diurnal
F = greater than 3.0 diurnal form

Unsurprisingly, this confirms the tide at Port Hedland as decidedly semi-diurnal.

Tidal planes for the port basin are shown in Table 2-2.

Table 2-2 Official tidal planes for Port Hedland (Pilbara Ports, 2025).

Tidal Plane	LAT (m)	MSL (m)
Highest Astronomical Tide (HAT)	7.6	+3.6
Mean High Water Spring (MHWS)	6.7	+2.7
Mean High Water Neap (MHWN)	4.7	+0.7
Mean Sea Level (MSL)	4.0	0.0
Mean Low Water Neap (MLWN)	3.3	-0.7
Mean Low Water Spring (MLWS)	1.3	-2.7
Lowest Astronomical Tide (LAT)	0.0	-4.0

The tidal character varies significantly along the length of the Port Hedland access channel as shown in Figure 2-2. This spatial variation must be accounted for when transferring between tidal datums to mean sea level (Schlack and Hewitt, 2015; Pilbara Ports, 2024). A typical year of predicted tide from the three stations, omitting seasonal variations in water level, is shown in Figure 2-3. The amplification in spring tidal range as shown into October is present every year. The spring tidal amplitude can thus be expected to increase toward the end of the proposed 15 Aug – 31 Oct construction period.

While the macrotidal character at Port Hedland implies that all other contributions to water levels are comparatively small, non-tidal contributions to total water level are still notable. Non-tidal contributions are the product of seasonal variations in mean water level, coastal trapped waves (CTWs), the inverse barometer effect from passing weather systems, local wind stress and wave-induced setup during extreme storms, as well as oceanic variations. Seasonal variations in water level are on the order of ±0.1m (AHO, 2025).

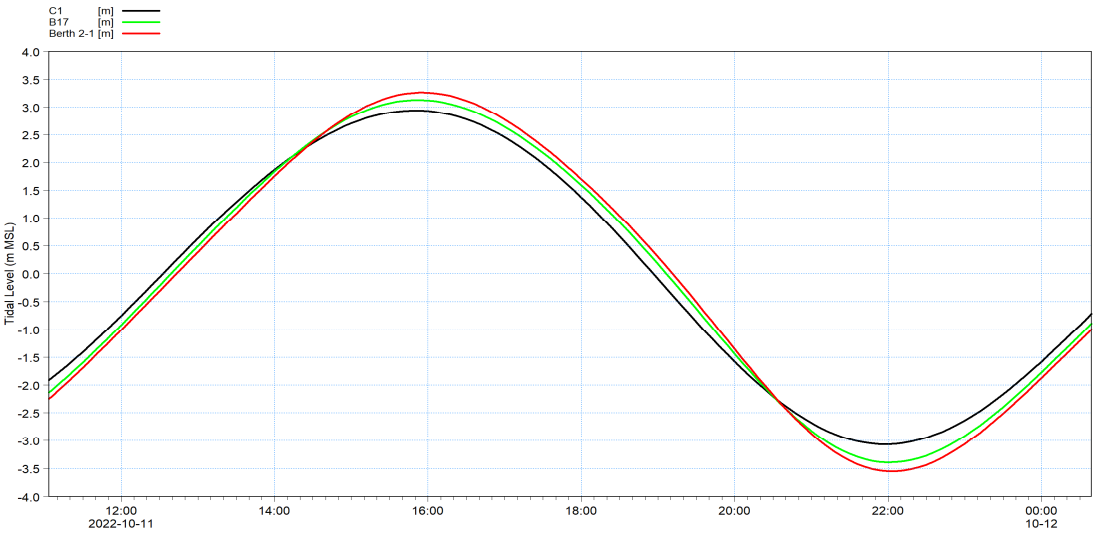

Figure 2-2 Variation in spring tidal character within study area, from C1 offshore into port basin Measurements show amplification as well as increasing phase lag approaching the port basin from offshore.

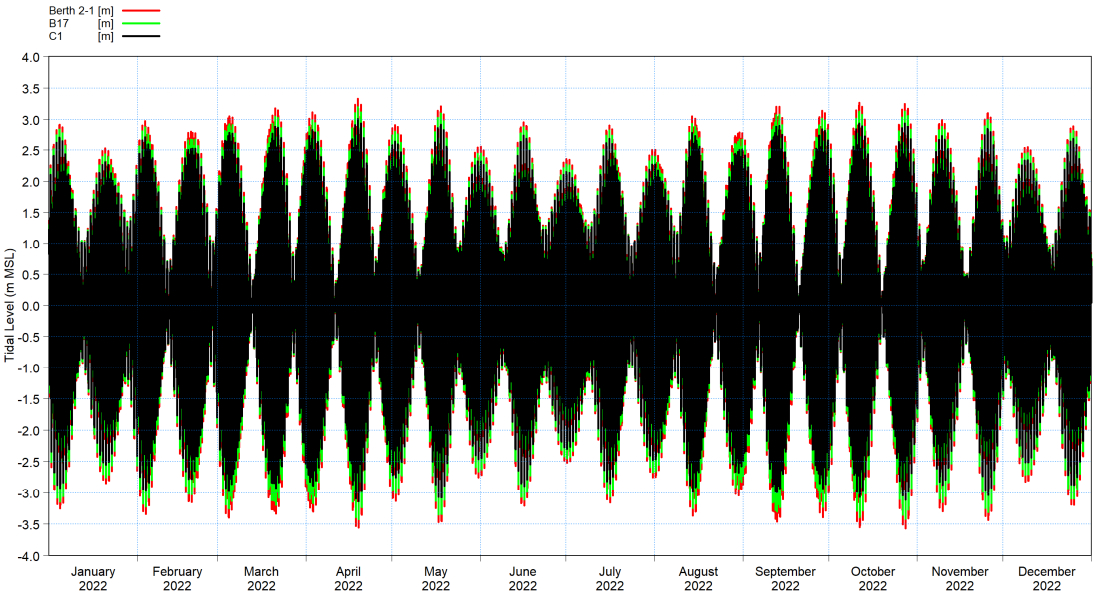

Figure 2-3 Annual variation of predicted tide within the study area, as derived from measurements using the methods of Foreman (1977), exclusive of seasonal changes to mean sea level.

The most substantial of the above are instantaneous cyclonic-induced surges and the lagged CTW response post-storm (Eliot and Pattiaratchi, 2010). Given the specific non-cyclonic seasonal focus of the present work, neither are relevant here.

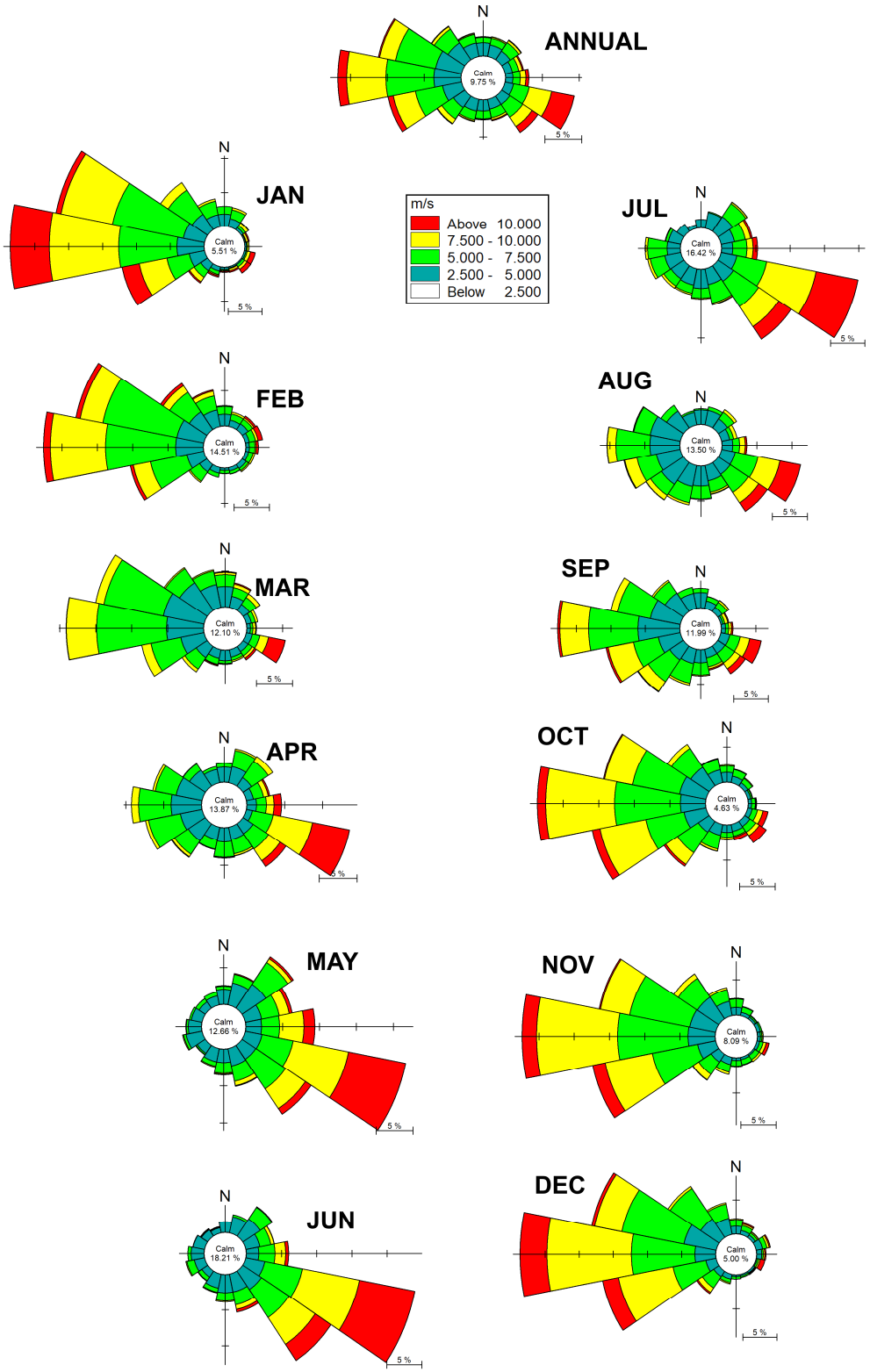

Figure 2-4 Long-term +10m overwater wind roses for all of 2020 – 2024, considering the full record at top and partitioned by month, based on BARRA-R2 reanalysis in the vicinity of station C1 offshore. The directional convention is blowing from.

2.2.4 Wind

Wind is of importance in the present work primarily in the context of local wave generation and for its contribution toward inducing residual current flow east or west along the coast, which is a key contributor to plume transport.

Aside from the particularly acute and variable effects of cyclones, the seasonal operational wind climate offshore of Port Hedland unfolds in a consistent pattern when averaged over multiple years. Figure 2-4 shows both the full annual wind rose over a five-year period as well as for monthly partitions thereof. It shows that from Sep-Mar the prevailing wind tends to blow from the west, while from May-Jul it tends to blow from the east, with Apr and Aug being mainly transitional months. These trends have significant implications on net longshore currents offshore of Port Hedland.

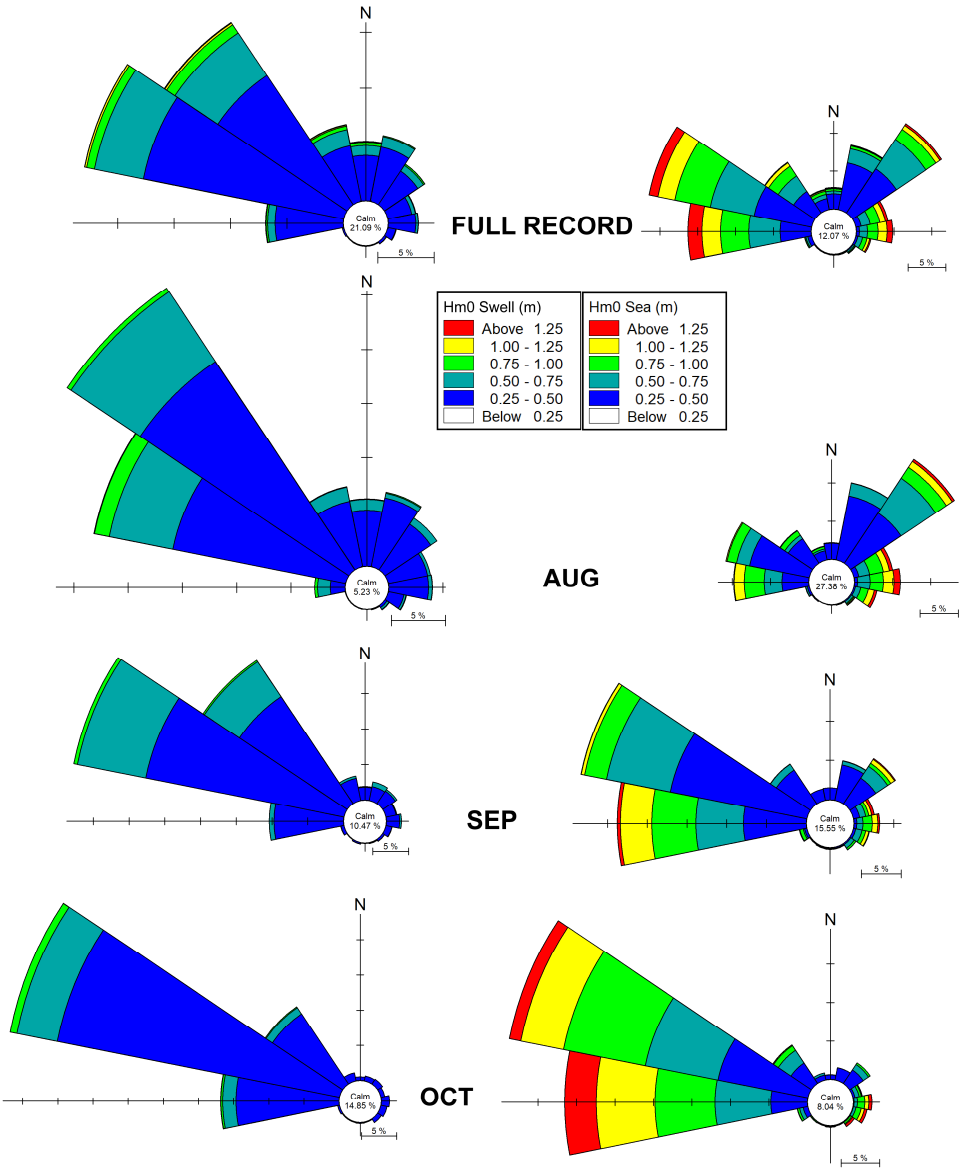

Figure 2-5 Wave roses of $Hm0_{SWELL}$ vs. MWD_{SWELL} (left) column and $Hm0_{SEA}$ vs. MWD_{SEA} (right column) for the E3 AWAC over a three-year period (Mar2020 – Feb2023), showing results from full three years (top row) as well as partitioned into monthly records for Aug, Sep and Oct. The directional convention is propagating from. Sea and swell are separated at 7s.

2.2.5 Waves

Wave exposure approaching Port Hedland follows seasonal patterns which differ for sea and swell components. Swell exposure has two energy peaks over the year, one being a peak in “base swell” energy in the winter months, which primarily originates from the Southern Ocean. A second range of brief and more intense peaks occur in summer in connection with active cyclones at distance from the port. Sea energy peaks in summer (also from cyclones, but not exclusively) but local generation by seabreeze is present throughout the year.

Figure 2-5 provides insight into wave climatology approaching the worksite within the proposed construction window of 15 Aug – 31 Oct. Based on three measurement years at the E3 AWAC, the construction window again is characterised by behaviour associated with the shoulder season between winter and summer conditions. The roses indicate a modest weakening of swell conditions as winter storm energy in the Southern Ocean eases. In contrast, the sea component pivots directions in lockstep with the wind climate (Figure 2-4) and increases in strength toward its summer peak.

Swell waves propagating to the work area are prone to significant refractive modification where the swell approaches the upwave side of the navigation channel. The effect is most prominent when the water depth change is large and abrupt. As such, this effect is most pronounced at low tide and at locations where the channel shoulder is most shallow. The channel will also affect the longer period portion of the sea partition, but less prominently.

2.2.6 Currents

Currents within the area of interest are dominated by macrotidal processes and the resulting oscillatory tidal currents. Superimposed upon the tidal currents are residual currents which, while substantially weaker aside from storm events, impart net transport. The transport of dredge plumes in the minutes and hours following spillage are typically dominated by oscillatory tidal currents, while the weaker residuals are responsible for plume transport east and west along the coast over longer distances and timescales.

Figure 2-6 provides a current rose as derived from long-term depth-averaged measurements from the B16 AWAC over the period of 2020-2024. Operational tidal currents peak at roughly 0.5 m/s, with a principal axis of motion of around 120° / 300°. Initial movements of spilled sediments can be expected to follow approximately this pattern, with some allowance for the distance between B16 and the spillage locations. The B16 record is applied here as it is the closest AWAC to the Zone 5 Bypass work area which has reliable long-term data coverage.

Residual currents are calculated from the same depth-averaged B16 AWAC record, by isolating the eastward U-velocity component and applying a simple running mean with a window of 7 days. The results of this analysis are shown in Figure 2-7 for the calendar years of 2021 and 2022. The results show residual currents of 0 to 10 cm/s, with a seasonal directional distribution that aligns well with the wind climate in Figure 2-4. Residual currents tend to set eastward for most of the year. Brief episodes of westward drift may occur any time of the year, but are most likely to occur in the winter months when the prevailing winds are also directed toward west. These observations are consistent with those reported in BHP (2011).

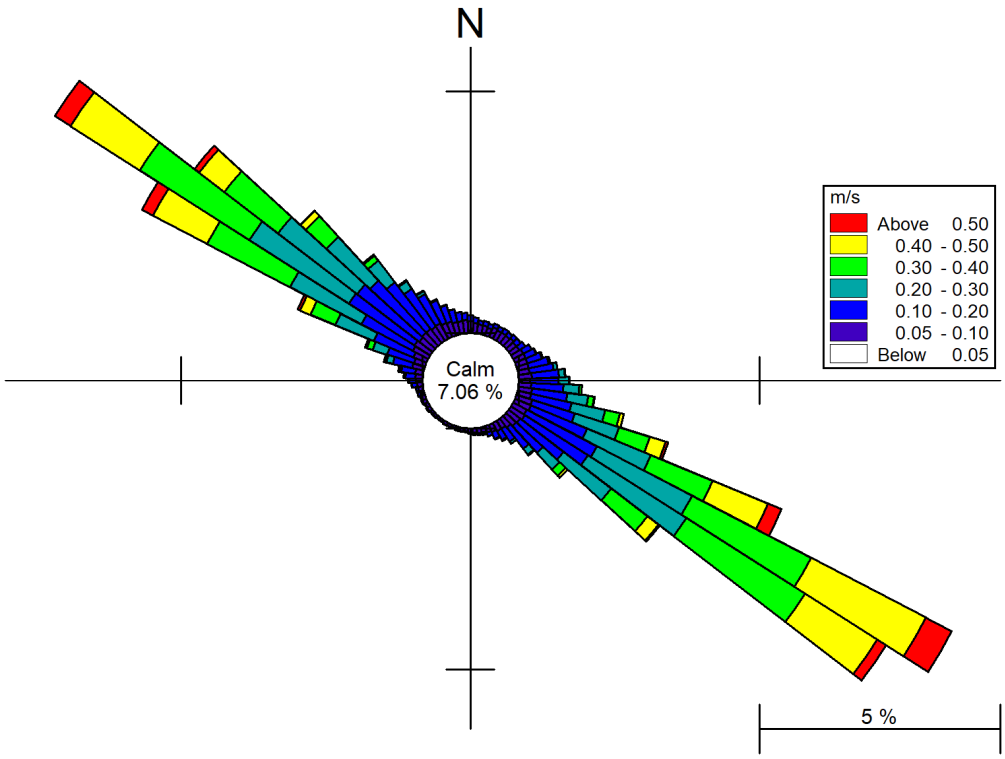

Figure 2-6 Current rose as derived from long-term depth-averaged measurements from the B16 AWAC over the period of 2020-2024. The directional convention is flowing towards.

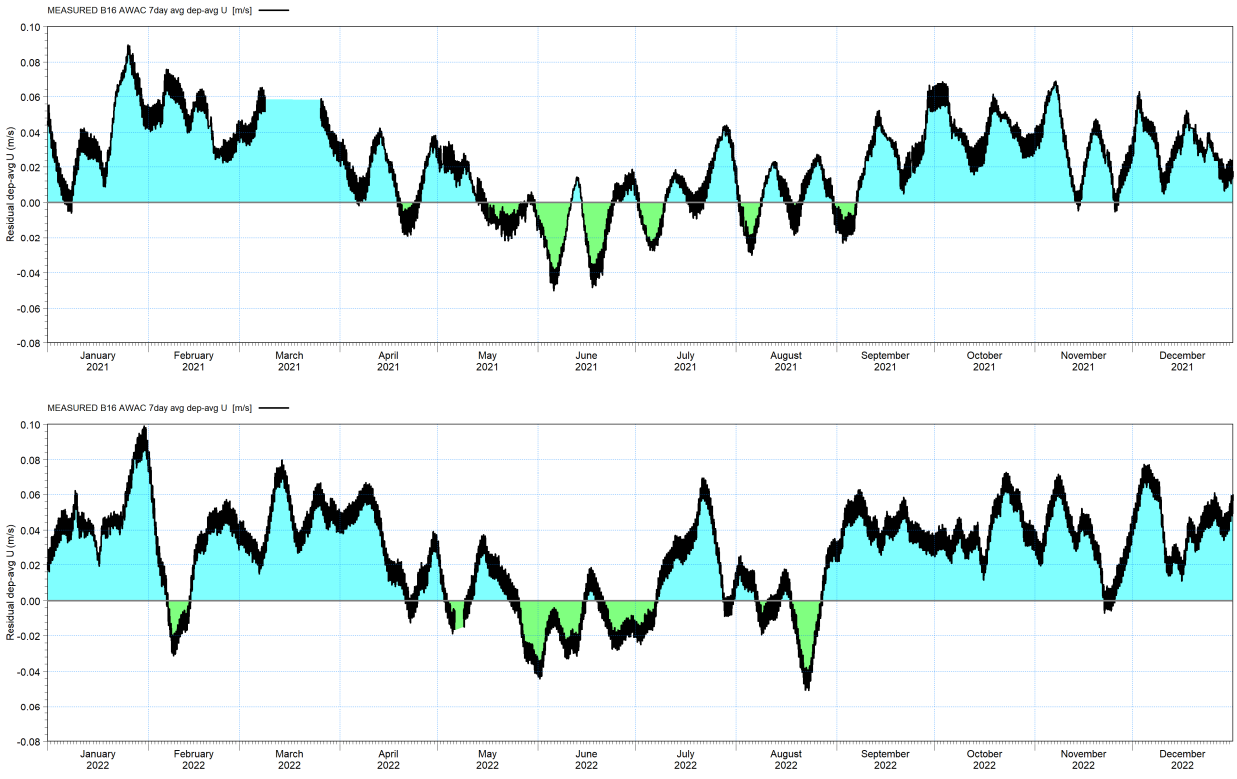

Figure 2-7 Annual residual current distribution, as 7-day running mean of depth-averaged U velocity component at B16 AWAC. Positive values shaded blue indicate eastward drift, negative in green denote westward drift.

3 Hydrodynamic Modelling

3.1 Introduction

Section 3.2 describes the establishment and validation of hydrodynamic models covering much of the Pilbara and Kimberley regions, as well as local features surrounding Port Hedland and at a very high resolution within the proposed work area of the Zone 5 Bypass project. The models have been established in both 2D and 3D, and serve multiple purposes.

The 2D Regional Hydrodynamic Model was executed for multiple years, which was necessary for fine tuning of tidal dynamics approaching Port Hedland as well as minimising nontidal errors in the model. The results from the long simulations within the 2D Regional Hydrodynamic Model were also used to characterise flow conditions and support the appropriate choice of simulation periods to characterise spillage from the proposed Zone 5 Bypass construction programme. The outputs of the 2D Regional Hydrodynamic Model provide boundary conditions to drive the 2D and 3D Local Hydrodynamic Models.

A 2D Local Hydrodynamic Model was applied as part of the model calibration process, and for initial screening of dredging spill scenarios to inform the choice of those retained in the 3D production simulations.

The 3D Local Hydrodynamic Model ultimately forms the basis for the transport and dispersion of sediments spilled during construction operations. As this model is computationally intensive, the duration of 3D simulations is generally limited to what is required to describe the construction scenarios.

3.2 2D/3D Hydrodynamic Models

3.2.1 Model Systems

A series of industry standard model systems have been applied for the present study. MIKE21 and MIKE3 FM HD (Hydrodynamics) and are mature industry standard (2D and 3D, respectively) numerical modelling tools which are developed and maintained by DHI. The modelling systems have been developed for complex applications within oceanographic, coastal and estuarine environments, with a constellation of other MIKE modules which can be coupled seamlessly. The present application involves a joint application of hydrodynamic, wave and mud transport modules.

The MIKE 21 Flexible Mesh hydrodynamic (FM HD) flow model is applied to describe the regional scale flow processes under the assumption that such flows are nearly horizontal (2D, depth-integrated) and that stratification can be neglected. This model is based on the numerical solution of the two-dimensional (2D) incompressible Reynolds averaged Navier-Stokes equations subject to the assumptions of Boussinesq and of hydrostatic pressure.

The MIKE3 Flexible Mesh hydrodynamic (FM HD) flow model is based on the numerical solution of the three-dimensional (3D) incompressible Reynolds averaged Navier-Stokes equations subject to the assumptions of Boussinesq and of hydrostatic pressure. The system is fully compatible with MIKE21, which is in many respects a direct simplification of MIKE 3. Numerous options of vertical turbulence closure schemes are available.

Both MIKE3 and MIKE21 utilize an unstructured mesh in the horizontal, consisting of triangular and/or quadrangular elements. This approach allows for increased resolution in

the areas of interest, while providing for larger more computationally efficient elements in the outer model areas.

MIKE3 utilizes a structured grid in the vertical, with numerous options available, including a σ (stretched) grid, a fixed z grid, or a mixed σ-z grid. The 3D model as applied here utilises a σ grid over the vertical and is barotropic in nature, ie it does not describe density stratification.

3.2.2 Computational Mesh

The domain established for the 2D Regional Hydrodynamic Model is shown in Figure 3-1. The domain covers the entirety of the Pilbara and much of the Kimberley regions with an unstructured triangular computational mesh at nominal resolutions ranging from 6km offshore down to 200m around the Port Hedland access channel.

The domain established for the 2D and 3D Local Hydrodynamic Model is shown in Figure 3-2. The domain extends roughly 125km west, 150km east and 100km offshore of Port Hedland. The domain features an unstructured computational mesh at nominal resolutions ranging from 3.5km offshore down to 35m within the Zone 5 Bypass dredged footprint. The same computational domain is also utilised for the Local Wave Model and for the dredging spill calculations.

Figure 3-3 shows intermediate and fine details of the domain. The existing navigation channel is described with a region of seven-wide quadrilateral elements to resolve flow. The dredged footprint is described with a series of structures triangular elements (five-wide across the channel) at a nominal resolution of 35m. Spoilgound 7C is described with a ~50m structured square grid.

All simulations are performed upon a rigid bed.

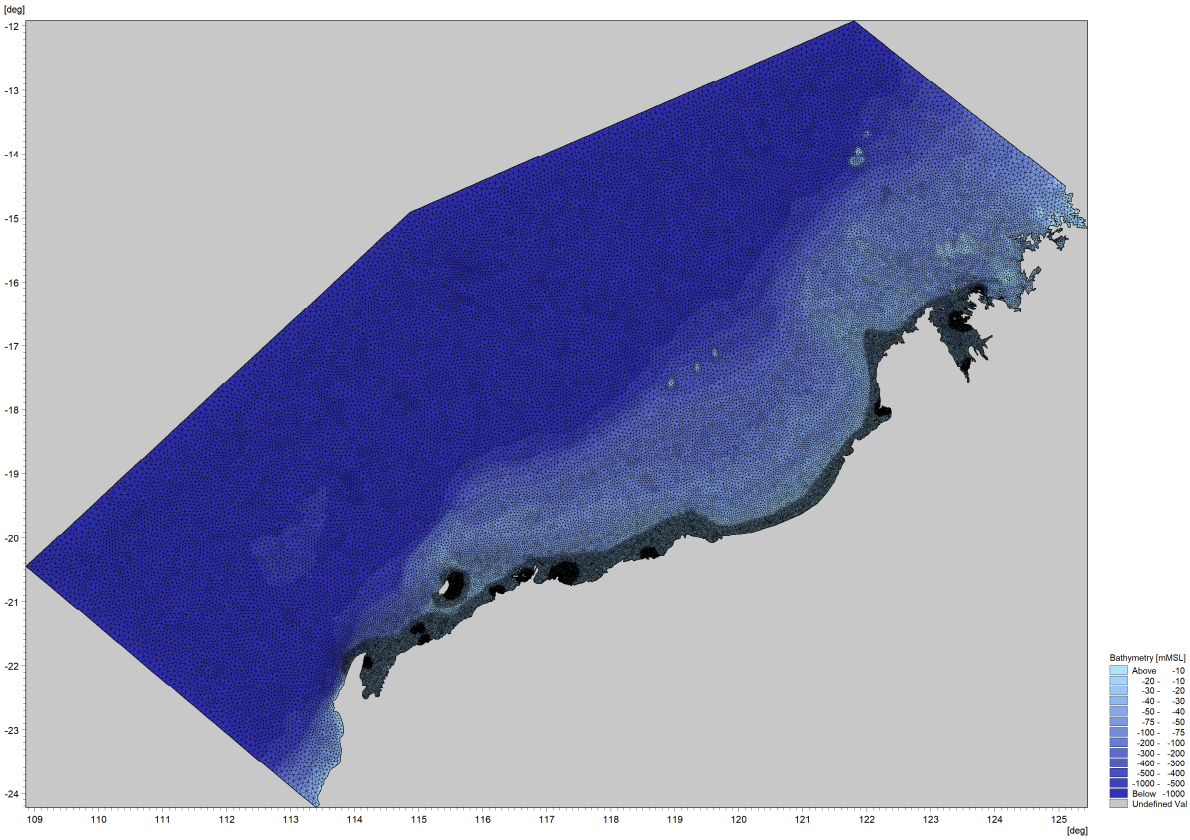

Figure 3-1 Domain and mesh arrangement of the (2D) Regional Hydrodynamic Model.

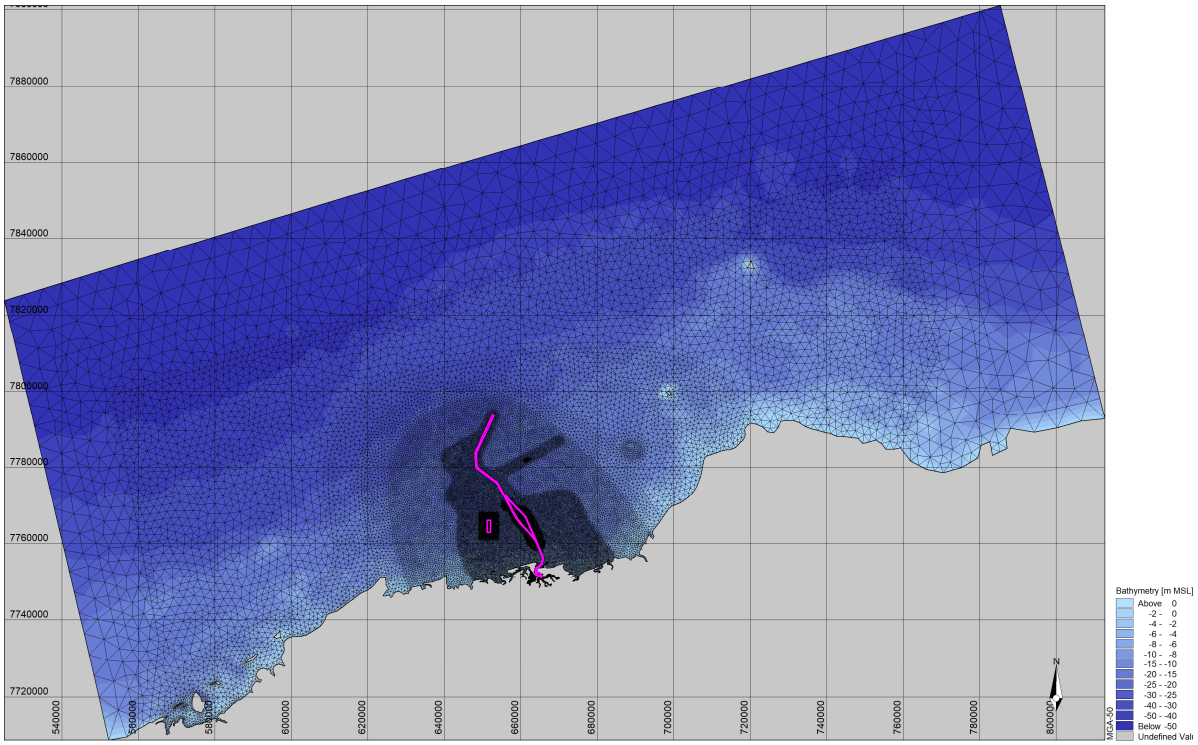

Figure 3-2 Domain and mesh arrangement of the (2D and 3D) Local Hydrodynamic Model. This domain is also applied for the Local Wave Model and for the Local Mud Transport (MT) model in which dredging spillage is simulated.

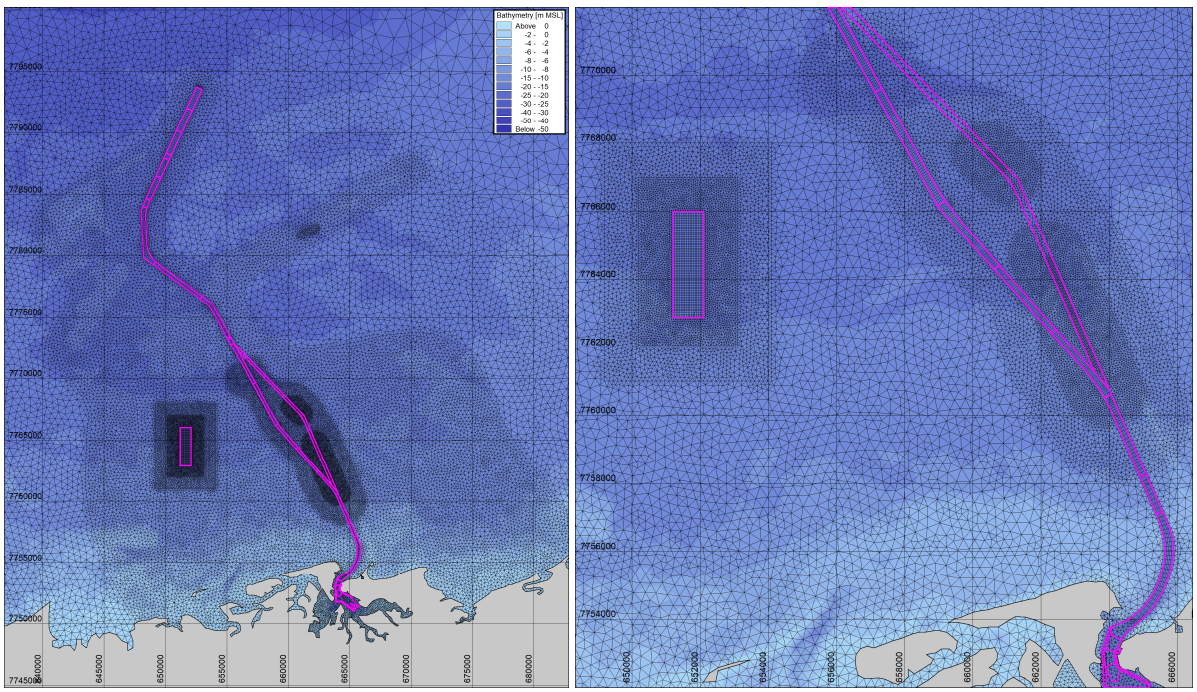

Figure 3-3 Intermediate and fine details of the Local Hydrodynamic Model mesh shown in Figure 3-2.

3.2.3 Bathymetry

Bathymetry within the model is specified based upon a hierarchy of data sources as listed below, where the first listed are applied within a given area if coverage exists:

- Multibeam acoustic surveys within port areas as provided by Pilbara Ports, within the domain shown in Figure 1-2. Areas within the port were described from published dredge depths and satellite imagery.
- Blending of 1m gridded LIDAR and multibeam data of the local area surrounding Spoilbank peninsula and Spoilbank Marina, dating from 2019 and 2025 (DoT, 2025).
- Remaining areas offshore to the ~25m MSL contour and ±50km longshore from the Port Hedland access channel were populated using the Geosciences Australia 30m gridded bathy/topo of NW Shelf (GA, 2020).
- Areas further afield within the Local domain, as well as the Regional Hydrodynamic Model domain were populated using Geosciences Australia AusBathyTopo (Australia) 250m grid (GA, 2024).
- The oceanic scale Southern Ocean Wave Model and the offshore portions of the Regional Wave Model were populated using a combination of GEBCO gridded bathymetry (GEBCO, 2024) and electronic navigation charting (Jeppesen, 2024).

The above data was merged into a unified archive with a consistent vertical datum of mean sea level (MSL).

3.2.4 Vertical Grid (3D Model)

The 2D Hydrodynamic and Wave Models have no vertical discretisation *per se*.

The vertical grid of the 3D model is applied as a so-called sigma "σ" grid, in which the water column is subdivided into an integer number of layers (in this case seven), each describing a fixed ratio of the total water column. Given the nature of dredging spill operations, the model is tailored to feature higher resolution toward the bottom of the water column.

Table 3-1 Vertical discretisation applied in Local 3D Hydrodynamic Model.

Layer # (from bottom)	σ-grid (% of water column)	Layer Thickness for Given Water Depth (m)		
		5m	10m	20m
7	20.0%	1.000	2.000	4.000
6	20.0%	1.000	2.000	4.000
5	15.0%	0.750	1.500	3.000
4	12.5%	0.625	1.250	2.500
3	12.5%	0.625	1.250	2.500
2	10.0%	0.500	1.000	2.000
1	10.0%	0.500	1.000	2.000

3.2.5 Offshore Boundary Conditions

The offshore boundary conditions of the Regional Hydrodynamic Model are generated in a hybridised manner from several separate sources.

The base spatially varying tidal variation along the open boundaries is specified from the 0.125° global tidal model DTU10 (Cheng and Andersen, 2011), which provides contributions from 10 primary constituents (M2, S2, K2, N2, O1, K1, P1, Q1, S1, M4). An additional 9 secondary constituents (J1, EPS2, 2N2, MU2, NU2, LDA2, L2, T2, R2) were added to the boundary signal using data from FES2014 (Avios, 2014) and tuned to minimise errors at the Port Hedland water level monitoring stations.

The modest annual / seasonal variation in water level at Port Hedland is described imperfectly by the inverse barometric effects associated with the BARRA-R2 met fields. The error in seasonal water level prediction within the model was calculated over five simulation years (2020-2024) and offset with compensatory SA/SSA constituents on the open boundaries of the Regional HD model for the final production simulations.

3.2.6 Meteorological Forcing

Meteorological forcing within the model domain is applied based upon the BoM BARRA-R2 reanalysis wind/pressure fields (Su et al, 2023). BARRA-R2 fields are available hourly at a spatial resolution of 0.11°, roughly 12km.

Table 3-2 Model settings applied in the 2D and 3D Hydrodynamic Models.

Property	2D Regional (depth-integrated)	2D Local (depth-integrated)	3D Local
Model System	MIKE21FM HD	MIKE21FM HD	MIKE3FM HD / MT
Vertical Grid	Depth-integrated (single layer)	Depth-integrated (single layer)	7σ layers, irregularly spaced
Density Effects	2D Depth-integrated	2D Depth-integrated	3D Barotropic
Roughness	Manning's M = 32	Manning's M = 32	k_s = 0.20m
Turbulence Closure	Smagorinsky, Cs=0.28	Smagorinsky, Cs=0.28	Smagorinsky, Cs=0.28 Vertical: k-ε
Coordinate System	Long/Lat	MGA-50	MGA-50
Nominal Mesh Resolution*	6km → 200m	3.5km → 35m	3.5km → 35m
Bathymetry	See Section 3.2.3		
Met Forcing	BARRA-R2 Reanalysis Fields. Inverse barometric effect included, wind drag coefficient = 0.0026		
Flooding & Drying	Enabled		
Wave radiation stress	Omitted	Included	Included
Boundary Conditions	Global tidal models, tuning per Section 3.2.5	Flather from 2D Regional Model	Flather from 2D Regional Model
Simulation Periods	Full years of 2020 through 2024, inclusive	01 Aug – 31 Oct 2021 01 Aug – 31 Oct 2022	Dredging spill: 15 Aug – 24 Sep 2021 22 Sep – 27 Oct 2022 15 Aug – 24 Sep 2022

* as sqrt(element area)

3.2.7 Miscellaneous Model Inputs and Settings

A summary of model settings is provided in Table 3-2 for all three hydrodynamic models applied in the present work. The 2D hydrodynamic model is simulated for a full year to support the generation of annual statistics and as a basis for the choice of shorter design periods for the more computationally demanding 3D model.

The 3D model is constructed as purely barotropic, ie vertical density gradients within the water column are omitted. The season of interest lies at the end of the dry season and prior to cyclone season, there is no reason to expect stratification to have a significant influence on transport mechanisms or plume dynamics.

3.2.8 Model Validation

Both the 2D and 3D models have been validated against long-term measured water levels and currents within the extensive network of metocean instrumentation maintained by Pilbara Ports (Figure 2-1).

Appendix A contains supplementary graphics and statistics related to validation of the hydrodynamic models.

Figures are presented in pairs, with each pair representing validation from 2021 and 2022 for a given combination of measurement station and measured quantity. Results from 2021 are in oddly numbered figures, 2022 evenly numbered.

Figures A-1 through A-8 present composite graphics of water level time series plots and performance statistics for year-long simulations of the 2D Regional Hydrodynamic Model for stations C1, E3, B17 and B31. As the focus of the present work is upon operational conditions outside the cyclone season, acute cyclone events are omitted from these comparisons. The results from these figures show a very high level of model proficiency, giving root mean square errors of 7 to 9 cm without bias correction.

Figures A-9 through A-16 present composite graphics of water level time series plots and performance statistics within the seasonal window of 15 Aug – 31 Oct from the 3D Local Hydrodynamic Model for the same stations C1, E3, B17 and B31. The results from these figures again show a very high level of model proficiency, giving root mean square errors of 7 to 11 cm without bias correction. The slightly elevated RMSE values in the Local Model results are not due to a degradation in performance vs. the Regional Model, but are a byproduct of a slightly elevated water level bias in the model (up to 6cm) which is specific to the15 Aug – 31 Oct 2022 period.

Figures A-17 through A-22 present composite graphics of current speed time series plots and performance statistics within the seasonal window of 15 Aug – 31 Oct from the 3D Local Hydrodynamic Model for the AWACs at stations E3 (depth-averaged), B16 (depth-averaged) and B31 (bottom AWAC bin, which is the only data available for these periods).

Figures A-23 through A-28 present time series comparisons of (u,v) current velocity components within the seasonal window of 15 Aug – 31 Oct from the 3D Local Hydrodynamic Model for the AWACs at stations E3 (depth-averaged), B16 (depth-averaged) and B31 (bottom AWAC bin).

The 3D Local Hydrodynamic Model clearly performs extremely well in terms of current speed magnitudes, directions and phase. A modest reduction in performance is seen in the B31 comparisons, owing to the only available measured information originating from the bottom AWAC bin.

Figures A-29 and A-30 present scatter plots of (u,v) current velocity components within the seasonal window of 15 Aug – 31 Oct from the 3D Local Hydrodynamic Model for the

AWACs at stations E3 (depth-averaged), B16 (depth-averaged) and B31 (bottom AWAC bin). The magnitudes and principal axes of motion are clearly captured very well in the model.

Validation of the 2D Local Hydrodynamic Model largely aligns with the depth-integrated comparisons of the 3D model, and is omitted here for brevity.

Two aspects of the hydrodynamic model performance of particular importance for dredging plume behaviour, are the principal axis of motion (mainly tidal) and the resultant nontidal residual flow. The former is responsible for short-term plume transport, while the latter dominates the net transport of the plume up-/down-coast over multiple tidal cycles.

Figure 3-4 shows the measured and modelled principal flow axes at the E3 and B16 AWACs. The tidal current component at E3 is oriented around an axis of almost exactly 135°-315°N, affected in part by the reef ridgeline on which the instrument resides. In contrast, B16 further inshore shows a reduced magnitude and a counter-clockwise rotation to align more closely with depth contours approaching shore. The orientations shown indicate the axes along which dredge plumes will be initially transported under the dominant tidal currents.

Figure 5-11 shows measured and modelled residual currents (as a 7-day running mean of depth-averaged U velocity component) during the candidate simulation periods of 15 Aug – 31 Oct 2021 and 2022. The figure confirms that both 2D and 3D Local Hydrodynamic Models perform extremely well in replicating the longshore residual current components. A useful rule of thumb is that a 1 cm/s longshore residual current results in a net plume migration of about 1 km/day (864m/day). Residual currents of the magnitude shown in Figure 5-11 thus result in substantial net plume transport along the coast within the dredging spill simulations.

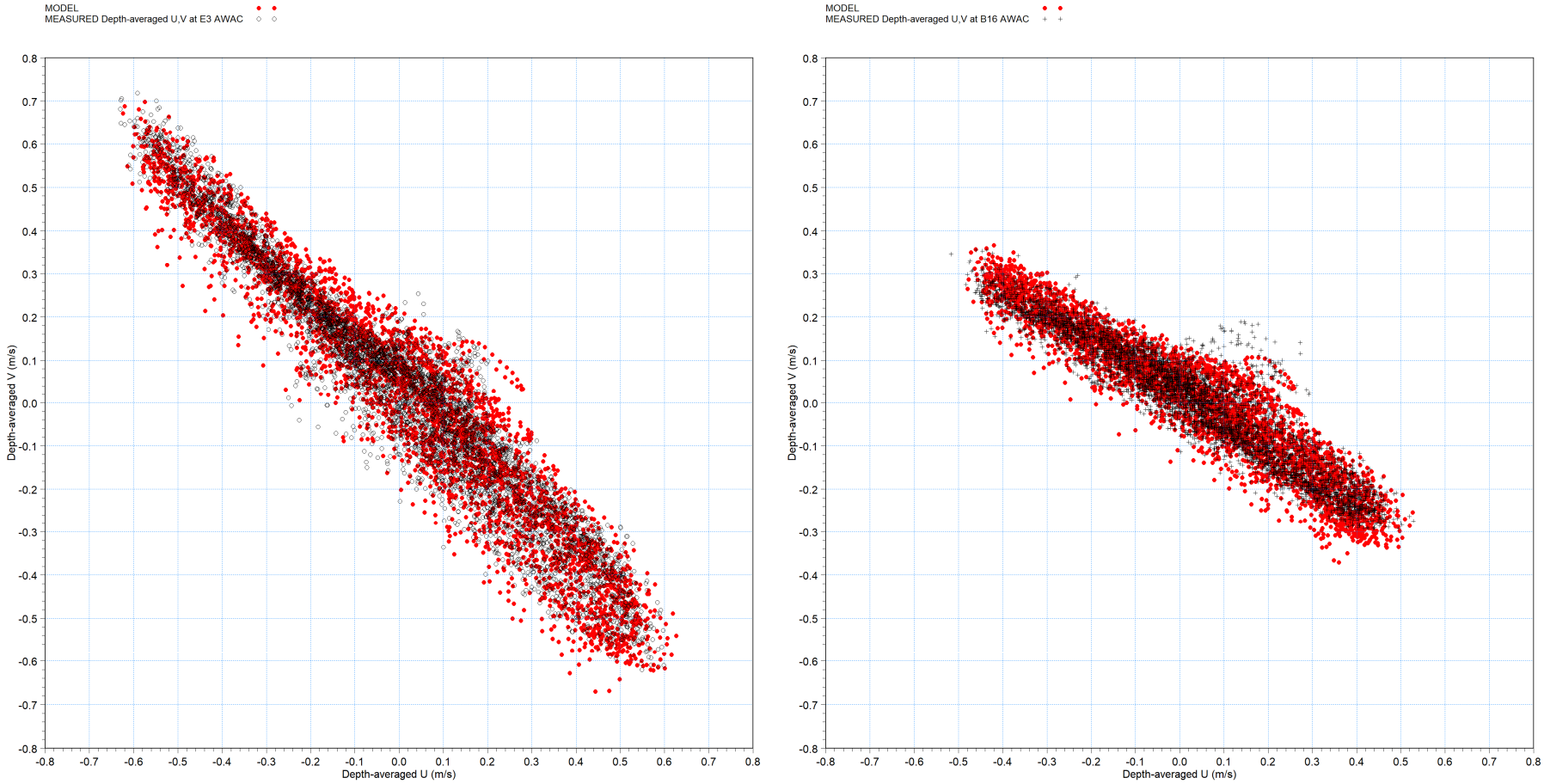

Figure 3-4 Measured scatter plots of depth-averaged current velocity (u,v) components from the E3 (left) and B16 (right) AWACs, overlain with depth-averaged results from the 3D Local Hydrodynamic Model.

4 Wave Modelling

4.1 Purpose

The purpose of wave modelling within the present study is to provide input to the calculation of combined wave/current shear stresses as required by the dredging spill (MIKE3 MT) model. The wave/currents shear stresses effectively control sediment interactions between the water column and the bed, determining when material in suspension may deposit, or when material on the bed may be resuspended.

4.2 Overview

A series of three spectral wave models covering a range of spatial scales have been applied to describe waves potentially influencing the area of influence of the Zone 5 Bypass project.

Operational wave conditions are addressed by first simulating wind growth over the Indian and Southern Oceans, forced by industry standard global wind fields. This Southern Ocean Wave Model (Figure 4-1) delivers temporally- and spatially variable directional spectra to a region roughly 2000km west of WA, where it is fed into the boundary conditions of the Regional Wave Model (Figure 4-2), which propagates wave energy onto the coastal shelf approaching WA. Directional spectra from the Regional Model is similarly applied to force the Local Wave Model (domain per Figure 3-2), which features higher mesh resolution and spatially variable water level conditions to more fully incorporate macrotidal effects.

As the proposed Zone 5 Bypass dredging operations are planned to occur outside the cyclone season, the focus of the model construction and validation is placed on the non-cyclonic portions of the year and more specifically within the proposed construction window of 15 Aug – 31 Oct.

The three models rely only upon windfields for third party input, and so can be operationalised should that be deemed useful.

4.3 Model System

MIKE 21 is DHI's modular, highly flexible modelling platform for the coastal ocean. It contains hydrodynamic, sediment transport, wave and water quality models. For this project, we utilise MIKE 21 SW, our spectral wind-wave model that simulates the growth, decay and transformation of wind-generated waves and swell. Typical applications of MIKE 21 SW include:

- Design wave conditions for offshore, coastal and port structures
- Accurate assessments of wave loads
- Simultaneous wave predictions and analysis
- Calculation of sediment transport determined by wave conditions and currents

DHI's MIKE 21 SW model is unique in the use of a cell-centred finite volume and unstructured (flexible) mesh method for discretisation of the governing equations in

geographic and spectral space. This approach provides significant advantages over contemporary fixed and fixed nested grid models by enabling the model resolution to be varied spatially within the model domain to provide very high resolution results at particular areas of interest, whilst enabling computational overhead to be limited in areas of lower interest or where wave transformation processes are varying slowly.

The MIKE21 SW computational engine also supports parallelisation in either OpenMP or MPI memory architecture. This enables simulations to be undertaken on High Performance Computers (HPC) using hundreds to thousands of computational cores in order to provide the ability to simulate very high spatial resolution models covering several years within reasonable computational time frames.

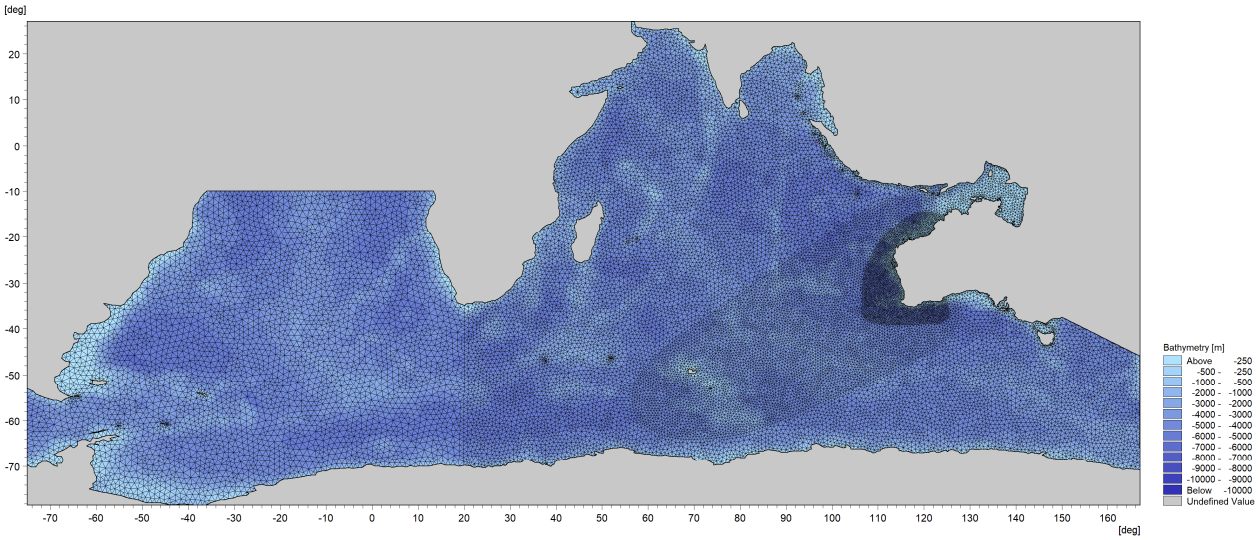

Figure 4-1 Domain and mesh arrangement of the Southern Ocean Wave Model.

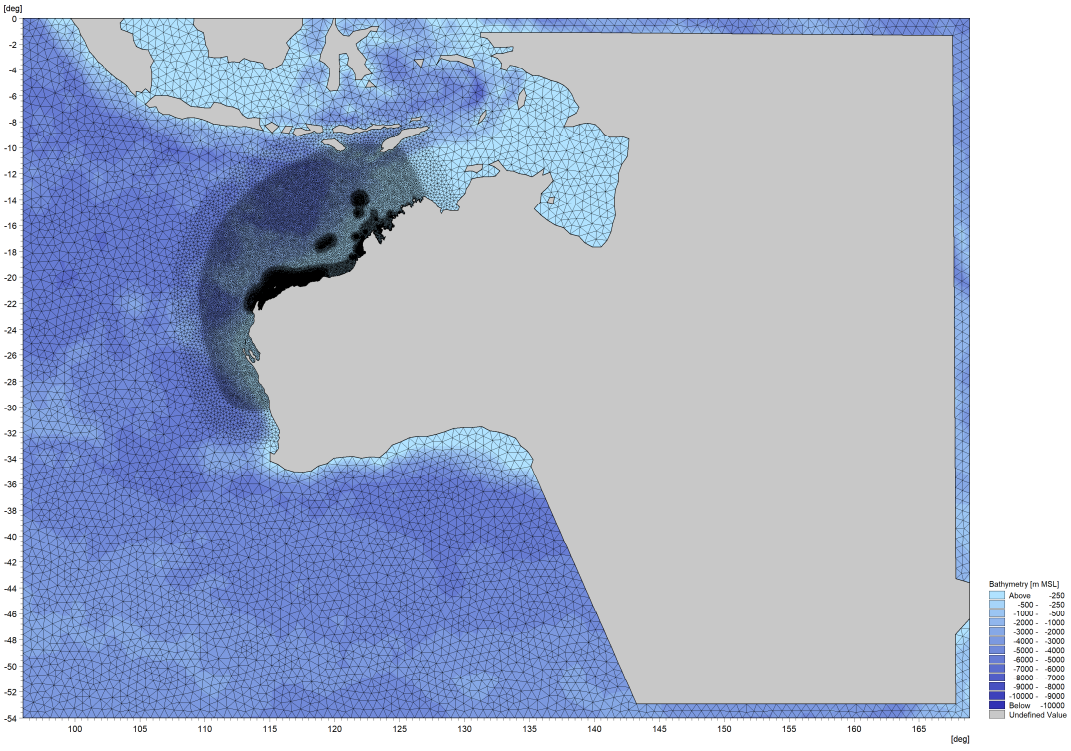

Figure 4-2 Domain and mesh arrangement of the Regional Wave Model.

Table 4-1 Model settings applied in the three wave models.

Property	Southern Ocean Wave Model	Regional Wave Model	Local Wave Model
Model System	MIKE21FM SW	MIKE21FM SW	MIKE21FM SW
Coordinate System	Long/Lat	Long/Lat	MGA-50
Nominal Mesh Resolution*	55km → 2.5km	50km →500m	3.5km → 35m
Bathymetry	See Section 3.2.3		
Model Engine	Fully spectral, dynamic		
Met Forcing	CFSRv2 Reanalysis Fields.	BARRA-R2 Reanalysis Fields.	BARRA-R2 Reanalysis Fields.
Frequency bins	30	25	25
Air/Sea	Coupled, Charnock=0.01	Coupled, Charnock=0.01	Uncoupled, Charnock=0.0185
Directions	36	24	24
Roughness	k_N = 3cm	k_N = 2cm	k_N = 2cm
Depth breaking	Omitted	Battjes & Jansson, γ=0.8	Battjes & Jansson, γ=0.8
Whitecapping	Enabled	Enabled	Enabled
Water Level Variations	Omitted	Port Hedland tide record	2D Local Hydrodynamic Model Fields
Boundary Conditions	none	Spatially varying dir spectra from Southern Ocean Wave Model	Spatially varying dir spectra from Regional Wave Model
Simulation Periods	Full years of 2020 through 2024, inclusive	01 Jun – 31 Oct 2021 01 Jun – 31 Oct 2022	02 Aug – 31 Oct 2021 02 Aug – 31 Oct 2022

* as sqrt(element area)

4.4 Model Construction

The builds of the Southern Ocean, Regional and Local Wave Models are summarised in Table 4-1.

Computational Mesh and Bathymetry

The computational mesh of the Southern Ocean Model is shown in Figure 4-1. The mesh is composed of unstructured triangular elements, with a spatially varying nominal resolution ranging from 1° (~55km) down to 0.025° (~2.5km) approaching the Australian continent. Bathymetry is populated based upon a hybrid dataset consisting of GEBCO (UNESCO, 2014) data at depths > 100m and C-MAP (Jeppesen, 2024) for depths < 100m.

The computational mesh of the Regional Wave Model is shown in Figure 4-2. The mesh is composed of unstructured triangular elements, with a spatially varying nominal resolution ranging from 50km down to 500km approaching the WA coastal shelf. Bathymetry is again populated based upon a hybrid dataset consisting of GEBCO (UNESCO, 2014) data at depths > 100m and C-MAP (Jeppesen, 2024) for depths < 100m.

The computational mesh of the Local Wave Model is identical to the Local Hydrodynamic Model, per Figure 3-2. The mesh is composed of unstructured triangular and quadrilateral elements, with a spatially varying nominal resolution ranging from 3.5km offshore down to 35m within the Zone 5 dredged footprint. Bathymetry is populated per Section 3.2.3.

Wind

Atmospheric forcing is provided via NOAA CFSRv2 global reanalysis wind fields (Saha et al., 2011). CFSR coverage is hourly, and available at a spatial resolution of 0.2°.

Wind forcing in the Regional and Local Wave Models is provided from the hourly high-resolution (0.11°) BoM BARRA-R2 reanalysis wind fields (Su et al, 2023).

4.5 Validation

The Southern Ocean and Regional Wave Models have been validated via previous projects within the Pilbara. For the present application, validation focuses upon the Local Wave Model.

Validation is presented in Appendix B, in the form of time series comparisons against measurements within the extensive network of metocean instrumentation maintained by Pilbara Ports (Figure 2-1).

As per Appendix A, figures are presented in pairs with each pair representing comparisons from 2021 and 2022 at a given measurement station. Results from 2021 are in oddly numbered figures, 2022 evenly numbered. The handling of the sea/swell separation within the measured data was inconsistent, at times occurring at 7s and in some instances at 9s as noted below. In all cases the sea/swell separation of the model outputs are aligned to follow the native processing of the measurements.

Figures B-1 and B-2 present time series plots of $Hm0_{TOT}$, $Hm0_{SEA}$ and $Hm0_{SWELL}$ for the waverider buoy at station C2. For 2021, the sea/swell split in the measurements was applied at 9s, while in 2022 it was applied at 7s.

Figures B-3 and B-4 present time series plots of $Hm0_{TOT}$, $Hm0_{SEA}$ and $Hm0_{SWELL}$ for the AWAC at station E3. The sea/swell split in the measurements was applied at 7s for both years.

Figures B-5 and B-6 present time series plots of $Hm0_{TOT}$, $Hm0_{SEA}$ and $Hm0_{SWELL}$ for the waverider buoy at station B15. For 2021, the sea/swell split in the measurements was applied at 9s, while in 2022 it was applied at 7s.

Figures B-7 and B-8 present time series plots of $Hm0_{TOT}$, $Hm0_{SEA}$ and $Hm0_{SWELL}$ for the AWAC at station B16. The sea/swell split in the measurements was applied at 7s for both years.

Figures B-9 and B-10 present time series plots of $Hm0_{TOT}$, $Hm0_{SEA}$ and $Hm0_{SWELL}$ for the AWAC at station B31. The sea/swell split in the measurements was applied at 7s for both years.

The figures show consistently strong performance between the modelled and observed wave heights for total, sea and swell components.

5 Dredging Spill Modelling

5.1 Introduction

Section 5 addresses construction-period impacts in relation to dredging spillage resulting from the handling of marine soils, and is arranged as follows:

- Section 5.2 lists basic conventions which are maintained in the description of dredging production and spillage.
- Section 5.3 addresses the planned timing of the Zone 5 construction works.
- Section 5.4 describes the detailed reference construction programmes as laid out by Pilbara Ports for the execution of the Zone 5 Bypass project
- Section 5.5 describes the reference CSD and TSHD vessels considered for the Zone 5 construction.
- Section 5.6 discusses the geotechnical baseline available to support the dredging spill assessment.
- Section 5.7 describes details of the parameterisation of the reference dredging programme into the numerical model
- Section 5.8 describes the construction and simulation periods applied for the production scenarios
- Section 5.9 describes the methodology applied for the estimation of spill rates
- Section 5.10 provides details of the dredge spill model (MIKE3 MT) setup
- Section 5.11 presents results from the dredging spill modelling.

5.2 Conventions

Unless stated otherwise, vertical references cited here are relative to Chart Datum (CD).

Unless stated otherwise, all volumes cited here refer to *in situ* values and do not incorporate a bulking factor for handled materials.

The term “fines” is frequently used in the context of dredging spill to describe the fraction of cohesive material prone to remaining in suspension in far-field, but that definition is not universal. For the avoidance of doubt, in the present document the terms “fines” and “fine material” refer to all sediments having a grainsize diameter of d < 75µm to align with the available particle size distributions (PSDs).

Production scenarios are referenced as a number and a letter (ie, Scenario 2A), with the number indicating the construction methodology (1 or 2) and the letter indicating the historical metocean period applied as forcing for the given simulation (A, B or C).

5.3 Timing of Proposed Construction Works

Per Pilbara Ports, the dredging campaign is to occur over a duration of 30 - 35 days within a specific seasonal target window. Dredging is planned to start in mid-August 2026, and

will be completed prior to the onset of cyclone season (formally 01 Nov). Specific production simulation periods are addressed in Section 5.8.

5.4 Overview of Reference Construction Programmes

The proposed Zone 5 bypass channel is shown in Figure 1-2 and Figure 5-1. The design depth within the indicated yellow polygons is -11.5m CD, with an overdredging allowance of 0.6m. For the purposes of spill modelling, it is conservatively assumed that the full overdredging allowance is utilised. Dredging within the yellow polygons in Figure 5-1 will thus be assumed to occur wherever the ambient seabed is shallower than -12.1m CD. This corresponds to a total dredging volume of approximately 800,000 m^3.

As indicated in the right pane of Figure 5-1, this implies that dredging will be concentrated in the southern end of the proposed Bypass Channel. The majority of the proposed channel footprint (about 75% by area) is already deeper than -12.1m CD. Isolated patches of hardbottom (indicated as coral by Client) in the northern portion of the dredging area (hereafter "Northern Patches") are of very limited volume, totalling roughly 1500 m^3 of material.

Two construction scenarios are considered in this report:

Scenario 1 Dredging
Scenario 1 assumes an all-TSHD operation removing 800,000 m^3 consisting of a mixture of granular and partially consolidated bed material. The total duration of Scenario 1 operations is 5 weeks. Scenario 1 cycling details are provided in Table 5-1.

Scenario 1 operations will occur 24/7.

Scenario 2 Dredging
Scenario 2 is a CSD-TSHD operation, under the assumption that the contractor deems the material to be too hard to be dredged efficiently with a TSHD alone.

A mega CSD will first crush the material in place within the channel design footprint south of BH-12, to a tooth depth of -12.5m CD. The volume pre-cut in this CSD operation is estimated at 325,000m^3.

Following completion of CSD operations, a TSHD will then remove the crushed material and remaining loose sediments within the dredging footprint, to a depth of -12.1m CD inclusive of overdredging. The total material moved by the TSHD thus aligns with the 800,000 m^3 assumed in Scenario 1. Of this total, an estimated 262,000 m^3 will be CSD pre-cut material. Pre-cut material below -12.1m CD will be left in place. The CSD operations are assumed to last for 1.6 weeks (~11.2 days, daylight only), while the following TSHD operations would last for 19 days (24/7). Scenario 2 will thus extend for just over 30 days in total.

Scenario 2 cycling details for the TSHD are provided in Table 5-1, with cycling information for the CSD in Table 5-4.

CSD operations will be constrained to daylight only (06:00-18:00), while Scenario 2 TSHD operations will be 24/7 as per Scenario 1.

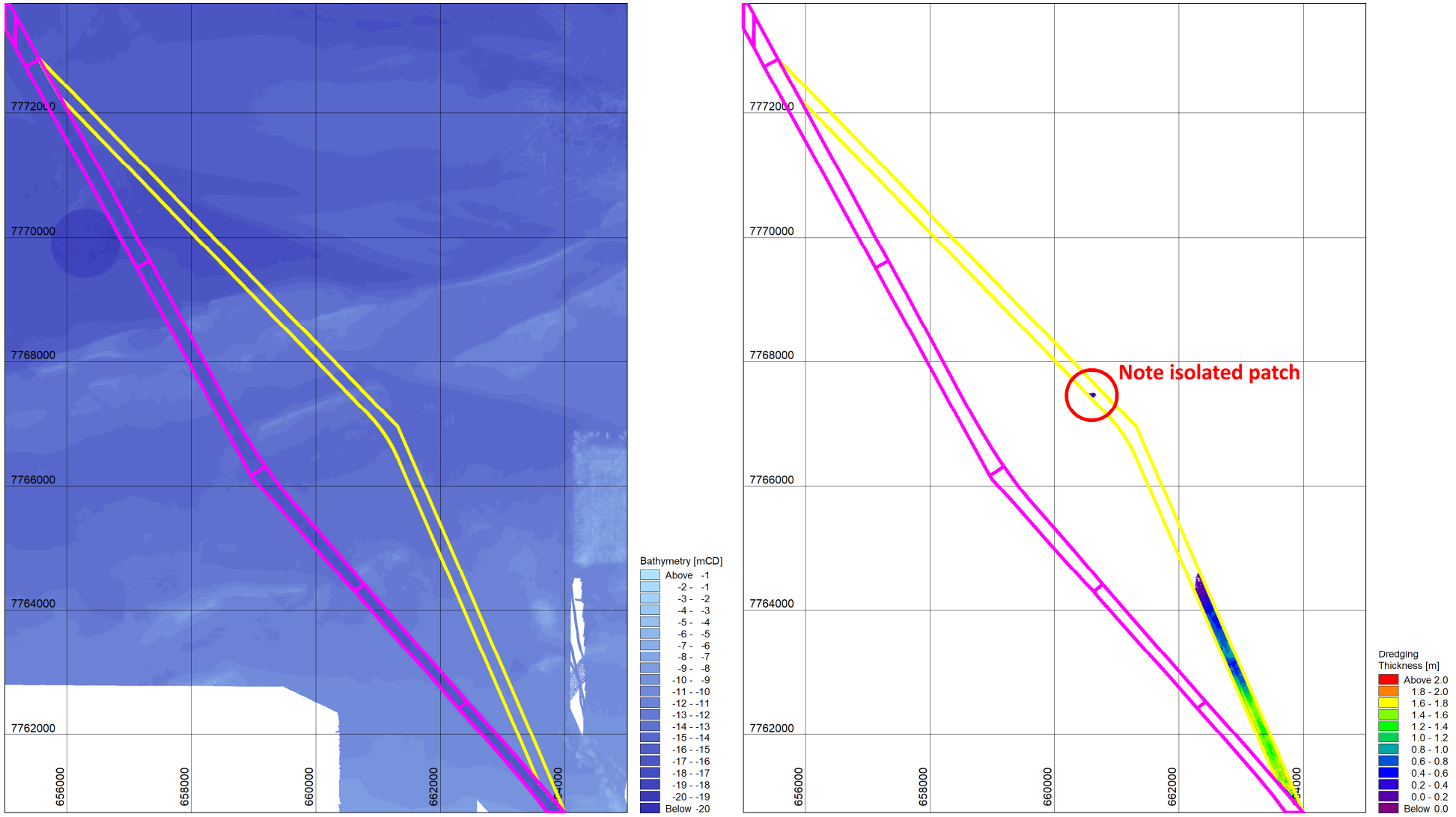

Figure 5-1 Left: Pilbara Ports bathymetric survey grid, overlain with existing access channel (magenta) and proposed Zone 5 bypass (yellow). Right: dredging thickness for a target depth of -12.1m CD (-11.5m design plus 0.6m overdredge).

Disposal

For both Scenarios 1 and 2, disposal of dredged materials will occur via TSHD bottom dumping within the designated Spoilground 7C (hereafter SG7C), as indicated in Figure 1-2. The dimensions of SG7C correspond to a rectangle of approximately 900m x 3120m.

5.5 Equipment and Methods

5.5.1 TSHD

The dredging equipment applied for the Zone 5 Bypass will ultimately be determined by commercial considerations and availability when the work is contracted.

The reference vessel considered here for the execution of the TSHD portion of the Zone 5 work is the TSHD *Juan Sebastián de Elcano* (hereafter TSHD *Elcano*, see Figure 5-2). The vessel is operated by Jan de Nul, and has previously worked at Port Hedland in connection with the CROP project. While the dredging spill simulations performed are based on this vessel specifically, the results of the simulations are broadly indicative of TSHDs within this size class.

The length overall (LOA) of TSHD *Elcano* is 157m, the beam 27.8m and its loaded draft 11.1m (JdN, 2025). Its unloaded draft is approximately 7.0m, per Pilbara Ports. It features two suction pipes and two cylindrical overflow pipes in the hopper, one fore and one aft (AET, 2016). For disposal, TSHD *Elcano* features 7 double bottom doors along the centreline of the ship (AET, 2016).

The TSHD is planned to operate with overflow. The hopper will be loaded until partially filled, after which time the (primarily) liquid portion will drain back to sea, along with an associated suspended sediment load. TSHD *Elcano* includes a central underkeel discharge arrangement where water is released via downward pipes through the keel. The elevation of the upper portion of this pipe is dynamically controlled based on the load of the vessel, so that the top of the overflow pipe remains just below the water surface of the hopper, thereby drawing off the lowest concentration of sediment.

During the initial period of loading prior to overflow, spillage will be a result of draghead / propwash contributions alone and will be relatively small. Once overflow is initiated, spillage will continue to occur via draghead / propwash and also via stripping from the overflow plume with the latter dominating total losses during the loading process.

Most modern TSHDs include an “environmental valve” or “green valve” on the overflow system, which is effectively a butterfly valve sitting within the pipe to limit the amount of air entrainment into the underkeel discharge. Dredgers overflowing without a green valve tend to generate larger plumes as the entrained air offsets the otherwise negative buoyancy of the sediment-laden plume and disrupts its descent to the seabed. Spillage rates are calculated here under the assumption that a green valve is active on the TSHD throughout its operations.

The TSHD *Elcano* hopper volume of 16,000 m^3 shown in Table 5-1 is based upon inputs from Pilbara Ports. Other references cite slightly higher volumes of 16,500 m^3 (JdN, 2025) or 16,700 m^3 (AET, 2016). This detail is not critical in the present context as the hopper is only ever partially filled during the Zone 5 campaign, and the vessel is at any rate indicative for what may be achieved by other similar “jumbo” class TSHDs.

Figure 5-2 TSHD *Juan Sebastián de Elca*no (photo JdN).

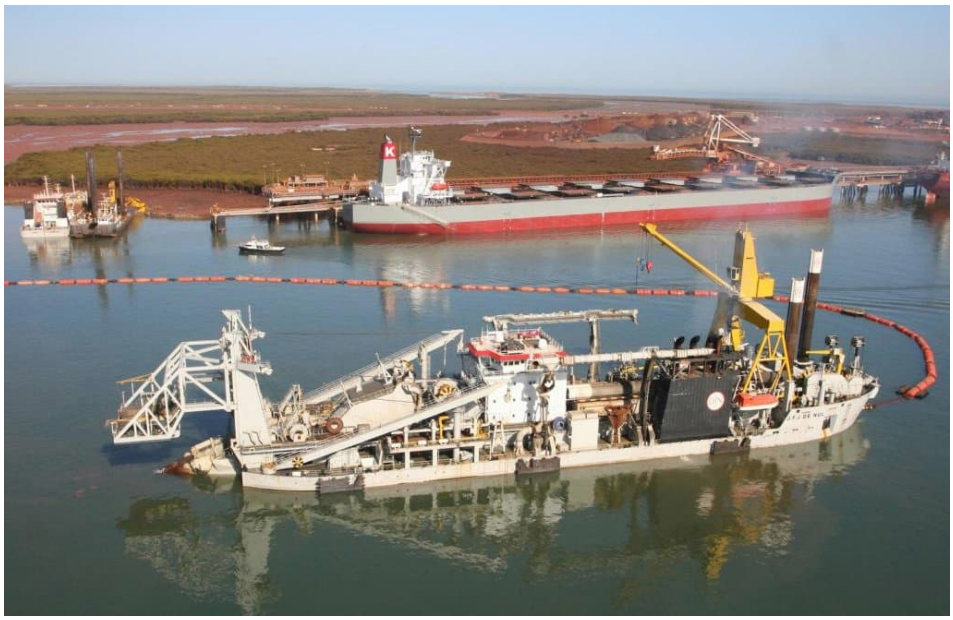

Figure 5-3 Mega cutter suction dredger (CSD) *J.F.J. de Nul* (photo JdN).

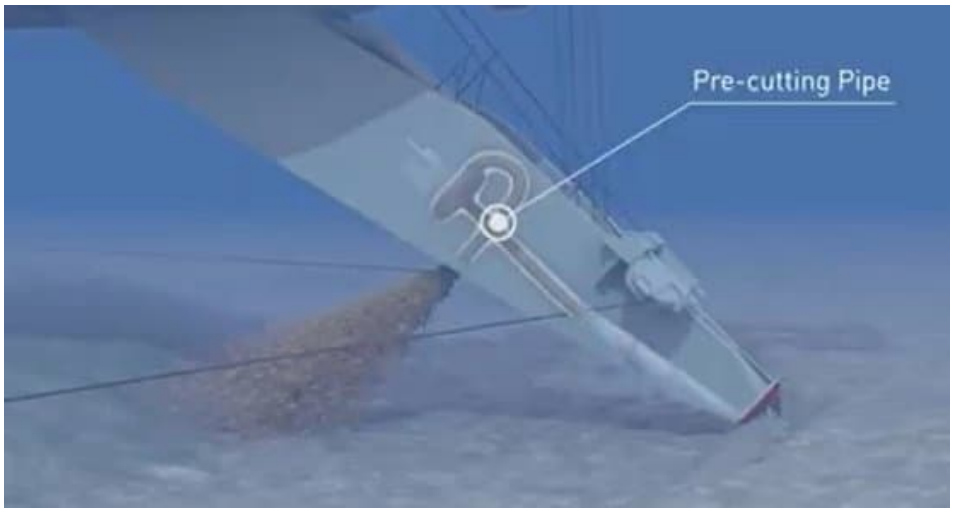

Figure 5-4 Near-bed pre-cutting discharge on the CSD ladder (Pilbara Ports).

Table 5-1 Key details assumed for the operation of TSHD *Elcano* for the Zone 5 activities.

Characteristic / Activity	Zone 5 TSHD Activity		Reference
	Scenario 1	Scenario 2	
Total *in situ* volume excavated	800,000 m^3		Owner email
Hopper capacity	16,000 m^3		Owner email
Draft Empty	7.0 m		Owner sharepoint
Draft Loaded	11.1 m		JdN (2025a)
Operational window	24 / 7		Owner email
Overflow arrangement	Underkeel, with “green valve”		Owner sharepoint
Estimated duration of activity	35 days	30.2 days	Owner email
Loading time prior to overflow	30 min		Owner email
Loading time with overflow	130 to 420 min	120 to 390 min	Owner email
Loading time total	160 to 450 min	150 to 420 min	Owner email
Avg sailing time to/from SG7C	32.4 min		Owner email
Disposal	15 min		Owner email
Traffic Interruptions per cycle	20 min		Owner email
Metocean-induced downtime	none		Owner email
Total cycle time	260 to 550 min	250 to 520 min	Owner email
Achieved cycles per day	2.62 to 5.54	2.77 to 5.76	Owner email
Total cycles	139.0	90.4	DHI calc

Table 5-2 and Table 5-3 both show reductions in productivity and load volume along with an increase in cycling times over the course of the TSHD operations. This reflects the progression to thinner dredging areas and isolated high spots requiring more time for vessel positioning. The latter weeks of work are more difficult to meaningfully describe in the model, as less active dredging occurs within each protracted loading cycle.

Table 5-2 Cycling details for the TSHD Elcano for Scenario 1, as provided by Pilbara Ports (top) and as slightly modified (below, where shaded green) for implementation in model.

As provided by Pilbara Ports

Volume m3	800,000
Hopper volume m3	16,000
ave. Sailing speed	12 knots
Distance to SG	12 km

Production	Sailing from SG (Mins)	Loading Time	Sailing to SG	Dumping	Shipping delay	Cycle Time (min)	Load per day	Ave Hopper load		Volume per day	Volume per week	Cum. Volume	Total loads
week 1	32.4	160	32.4	15	20	259.79	5.54	60%	9,600	53,211	372,479	372,479	38.78
week 2	32.4	190	32.4	15	20	289.79	4.97	40%	6,400	31,802	222,613	595,091	34.79
week 3	32.4	300	32.4	15	20	399.79	3.60	25%	4,000	14,407	100,852	695,943	25.20
week 4	32.4	360	32.4	15	20	459.79	3.13	20%	3,200	10,022	70,153	766,096	21.91
week 5	32.4	450	32.4	15	20	549.79	2.62	10%	1,600	4,191	29,335	795,431	18.34
												total →	139.02

As parameterised in Model

Volume m3	800,000
Hopper volume m3	16,000
ave. Sailing speed	12 knots
Distance to SG	12 km

PARAMETERISED TO = 800,000 total and to have integer # of loads per week

Production	Sailing from SG (Mins)	Loading Time	Sailing to SG	Dumping	Shipping delay	Cycle Time (min)	Load per day	Ave Hopper load		Volume per day	Volume per week	Cum. Volume	Total loads
week 1	32.4	160	32.4	15	18.67	258.46	5.571	60.42%	9,668	53,863	377,039	377,039	39.00
week 2	32.4	190	32.4	15	18.21	288.00	5.000	40.28%	6,445	32,226	225,579	602,618	35.00
week 3	32.4	300	32.4	15	23.41	403.20	3.571	25.18%	4,028	14,386	100,705	703,323	25.00
week 4	32.4	360	32.4	15	40.21	480.00	3.000	20.14%	3,223	9,668	67,674	770,997	21.00
week 5	32.4	450	32.4	15	30.21	560.00	2.571	10.07%	1,611	4,143	29,003	800,000	18.00
												total →	138.00

Table 5-3 Cycling details for the TSHD Elcano for Scenario 2, as provided by Pilbara Ports (top) and as slightly modified (below, where shaded green) for implementation in model. Note that time references in this table (Day1-4, etc) starts upon completion of the CSD pre-cutting.

As provided by Pilbara Ports

Volume m3	800,000
Hopper volume m3	16,000
ave. Sailing speed	12 knots
Distance to SG	12 km

Production	Sailing from SG (Mins)	Loading Time	Sailing to SG	Dumping	Shipping delay	Cycle Time (min)	Load per day	Ave Hopper load		Volume per day	Volume per period	Cum. Volume	Total loads
Day 1-4	32.4	150	32.4	15	20	249.8	5.76	70%	11,200	64,565	258,260	258,260	23.04
Day 5-8	32.4	160	32.4	15	20	259.8	5.54	60%	9,600	53,211	212,845	471,105	22.16
Day 9-12	32.4	170	32.4	15	20	269.8	5.34	50%	8,000	42,699	170,796	641,901	21.36
Day 13-16	32.4	270	32.4	15	20	369.8	3.89	40%	6,400	24,922	99,688	741,589	15.56
Day 17-19	32.4	420	32.4	15	20	519.8	2.77	30%	4,800	13,298	39,893	781,482	8.31
												total →	90.43

As parameterised in Model

Volume m3	800,000
Hopper volume m3	16,000
ave. Sailing speed	12 knots
Distance to SG	12 km

PARAMETERISED TO = 800,000 total and to have integer # of loads per week

Production	Sailing from SG (Mins)	Loading Time	Sailing to SG	Dumping	Shipping delay	Cycle Time (min)	Load per day	Ave Hopper load		Volume per day	Volume per week	Cum. Volume	Total loads
Day 1-4	32.4	150	32.4	15	20.63	250.43	5.750	72.61%	11,618	66,805	267,220	267,220	23.00
Day 5-8	32.4	160	32.4	15	22.02	261.82	5.500	62.24%	9,959	54,772	219,087	486,307	22.00
Day 9-12	32.4	170	32.4	15	24.49	274.29	5.250	51.87%	8,299	43,568	174,274	660,581	21.00
Day 13-16	32.4	270	32.4	15	34.20	384.00	3.750	41.49%	6,639	24,896	99,585	760,166	15.00
Day 17-19	32.4	420	32.4	15	40.20	540.00	2.667	31.12%	4,979	13,278	39,834	800,000	8.00
												total →	89.00

5.5.2 CSD

The southern portion of the Zone 5 work area features partially consolidated materials which are marginally dredgeable with a TSHD. Scenario 2 considers an initial pre-cutting phase whereby a mega CSD crushes the material in place within the channel design footprint south of BH-12, to a tooth depth of -12.5m CD. The volume pre-cut in this CSD operation is estimated at 325,000m^3.

The reference dredger for this operation is the CSD *J.F.J. de Nul* as shown in Figure 5-3. This vessel features an LOA of 141m, a beam of 27.8m a draught of 5.5m and a maximum dredging depth of 36m (JdN, 2025b). The installed cutter power of 7600 kW is more than adequate for crushing the Zone 5 materials. Slurry will be discharged immediately (~15-20m) behind the cutterhead, at an elevation nominally ~3m above the seabed (mASB) as illustrated in Figure 5-4.

CSD *J.F.J. de Nul* is indicative of the given class of vessels. Market forces will determine the equipment ultimately applied for the work.

Table 5-4 Key details assumed for the operation of CSD *J.F.J. de Nul* for the Zone 5 activities, as provided by Client.

Characteristic / Activity	Zone 5 CSD Activity	Reference
Total *in situ* volume excavated	325,000 m^3	Owner email
Expected max tooth depth	-12.5m CD	Owner email
Draft	5.5 m	JdN (2025b)
Total duration of activity	1.6 weeks = 268.8 hrs *[1]	Owner email
Operational window	Daylight only (0600-1800)	Owner email
Production rate as *in situ* vol	2,725 m^3/hr	Owner email
Production rate as slurry	18,240 m^3/hr	Owner email
Operational downtime	20min every 2hrs *[2]	Owner email
Discharge point	15-20m behind cutterhead, ~3m ASB	Owner email

*[1] Modelled as 278.2 hrs (11.59 days) to align with stated total volume and production rate

*[2] Interpreted as a 140min cycle, ie 120min continuous dredging then 20min downtime

5.6 Geotechnical Inputs

Project-specific geotech information is available in Worley (2025). This work incorporated 14 boreholes as well as geophysical surveys of the regions bounded by the rectangles indicated in Figure 5-5. The distribution of the boreholes was specifically chosen to address dredgeability of the material, and therefore targeted areas for which harder materials were likely to be located. A total of 23 particle size distributions (PSDs) are available from samples within 9 boreholes (BH-06 through BH-14), all of which lie within the southern portion of the Zone 5 work area.

The soil units present in the survey are characterised as Alluvium, Coastal Limestone or Upper Red Beds. Dredging will mainly occur within the Alluvium and Coastal Limestone units, with Upper Red Beds generally lying below the active dredging prism.

Table 5-5 provides a breakdown of the fines content present in the Zone 5 PSDs in Worley (2025), with grading curves from all PSDs provided in Figure 5-6. Several observations can be made:

- While substantial scatter is present, the mean fines percentage occurs within a relatively narrow range (26.0 to 31.3%) for all subsets by either depth or soil unit.
- Most of the PSDs analysed are deeper than the proposed dredging (including overdredging). Only 5 lie specifically within the material to be moved as part of the Zone 5 project.

Table 5-5 Summary of PSDs generated from the Worley (2025) borehole campaign.

Subsets of PSDs acquired in Worley (2025) boreholes	# of PSDs	Mean fines content (< 75m)
All available from Worley (2025)	23	29.8 %
All within Alluvium unit	16	30.8 %
All within Coastal Limestone unit	4	26.0 %
All within Upper Red Beds unit	3	29.7 %
All above -12.1m CD, full work area	4	31.3 %
All above -12.1m CD, or above -12.5m CD within CSD pre-cut area	5	29.2 %

The boreholes paint a complex picture in space, in terms of both a) the relative distribution of Coastal Limestone vs. Alluvium within the dredged material and b) the degree of consolidation within the Coastal Limestone unit where present. It is expected that the dredging operations under consideration will typically handle a commingling of the Alluvium and Coastal Limestone units at any given time.

The following geotechnical inputs are applied in the modelling of dredging spill:

- A uniform fines percentage of 29.2%, based upon the mean PSD from the five samples available from within the dredging material to be handled (bottom row of Table 5-5, Figure 5-6).
- A uniform *in situ* dry density of 1800 kg/m^3
- Grain density of 2.67 g/cm^3

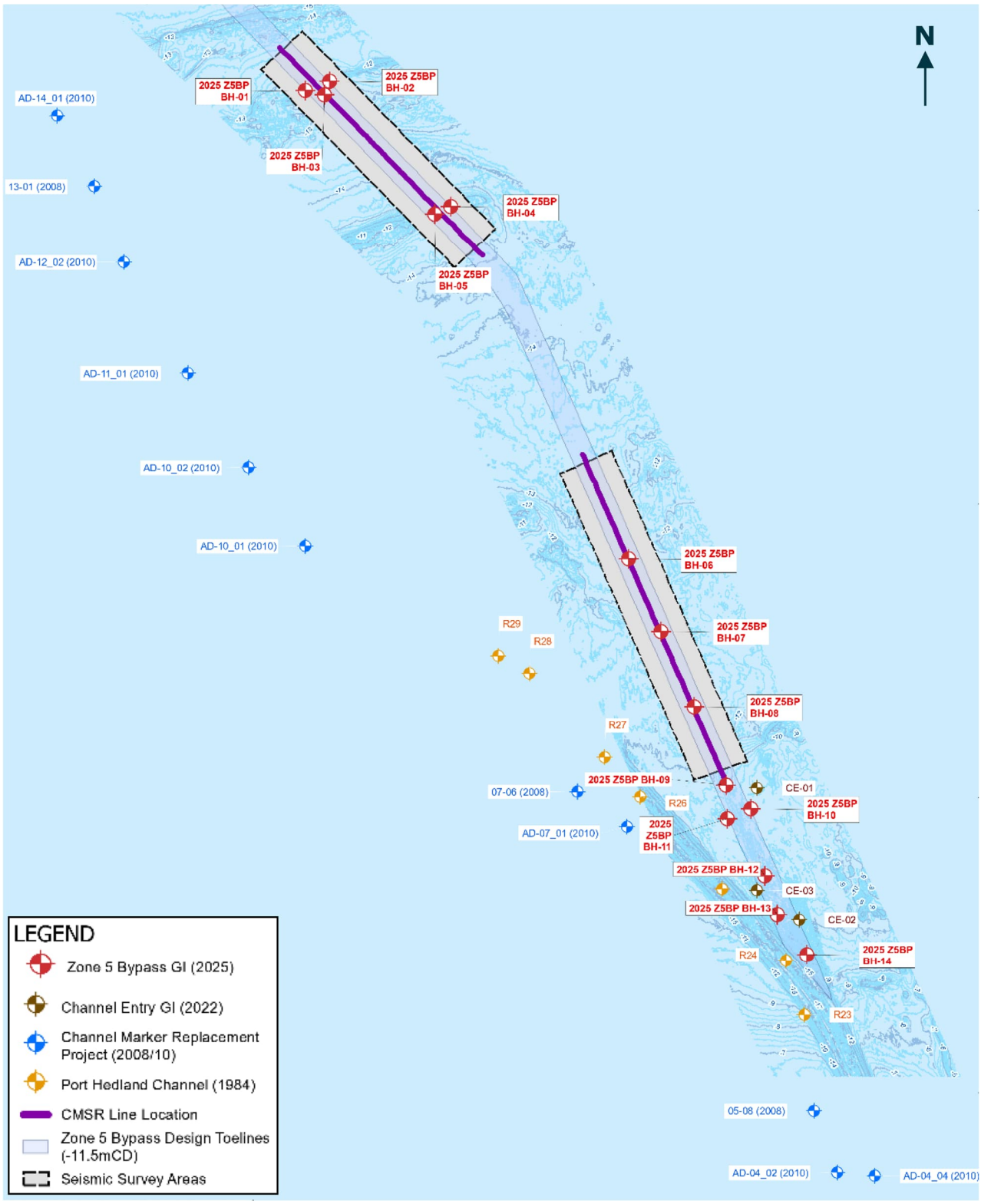

Figure 5-5 Locations of the 14 boreholes and coverage of geophysical surveys describing the Zone 5 dredging area, with boreholes acquired in support of previous projects as indicated (after Worley, 2025).

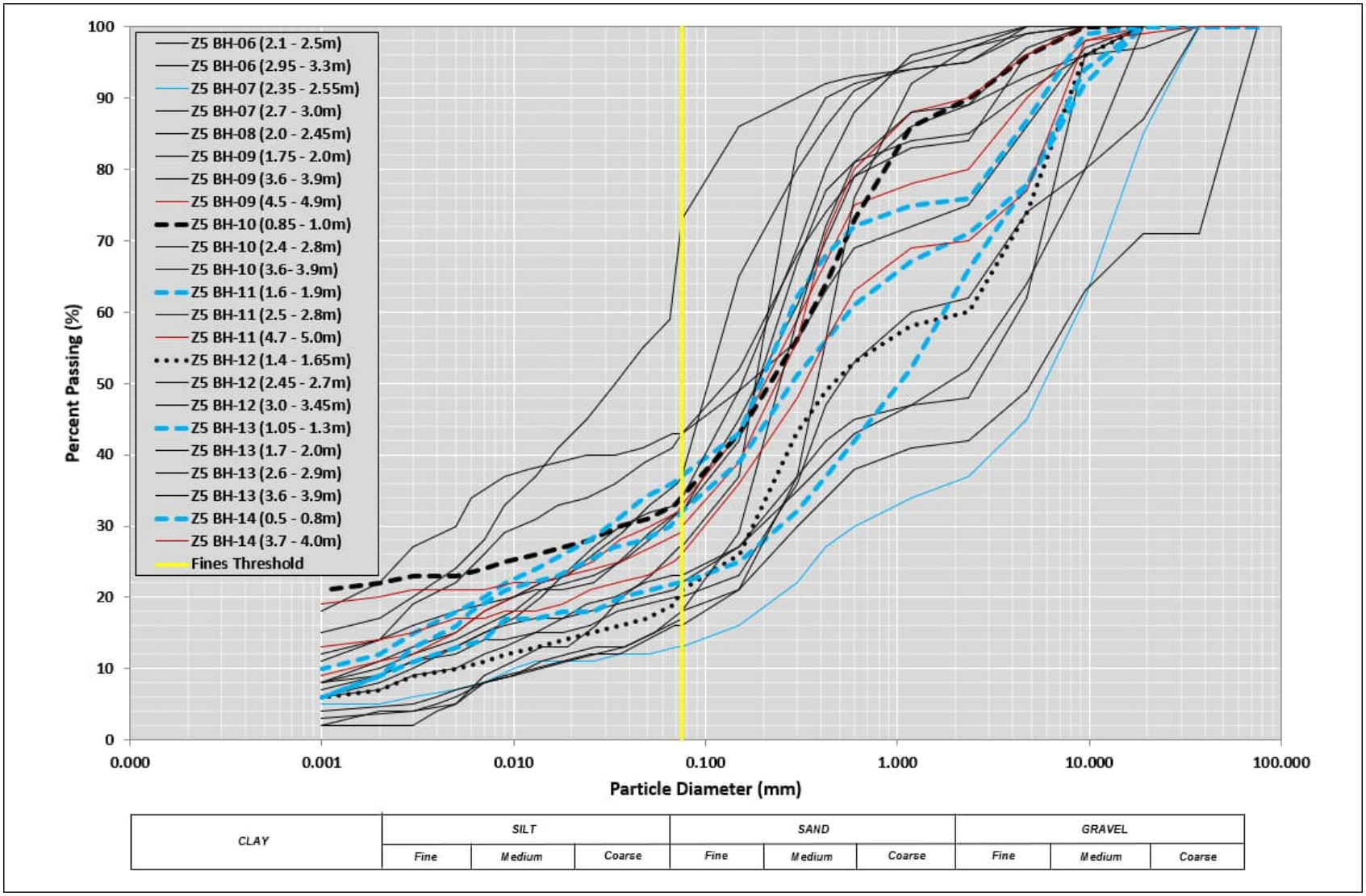

Figure 5-6 Visualisation of all 23 PSD curves reported in Worley (2025). Depths below seabed noted in parentheses.
Black: Alluvial unit, blue: Coastal Limestone, red: Upper Red Beds.
Bold dashed: depth > -12.1mCD, full Zone 5 area. Bold dotted: -12.5mCD < depth < -12.1mCD within CSD operating area.

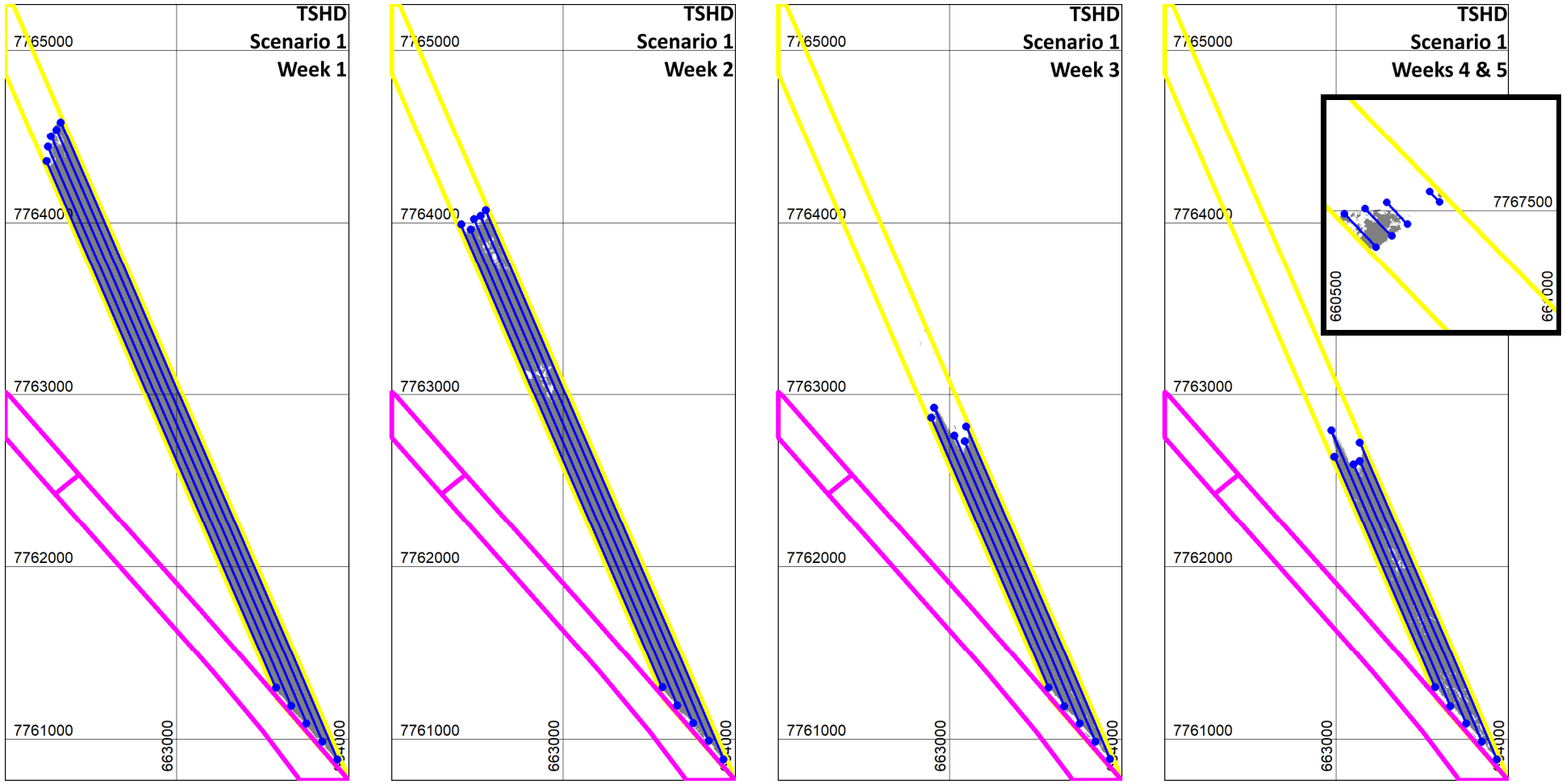

Figure 5-7 Scenario 1: Spatial parameterization of spill sources proposed for TSHD loading for each week, as indicated by blue lines. Week 5 also includes removal of the isolated northern patch as shown in rightmost pane. Shaded area in channel denotes areas in which TSHD assumed to operate over the given week.

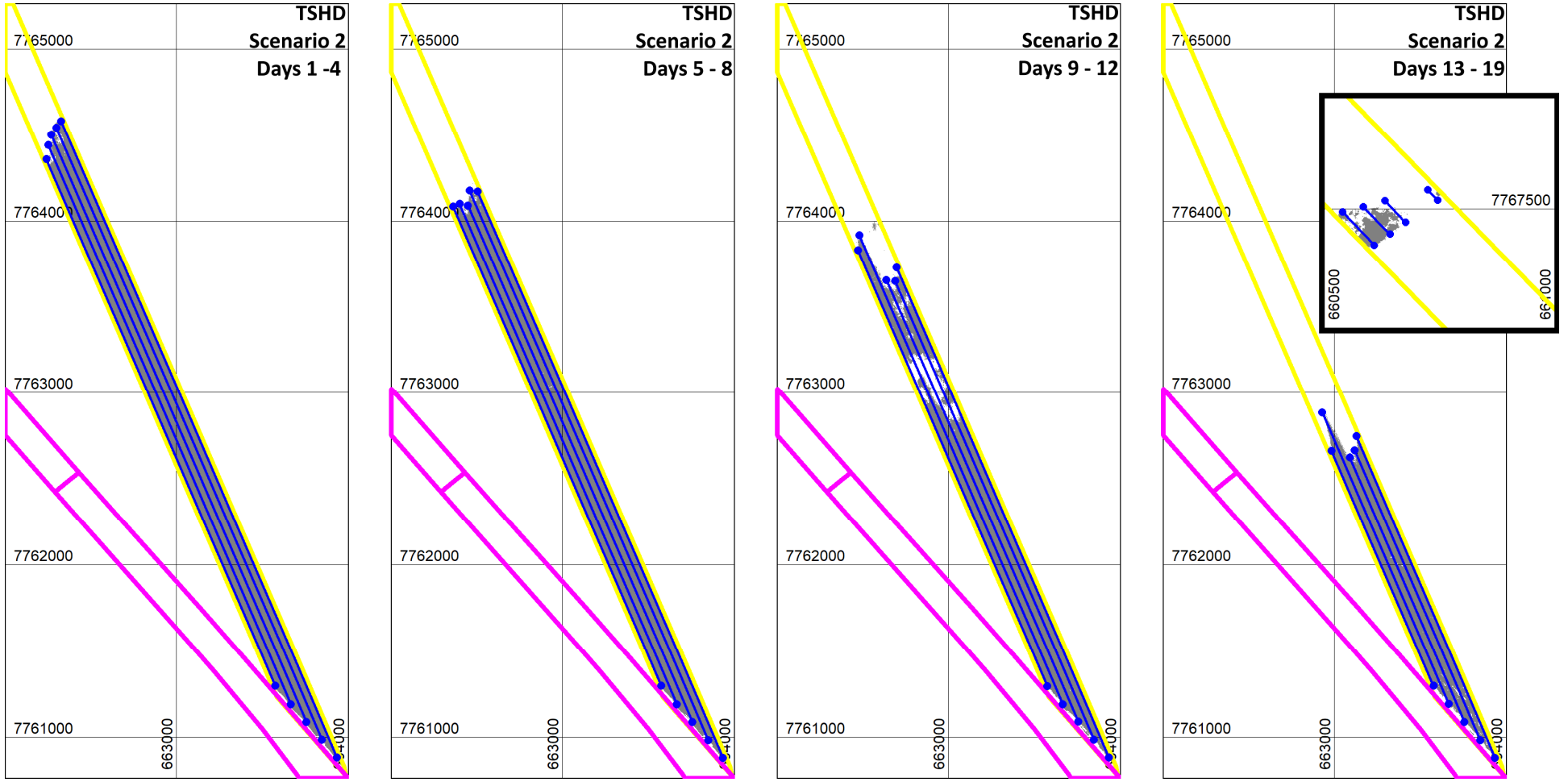

Figure 5-8 Scenario 2: Spatial parameterization of spill sources proposed for TSHD loading for each period of construction, as indicated by blue lines. Days 17-19 also includes removal of the isolated northern patch as shown in rightmost pane. Shaded area in channel denotes areas in which TSHD is assumed to operate over the given period.

5.7 Parameterisation of Construction Operations into Model

5.7.1 General

The parameterisation of the dredging programme into the numerical model seeks to strike a balance between being as realistic a depiction as possible, while acknowledging that the ultimate execution of the works will likely differ from whatever assumptions are made at this stage of the planning process. Furthermore, they are likely to be affected by operational constraints which cannot be anticipated.

The programme proposed below is fairly detailed, but still highly idealized.

5.7.2 Forcing Models

The transport, dispersion, deposition and resuspension of spilled dredge material are driven using the coupled 3D hydrodynamic and wave models as described in Sections 3 and 4 respectively, which have been extensively validated against measurements provided by Pilbara Ports. The wave and hydrodynamic calculations are performed on a rigid bathymetry, ie the modest changes to depth which occur due to the construction activities do not feed back to the model geometry. The proposed dredging thickness is small relative to the water depth, and there is no reason to expect significant changes metocean behaviour (in the context of affecting dredging spill calculations) as a result of the modest deepening.

The nominal mesh resolution within the immediate work area is <50m. For perspective, the last significant spill model executed for dredging of the outer channel featured a finest resolution of 100m (BHP, 2011).

5.7.3 TSHD Loading

Minor adjustments have been applied in the lower versions of Table 5-2 and Table 5-3, which force the total TSHD volume for each scenario to be 800,000 m^3 and impose the number of dumps for each line item to be an integer. In practice this entails making small changes to the cells shaded in green. The most notable changes in percentage terms occurs for the assumed traffic delay, which doubles for some activities. The changes are imposed such that the traffic delay tends to increase with the total duration of the TSHD cycle, which is entirely reasonable. Given the uncertainties associated with forecasting dredging operations, the scenarios as modelled are considered to be fully representative of the construction scenarios laid out by Pilbara Ports.

The exact sequence over which material will be removed in space by the TSHD is not known at this stage of project planning – only the temporal cycling of the work has been defined. In order to distribute spillage in time and space in a manner which is faithful to programme laid out by Pilbara Ports, it is necessary to assume a certain sequence for the dredger operations in both time and space.

The parameterisation of TSHD operations need to meet several fundamental requirements:

- The timing and duration of the spillage in the model must align with the cycling details for loading and dumping as laid out in Table 5-2 and Table 5-3.
- Spillage during loading is a direct function of rate of fines production, which is a direct function of total production for the TSHD. The total mass of spillage inserted

into the model from loading must thus align with production over each cycle, and when integrated over the full programme.

- Spillage during dumping is a direct function of fines remaining in the hopper after loading, which is a direct function of total production for the TSHD. The total mass of spillage inserted into the model from dumping must thus align with production over each cycle, and when integrated over the full programme.

- When integrated over the full programme, the areal distribution of spillage introduced into the model during dredging (loading) should approximately align in space with the areal distribution of fines by mass that are removed from the seabed.

Pilbara Ports have stated that latter portion of the TSHD activities would likely be focussed on the southern portion of the work area. The progression of the TSHD through the work area has been arranged in an idealised manner which is consistent with that guidance. The movement of the TSHD is based upon the assumed removal of fixed *thicknesses* of material during each time period (each week for Scenario 1, or each 3-4 days for Scenario 2). In this manner the final weeks of the campaign focus upon the southern portion of the work area where the dredging thickness is largest.

The sailing circuit followed by the model TSHD is shown in Figure 5-7 and Figure 5-8 for Scenarios 1 and 2, respectively. The nominal thickness of material removed for each time period is based upon the active dredging area and target volumes indicated in Table 5-2 and Table 5-3. As construction progresses, the design depths (incl overdredging) are achieved in the northern portions of the work area such that the active dredging area in subsequent periods becomes more concentrated to the south. The dredging area is held constant for the final two periods (Weeks 4 and 5 for Scenario 1, Days 13-19 for Scenario 2).

The removal of the isolated northern patches shown in Figure 5-1 is assumed to occur at the very end of the TSHD operations.

General Rules

a) A series of five longitudinal lines along the bypass channel are identified which the model dredger is assumed to sail at each step of the dredging campaign, as illustrated in Figure 5-7 and Figure 5-8. These lines form a circuit along which the model vessel advances.

b) All circuits are arbitrarily assumed to start at the southern end of the channel, with the five lines being sailing in sequence from the westernmost line to the easternmost line.

c) When loading, the vessel advances along the above circuit at a constant rate of 1 m/s (~2 knots), which is a realistic sailing speed for a TSHD when loading.

d) When the northern end of a line is reached, the vessel immediately reverses and returns to the starting (southern) point of the line. It then advances to the next line to east. When the easternmost line is completed, the circuit begins again at the southern point of the westernmost line.

e) The location of the vessel along the circuit at the termination of a given loading cycle is retained. When the subsequent loading cycle begins, it resumes sailing from its previous position.

f) The production rate of the vessel is assumed to be constant over the specified loading time of each cycle. Per Table 5-2, this will change weekly for Scenario 1. Per Table 5-3, this will change every 3-4 days for Scenario 2.

g) Traffic delays are in practice random, but are accounted in the model as always occurring between the dumping phase and the start of the next loading phase.

5.7.4 Pre-cutting by CSD

In order to limit disruptions of the existing main navigation channel, it is assumed that the CSD will work southward from BH-12. Its progression within the model is illustrated in Figure 5-9, which encompasses 163 mesh elements. The path as indicated shows a southward movement with cross-channel sweeps which crudely mimics the actual operations of the vessel – in reality each sweep will be only a few meters wide. Unlike the TSHD, the progression of a CSD is slow in relation to the transport of the plume, so this is an acceptable simplification within the model.

The rate of advance of the numerical CSD from one model element to the next along the indicated path is a function of the production rate as well as the volume of material being removed from each model element to achieve the specified cut depth of -12.5mCD. This process will pause for designated nighttime hours (18:00-06:00) and for the designated 20 min break every 2hrs.

When the progression of the vessel and associated spillage is calculated, the volume in each cell will be scaled such that the total in situ volume handled within the 163 cells aligns with the target volume of 325,000 m^3 to be pre-cut by the CSD. The model does not discriminate between spillage in the centre of an element vs the fringe of the element. Spillage at the coordinates of one of the red dots indicated in Figure 5-9 thus indicates spillage distributed over the entire respective element.

Changes in bathymetry as a result of the CSD activities, including bulking, are ignored in the model.

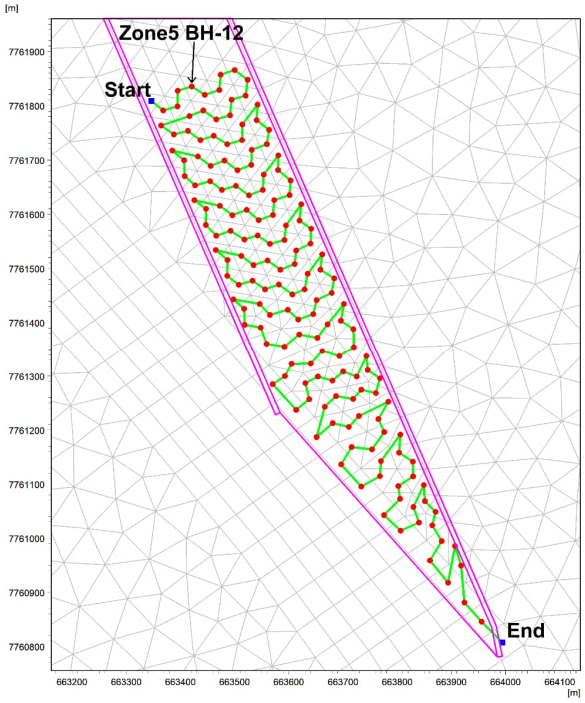

Figure 5-9 Parameterised progression of CSD from north to south in spill model.

5.7.5 Disposal by TSHD Bottom Dumping

The dimensions of SG7C correspond to a rectangle of approximately 900m x 3120m. Pilbara Ports have communicated the intent to partition this area into a grid of roughly 150m x 150m within which to manage dumping operations. As such, the dimensions of SG7C accommodate 124.9 grids each of 150m x 150m dimensions.

SG7C is described in the unstructured model mesh with a structured 50m x 50m grid, such that the model resolves each 150m x 150m disposal cell with 9 model elements. Spillage related to bottom dumping is released into the centre of the 9 model elements describing the respective disposal cell. As indicated in Table 5-1, each dump is assumed to last 15 min.

The model description of SG7C adjusts the grid dimensions slightly to achieve an integer number, with the dimensions of each grid being modified to 150m x 148.67m. In this manner SG7C becomes exactly 6 cells x 21 cells = 126 in total.

Per Table 5-2 and Table 5-3, the number of dumps required for Scenarios 1 and 2 are 138 and 89, respectively. This difference occurs as THSD operations in Scenario 1 last far longer and generate smaller loads per cycle. As such, some of the 126 dump cells in the model are used twice in Scenario 1 while for Scenario 2 many cells are unused.

The order of the dumps within this grid is randomised while constraining that each disposal cell receives at most one disposal over the course of the campaign (Scenario 2) and at most two for Scenario 1. The randomisation of dumps into the disposal cells is only performed once, ie the order and arrangement of dumps into SG7C is consistent for Scenarios 1A, 1B and 1C. Similarly, the order of dumps is identical between Scenarios 2A, 2B and 2C.

5.8 Simulation Periods

A total of six production simulations have been executed. Production scenarios are referenced as a number and a letter (ie, Scenario 2A), with the number indicating the construction methodology (1 or 2) and the letter indicating the historical metocean period applied for the given simulation (A, B or C).

Table 5-6 shows the duration of construction operations as well as the total simulation duration for each production scenario. An overview of metocean forcing conditions for the historical simulation periods A, B and C are shown in Figure 5-10 and Figure 5-11. Additional explanation follows.

Each of Scenarios 1A, 1B and 1C are identical in terms of the schedule of dredging and disposal activities, the only difference between them relates to the start time of the construction -- and hence the specific sequence of metocean conditions which occurs over the course of the dredging campaign. Similarly for Scenarios 2A, 2B and 2C

Per Pilbara Ports inputs, the dredging campaign is to occur over either 35 days (Scenario 1) or 30.6 days (Scenario 2) with a provisional start in mid-August 2026, and will be completed prior to the onset of cyclone season (01 November). The works are thus considered to occur within some subset of the window spanning 15 Aug - 31 Oct.

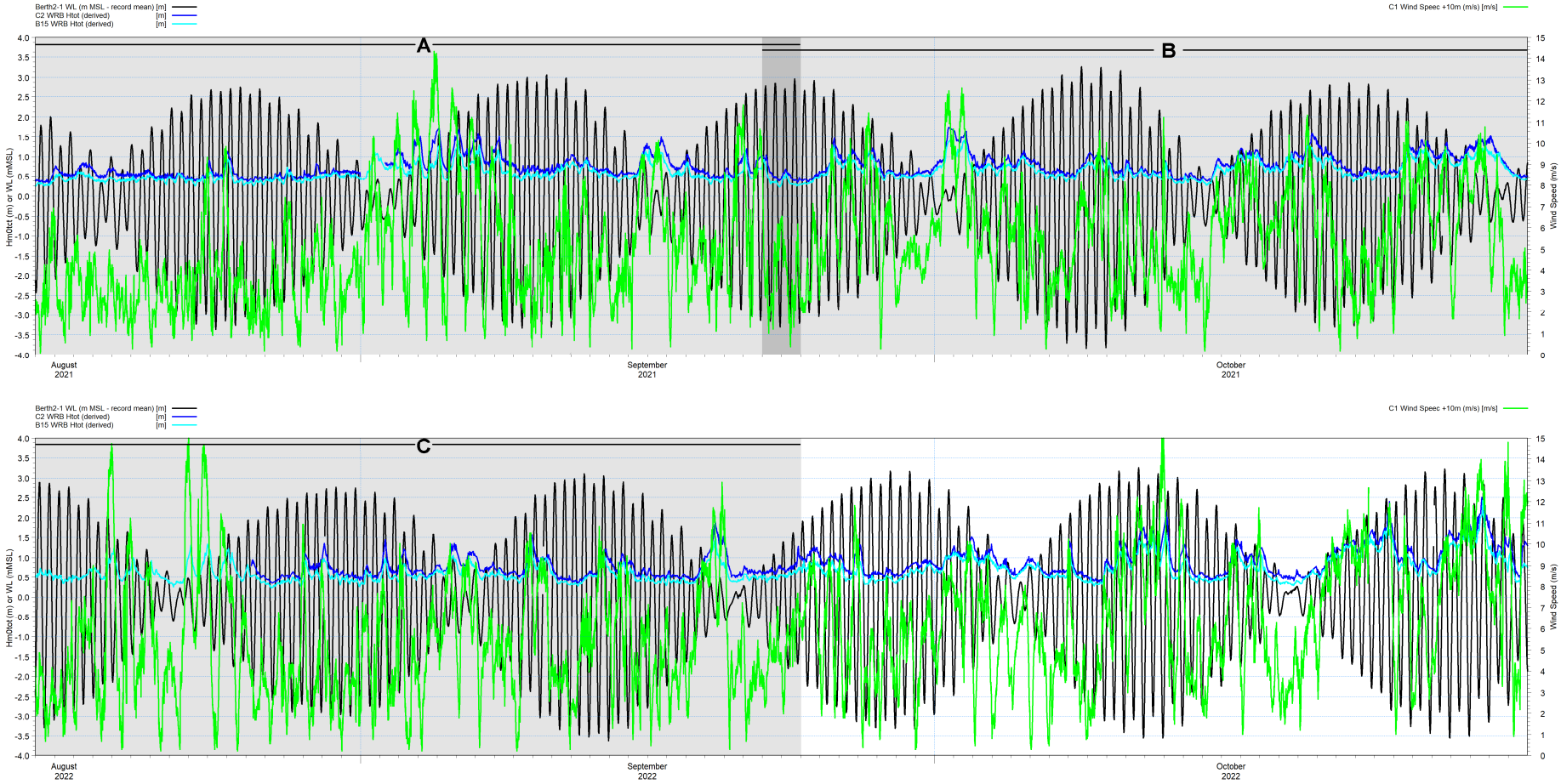

Figure 5-10 Instantaneous metocean measurements during the candidate simulation periods of 15 Aug – 31 Oct 2021 and 2022, showing water levels (black), windspeed (green) and wave heights at C2 (dark blue) and B15 (light blue), Grey shading and straight black lines / lettering indicates the three 40-day periods applied for production simulations in the 3D dredging spill model. Dark grey band in upper pane indicates a 2-day overlap between periods A and B.

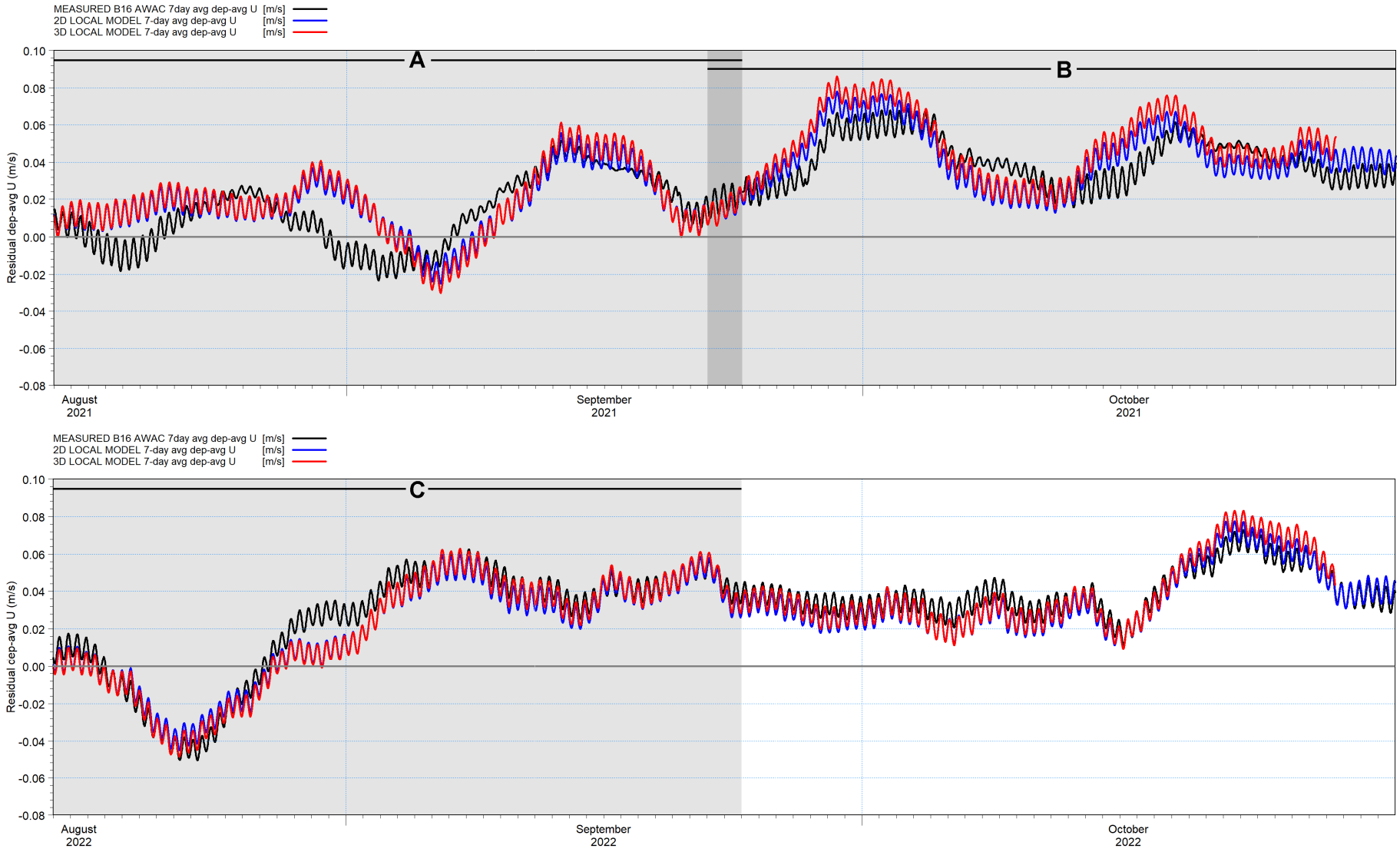

Figure 5-11 Measured and modelled residual currents (as 7 day running mean of depth-averaged U velocity component) during the seasonal construction window of 15 Aug – 31 Oct, shown here from 2021 and 2022. Grey shading and straight black lines / lettering indicates the three 40-day periods applied for production simulations in the 3D dredging spill model. Positive values indicate net eastward transport, negative westward.

There is appeal to select a historical simulation period from within the period during which the most/best measured data is available, such that the wave and hydrodynamic models can be directly validated during the production period. Based upon a review of interannual and intraseasonal metocean statistics, the 15 Aug – 31 Oct periods in 2021 or 2022 were assessed to be broadly indicative of the seasonal metocean envelope and are applied for the screening and production simulations. These periods also feature good availability of measured data from within the Pilbara Ports metocean instrumentation network.

Table 5-6 Construction and simulation periods as applied for Scenarios 1 and 2.

Construction / Metocean Scenario		Construction Activities	Simulation Period
Scenario 1A	TSHD	15Aug2021 00: – 19Sep2021 00:	15Aug2021 00: – 24Sep2021 00:
Scenario 2A	CSD TSHD	15Aug2021 00: – 26Aug2021 14: 26Aug2021 14: – 14Sep2021 13:	
Scenario 1B	TSHD	22Sep2021 00: – 27Oct2021 00:	22Sep2021 00: – 01Nov2021 00:
Scenario 2B	CSD TSHD	22Sep2021 00: – 03Oct2021 14: 03Oct2021 14: – 22Oct2021 13:	
Scenario 1C	TSHD	15Aug2022 00: – 19Sep2022 00:	15Aug2022 00: – 24Sep2022 00:
Scenario 2C	CSD TSHD	15Aug2022 00: – 26Aug2022 14: 26Aug2022 14: – 14Sep2022 13:	

* Simulation start indicates initiation of spillage. All simulations incorporate a 3 day spin-up period of the HD model prior to this.

As the proposed dredging campaign is relatively brief, the alignment of construction activities with metocean forcing is a key consideration. It is unrealistic to fully characterise the joint statistics of metocean variables (directional wind, directional waves, directional currents, water level / tide range) into a single indicative period. In order to provide insight to the range of potential effects of metocean timing, 2D screening simulations of dredging spillage were performed to provide an initial view of the sensitivity of results to the specific start date of the campaign within the 15 Aug - 31 Oct construction window. From this screening process, three periods were carried forward into 3D production which provide a range of plume responses. In this manner, three historical metocean forcing periods were identified, which are indicated here as A, B and C.

Figure 5-10 provides an overview of the primary instantaneous metocean forcing mechanisms present during the periods of 15 Aug – 31 Oct 2021 and 2022. Tidal level, wind speed, wave height are all indicated. The shaded boxes denote the temporal coverage of the three historical simulation periods A, B and C. It is clear from Figure 5-10 that each scenario initiates at a different phase of the fortnightly tidal cycle, and is exposed to stormy conditions at different stages of the construction sequence.

Figure 5-11 presents another key mechanism which dominates plume character, which is the prevailing residual current conditions. It was seen in Figure 2-7 that the residual current climate at the project site varies over the year, with a neutral or eastward drift prevailing much of the year but with periods of briefly sustained westward drift frequently occurring during the winter months. As the Zone 5 dredging campaign is proposed to occur in late winter / spring shoulder season, this implies that a westward residual current is more likely to be experienced early within the construction window and toward the earlier portion of the dredging sequence. As the bulk of production and spillage tends to occur in the first weeks of the programme, this increases the chances of the initial heavy production rates overlapping with a western residual. However, any of neutral, westward or eastward residual character is possible. From Figure 5-11:

- Metocean Scenario A is characterised as variable and roughly **neutral** residual character.
- Metocean Scenario B is characterised as sustained **eastward** residual character.
- Metocean Scenario C is exposed to mixed residual conditions, but is characterised as having **westward** residual character as this prevails toward the beginning of the simulation when the bulk of the production and spillage occurs.

All simulations cover a production period of 40 days, preceded by a 3 day spin-up period for the hydrodynamics and waves prior to the initiation of spillage. The 40 day duration is sufficient to cover the full construction period as well as several days of sediment draw-down following the cessation of works. As the construction scenarios differ in duration, this post-construction drawdown period in the model ranges from 5 days (Scenario 1) to 9.5 days (Scenario 2).

5.9 Spill Rate Estimation

5.9.1 General

Spillage from the respective dredging activities have been quantified using the protocol outlined in Becker et al (2015), van Eekelen et al (2015) and CEDA/IADC (2018). This defines the spill rate in direct proportion to the production rate at which fine material is handled during a given activity within the operation. The spill rates so calculated represent the rate of fine materials released into the far-field of the work area. Near-field details of plume dynamics within the immediate vicinity (typically a few tens to a few hundreds of meters) of the equipment are not described.

5.9.2 TSHD Loading

Spillage from TSHD loading operations occurs as two components. Spillage from the action of the draghead on the seabed has a modest effective spill rate of 1.5% of instantaneous fines production, but is active throughout the loading cycle. TSHD draghead spillage is distributed equally over the bottom three layers (effectively the bottom third of the water column) in the 3D model.

Spillage from TSHD overflow is far larger at 10.5% of instantaneous fines production, but is only active for the latter portion of the loading cycle once the hopper level has reached the top of the overflow pipe. This spill rate corresponds to of 15% of the fines present within the actual overflow stream, but is a smaller percentage in terms of instantaneous fines production (10.5%) to account for the portion of fine materials retained within the hopper (Becker et al, 2015).

Given the large tide range and variable draft of the TSHD, as well as the variable ambient currents which will be encountered over the campaign, the vertical distribution of the overflow plume can be expected to vary widely. We have applied an indicative static vertical distribution of overflow spillage for insertion into the 3D model as shown in Figure 5-12. Figure 5-12 is derived from the semi-empirical relations in de Wit et al (2014) to characterise a TSHD overflow plume at the end of the near-field. The left pane of Figure 5-12 shows the non-dimensional profile as output from the de Wit relations, while the right pane illustrates a sample dimensionalised SSC profile. While the right pane suggests that the concentration approaches zero at the surface, this does not occur within the model as the upper layer is typically 3-4m thick (Table 3-1).

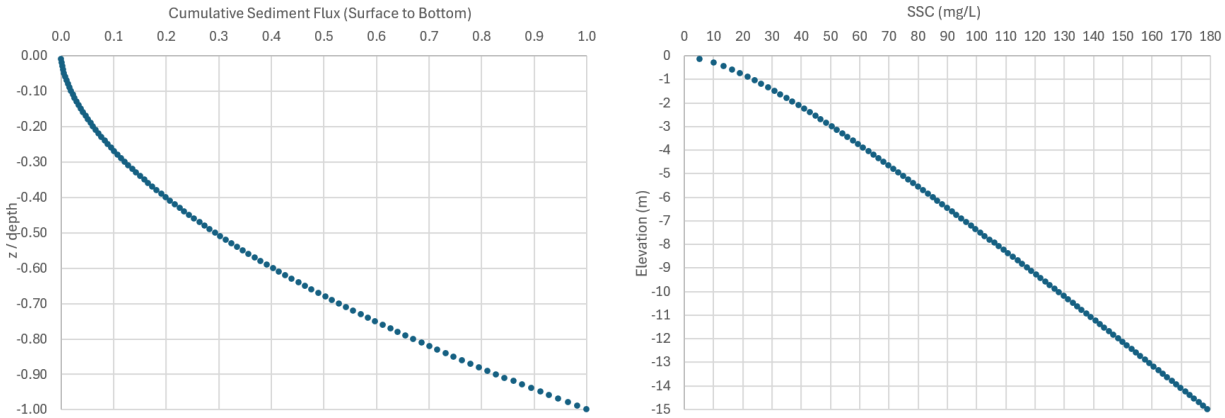

Figure 5-12 Left: Non-dimensional profile of suspended sediment flux applied for the insertion of the TSHD overflow plume into the 3D model, based on relations in de Wit et al (2014). Right: Sample dimensionalised SSC profile, for a situation with depth-averaged SSC = 100 mg/L in 15m water depth.

5.9.3 TSHD Disposal

For the TSHD loading operations, spillage to the far field is described as 8.0% of the fines remaining within the TSHD hopper.

The vertical distribution of material spilled during TSHD dumping operations is described using a parameterised version of the STFATE model (Johnson and Fong, 1995). An emulator of the STFATE model is embedded within MIKE3, which allows for on-the-fly calculation of spillage associated with individual disposal events. The inputs within the STFATE formulation are tuned such that the total spillage of fines from disposal activities aligns with the abovementioned far-field target of 8.0% of hopper fines per Becker et al (2015), CEDA/IADC (2018). As such, the STFATE emulator is effectively utilized only to inform the vertical distribution of the material when inserted into the 3D model. In practice this results in the vast majority of material being inserted near-bed, which is redistributed over the vertical by the balance between settling and dispersion in the far-field.

5.9.4 CSD Pre-cutting

Pre-cutting of material by a mega-CSD will involve crushing of material by the cutterhead, in combination with the discharge of high density slurry back to the seabed immediately (15 - 20m) aft of the cutterhead. Guidance for estimating cutterhead spillage is well documented in the literature. In contrast, guidance for estimating spillage resulting from the immediate discharge of cut material back to the seabed is minimal (WAMSI, 2020).

For the CSD cutterhead, spillage to the far field is described as 5.0% of *in situ* fines, based upon the recommended planning stage estimate in CEDA/IADC (2018).

The TSHD overflow plume is an available but imperfect analogue to the CSD discharge. The CSD discharge occurs closer to the bed, has far higher density than the TSHD overflow, and the CSD discharge incorporates far more coarse material within which fines will be buried upon reaching the bed. Further, spillage mechanisms induced by the mobility of the TSHD (hull interactions, propwash) are not present. While both activities involve a moving reference frame for the discharge point, this is far less of a factor for the CSD discharge. While a loading TSHD typically progresses at ~ 1 m/s, the swing speed of a CSD ladder is normally several times slower (Vlasbom, 2005). For the above reasons, it is reasonable to expect that spillage from the CSD discharge to be less than THSD overflow

in terms of fines percentage. We have described CSD discharge losses as 5% of the fines present in the discharged slurry. A similar estimate was applied in RPS (2023).

CSD spillage from the cutterhead and near-bed slurry discharge are both distributed equally over the bottom three layers of the 3D model, which is effectively the bottom third of the water column.

5.9.5 Spillage Statistics over Project

Table 5-7 presents spill statistics for each dredging activity over the life of the project, as well as the maximum instantaneous spill rate, which are key statistics for appreciation of construction spillage. The largest total spillage is associated with the TSHD overflow, while the largest instantaneous spillage occurs during the relatively brief disposal operations.

The spill rates shown in Table 5-7 are indicators of the magnitude of SSC that results from the respective operations. However, the spatial distribution of the material also plays a key role for the concentrations which ultimately result, both in reality and in the model. While the TSHD spillage is large in terms of total spillage over the project, it is inherently associated with a rapidly moving source, which limits the degree to which far-field concentrations accumulate.

Table 5-7 Estimated spill rates and spill budget of fine material into the far-field for Scenario 1 of the Zone 5 Bypass project. Decimals as presented are for the sake of inter-comparison, and are not intended to imply accuracy.

Construction Activity	Effective Spill Rate of Fines to Far-field	Total Spillage over Project (tons)	Max Instantaneous Spillage (kg/s)
TSHD Draghead	1.5% of fines production	6.300	7.9
TSHD Overflow	15.0% of overflow fines	37,400	55.7
TSHD Bottom Dumping	8.0% of fines in hopper	13,200	187.3
Total	**13.5% of total fines**	**56,900**	**187.3**

Table 5-8 Estimated spill rates and spill budget of fine material into the far-field for Scenario 2 of the Zone 5 Bypass project. Decimals as presented are for the sake of inter-comparison, and are not intended to imply accuracy.

Construction Activity	Effective Spill Rate of Fines to Far-field	Total Spillage over Project (tons)	Max Instantaneous Spillage (kg/s)
CSD Cutterhead	5% of in situ fines	8,500	19.9
CSD Discharge	5% of remaining fines	8,100	18.9
TSHD Draghead	1.5% of remaining fines	6,100	9.9
TSHD Overflow	15.0% of overflow fines	35.400	69.1
TSHD Bottom Dumping	8.0% of fines in hopper	13,200	222.6
Total	**17.0% of total fines***	**71,400**	**222.6**

* calculated as (Total spillage) / (In situ fines in the 800,000 m^3 ultimately removed)

The aggregated spill rate for the full Scenario 1 project is seen to be 13.5% of the total *in situ* fines handled. The maximum instantaneous spill rates for all TSHD operations occur in the first time period (Week 1 for Scenario 1, and Days 1-4 for Scenario 2) when production rates are highest and hopperloads are largest.

The aggregated spill rate for the full Scenario 2 project is seen to be 17.0% of the total *in situ* fines handled. The maximum instantaneous spill rates for all TSHD operations occur in the first time period (Week 1 for Scenario 1, and Days 1-4 for Scenario 2) when production rates are highest and hopperloads are largest.

5.10 Sediment Spill Modelling Details

5.10.1 General

The purpose of the Dredging Spill Model is to describe the transport, deposition and resuspension of material spilled during construction operations. The dredging operations are parameterised in considerable detail in terms of the movements, cycling and spillage associated with the numerous activities as described in previous sections.

The model describes spilled sediment only, and does not simultaneously describe ambient sediment transport processes. The model considers a single bed layer which is initiated as being devoid of sediment. As such, the water column suspended concentrations and bed deposition fields outputted from the model are entirely a product of the Zone 5 Bypass construction operations.

The dredging spill model is constructed within the MIKE3 FM Mud Transport (MT) model, which is a model engine executed seamlessly in combination with to the 3D hydrodynamic model described in Section 3 and the wave model described in Section 4. The MT model is effectively an add-on module which manages the transport of suspended sediment within the domain as well as the interactions between the water column and bed in terms of deposition and resuspension.

The setup of the 3D hydrodynamic model which drives the dredging spill simulations is identical to that described in Section 3. Wave inputs to the spill model are as described in Section 4

5.10.2 Modelled Sediment Fractions

Per Section 5.6, the material to be dredged is described as having a uniform fines (< 75µm) percentage of 29.2%.

The suspended fine material present in the dredge plumes will in practice not consist of single grains, but rather a mix of several contributions (Smith and Friedrichs, 2011) the details of which are material- and activity-specific:

1) Suspended bed aggregates which were not fully broken apart by the dredging process

2) Fully dis-aggregated single grains

3) A flocculated component, formed primarily from 2)

In practice, the degree of dis-aggregation which will occur in the disturbed material (in particular the Coastal Limestone unit) is unknown and will vary by the dredging method. The degree of flocculation that will occur is also unknown *a priori*.

The settling characteristics of the spilled material have been described within the model via two sediment fractions:

- Fraction 1: A finer cohesive fraction indicative of fine silt and clay, described with a generic concentration-dependent settling velocity (Whitehouse et al, 2000) of w_s = 0.001C, where w_s is the settling velocity in mm/s and C is the suspended sediment concentration in kg/m^3. This relation is applied with a lower limit of $w_s \geq$ 0.05 mm/s. When unaffected by flocculation, the 0.05 mm/s rate corresponds to a Stokes diameter near the boundary between fine silt and clay.

- Fraction 2: A coarser cohesive fraction indicative of the silt component is described with a static settling velocity of 0.4 mm/s. This rate corresponds to a Stokes diameter near the boundary between medium and coarse silt.

Fractions 1 and 2 are nominally partitioned at a particle diameter of 10 µm, using the mean of the five PSD curves plotted in bold in Figure 5-6. This yields a split within the fine material which is of 67% Fraction 1 and 33% Fraction 2. These percentages are maintained in the spill sources of fine material inserted into the model from all construction activities.

5.10.3 Deposition and Erosion

The movement of materials between the bed and water column is managed by widely applied formulations based upon exceedances of critical bed shear stresses for erosion and deposition.

The combined wave/current shear stresses are calculated using the Soulsby RMS formulation as described in Whitehouse et al (2000). A uniform bed roughness of k_N = 1 mm has been applied in the bed shear stress calculation

The deposition sink term in the model is described via the usual relation based on Krone (1962):

$$S_D = w_s c_b (1 - \frac{\tau_b}{\tau_{cd}})$$

where: S_D = deposition rate (kg/m^2/s)
w_s = settling velocity (m/s)
c_b = near-bed concentration (kg/m^3)
τ_b = instantaneous bed shear stress (N/m^2)
τ_{cd} = critical shear stress for deposition (N/m^2)

The critical shear stress for deposition has been set to 0.1 N/m^2.

Erosion

The erosion source term in the model is described via the commonly used relation from Partheniades (1965), with erosion in kg/s:

$$S_E = E(\frac{\tau_b}{\tau_{ce}} - 1)^n$$

where: S_E = erosion rate (kg/m^2/s)
E = erosion coefficient (kg/m^2/s)
τ_b = instantaneous bed shear stress (N/m^2)
τ_{ce} = critical shear stress for erosion (N/m^2)
n = power of erosion, set to 1 here

Values for *E* and τ_{ce} vary widely in the literature and are material-specific. The critical shear stress for erosion coefficient has been set to τ_{ce}= 0.3 N/m^2 and applied in combination with an erosion coefficient of *E* = 5 x 10^{-5} kg/m^2/s, Both are commonly used settings within DHI in the absence of site- and material-specific guidance.

5.10.4 Additional MT Model Settings

A deposited dry density of 400 kg/m^3 has been assumed. For the present application, this parameter is of relevance only in terms of defining the thickness of deposited material. Deposited density will in practice be highly variable. Short-term deposits which are dominantly fines may be fluffier than this value, whereas long-term deposits may be denser due to consolidation. The dispersion of suspended sediment within the model is proportional to the eddy viscosity with a horizontal scaling factor of 1 and vertical scaling factor of 0.1. Density effects associated with high sediment concentrations are neglected.

Total suspended sediment concentration (SSC) is output at a timestep of 30min. Other quantities such as deposition fields and results by individual sediment fractions are output hourly.

5.11 Results

The production simulations of the six dredging scenarios was performed in the 3D model. As 3D fields are visually challenging to present in print, they are visualised here in the simplest and most conservative manner. Each time-varying 3D field of SSC have been pre-processed into a 2D field which retains the maximum concentration over the water column at each location at each timestep. In most circumstances, this depth-maximum value occurs in the bottom of the seven model layers. All results presented in the remainder of the report are based upon 2D fields which have been derived as the depth-maximum of the native 3D fields.

Appendix C presents a sequence of ten instantaneous snapshots of depth-maximum SSC fields, advancing at a timestep of half a week (84hrs) for each of the six scenarios.

Appendix D presents statistical fields (median, 95th percentile and max envelopes) derived from the depth-maximum SSC over the dredging campaign for all scenarios.

General Observations – Appendix C

Figures C-1 through C-6 present a chronology ten instantaneous depth-maximum SSC fields over the course of each scenario.

All scenarios feature a reduction in spill rates over the latter weeks of the respective dredging campaigns. Consequently, plumes in the latter weeks are more likely to present as isolated “puffs” which are sheared off by tidal flows.

Notable differences are visible in the first three panes within the figures in Appendix C between Scenarios 1 and 2. During the first 1.5 weeks of operations the TSHD is loading and dumping at its highest rate in Scenario 1 while the CSD is active pre-cutting for Scenario 2. As Scenario 1 leads to far higher spillage in this period, the Scenario 1 plumes are more prominent. For T = t0 + 2.0 through T = t0 + 4.5 weeks, Scenario 2 spillage exceeds that of Scenario 1 and plumes are correspondingly heavier.

Scenarios 1A and 2A (Figures C-1 and C-4) feature variable directionality in residual transport, leading to both the smallest plume extension in space and the highest persistent SSC values around the work areas. These two characteristics are inherently related, as

residual flows tend to stretch the plume extent, which increases the footprint but reduces concentrations in the process. A period of westward residual is present in early Sep 2021 (Figure 5-11), which briefly induces westward setting plumes for T = t0 + 3.5 weeks in Figures C-1 and C-4.

Scenarios 1B and 2B (Figures C-2 and C-5) feature eastward residual character, leading persistently eastward setting plumes from T = t0 + 2.0 weeks onward and a corresponding reduction in concentration within the stretched areas of the plume. The plume becomes sufficiently stretched that its extent becomes non-contiguous as it is sheared by tidal flow, reduced by deposition and dispersed.

Scenarios 1C and 2C (Figures C-3 and C-6) feature westward residual character, leading persistently westward setting plumes over the first three weeks of the simulations. The plumes again become sufficiently stretched that they becomes non-contiguous. For T = t0 + 3.5 through T = t0 + 5.0 weeks, a modest eastward residual is present and the plume reverses its extent.

General Observations – Appendix D

The 95th percentile and max SSC fields shown in Figures D-1 through D-6 clearly demonstrate the degree to which the plume excursion from the immediate work area follows the principal axis of tidal motion as indicated in Figure 3-4 from both measurements and model.

The max SSC fields in Figures D-1 through D-6 also illustrate the degree to which the prevailing residual currents affect the extent of the sediment plumes. The simulations exhibiting neutral residual character (Scenarios 1A, 2A) feature the smallest longshore footprints. In contrast, the simulations with eastward residual character (Scenarios 1B, 2B) lead to 1 mg/L contours extending ~50km NE of the Zone 5 Channel. Simulations with westward residual character (Scenarios 1C, 2C) lead to 1 mg/L contours extending ~30km NE of the Zone 5 Channel. The smaller westward vs. eastward extent is largely a result of the season being simulated, during which the predominant residual direction tends to be transitioning from westward to eastward. As seen in Figure 5-11, the duration during which the residual sets westward in the C hindcast period is relatively brief vs. the more persistent eastward residual present in the B hindcast period.

The “speckled” character of the max SSC fields around SG7C in Figures D-1 through D-6 is due to highly mobile, very localised high resolution disposal plumes being resolved at a timestep of 30 min.

Figures D-1 through D-6 also show that the maximum SSC occurring within the TSHD loading footprint is between 200 and 300 mg/L, which for both Scenarios 1 and 2 tends to occur in the first week of TSHD operations when spill rates are highest. For Scenario 2 (Figure D-4 through D-6), the CSD operations lead to localised suspended concentrations within the work area in excess of 1000 mg/L during weak current conditions, due to the slow-moving nature of this activity.

Localised max SSC within SG7C is somewhat higher, in excess of 1000 mg/L due to the short duration of the dump events and its insertion into a fixed location. Outside the delineated disposal area, the maximum SSC is comparable to that within the TSHD loading footprint. Unlike the TSHD work area, the high concentrations within the disposal site are very short-lived and only occur once within each disposal cell. Consequently, the disposal area is visually prominent within the maximum SSC fields but much less so within the 95% or median SSC fields.

Deposition Fields

Figure 5-13 and Figure 5-14 present the deposited bed thickness at the end of active construction operations for Scenario 1 and Scenario 2, respectively, assuming a deposited dry density of 400 kg/m^3.

For Scenario 1, deposition adjacent to the TSHD loading area is on the order 2-3mm for all of Scenarios 1A, 1B and 1C, approaching 1cm within the dredged footprint itself. However, in the latter case most of the material depositing within the work area will have been re-dredged so the quantities are not meaningful. Scenario 1A has the largest region of 2-3mm deposition of the three simulations, as less material is transported out of the work area and more remains to locally deposit.

For Scenario 2, deposition again reflects the staged CSD/TSHD methodology, with distinct deposition regions originating from the respective CSD pre-cutting and TSHD loading operations. Owing to the slow-moving nature of the CSD, Scenario 2 spillage is locally concentrated in the southern portion of the work area. In the northern portion of the work area plied only by the TSHD, deposition adjacent to the Zone 5 channel is on the order of 5-8mm. In the southern portion worked by both the CSD and TSHD, deposition is an order of magnitude larger. Localised areas with deposition in excess of 10cm exist within the channel, but these are unrealistic as CSD spillage will have been later dredged by the TSHD.

Deposition fields for both Scenarios 1 and 2 show apparent holes and sharp features with no net deposition. These indicate reefs or other shallow areas over which bed shear stress is elevated by wave and/or tidal action, thereby preventing deposition and/or inducing erosion.

Throughout the model, deposited material originates from one of the two fine fractions spilled into the water column during construction operations. An exception to this lies within SG7C, as a portion of the fine material is placed directly onto the seabed by the STFATE emulator, along with a sand component. The former ensures that there is fine material within the disposal area available for resuspension by waves and currents as the simulation progresses. Modelled deposition thickness within the delineated SG7C should not be interpreted in the same manner as the rest of the domain, and there is no regulatory requirement to quantify deposition there in the context of dredging spillage.

It is again emphasised that the model applied here inherently describes far-field processes, as is typical in the context of dredging project permitting. Model spill sources are estimated as material prone to reaching the far-field. Concentrations and deposition rates in the immediate vicinity of the spill sources will both exceed those shown in the model. This is of particular relevance to potential localised sedimentation in the existing main channel, which will need to be monitored during adjacent Zone 5 dredging activities to ensure continued safe navigation.

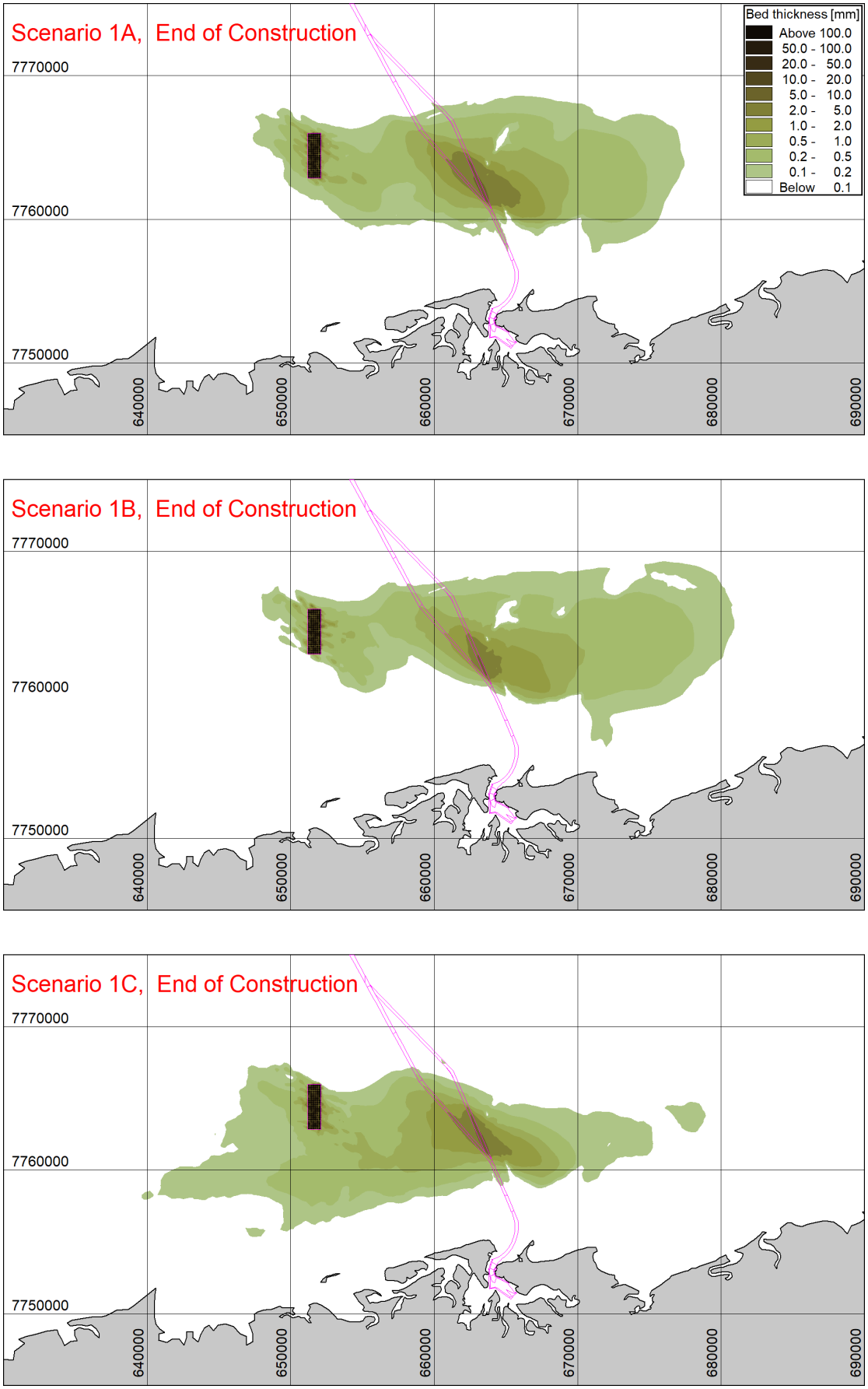

Figure 5-13 Net deposition fields at the completion of dredging operations for Scenario 1.

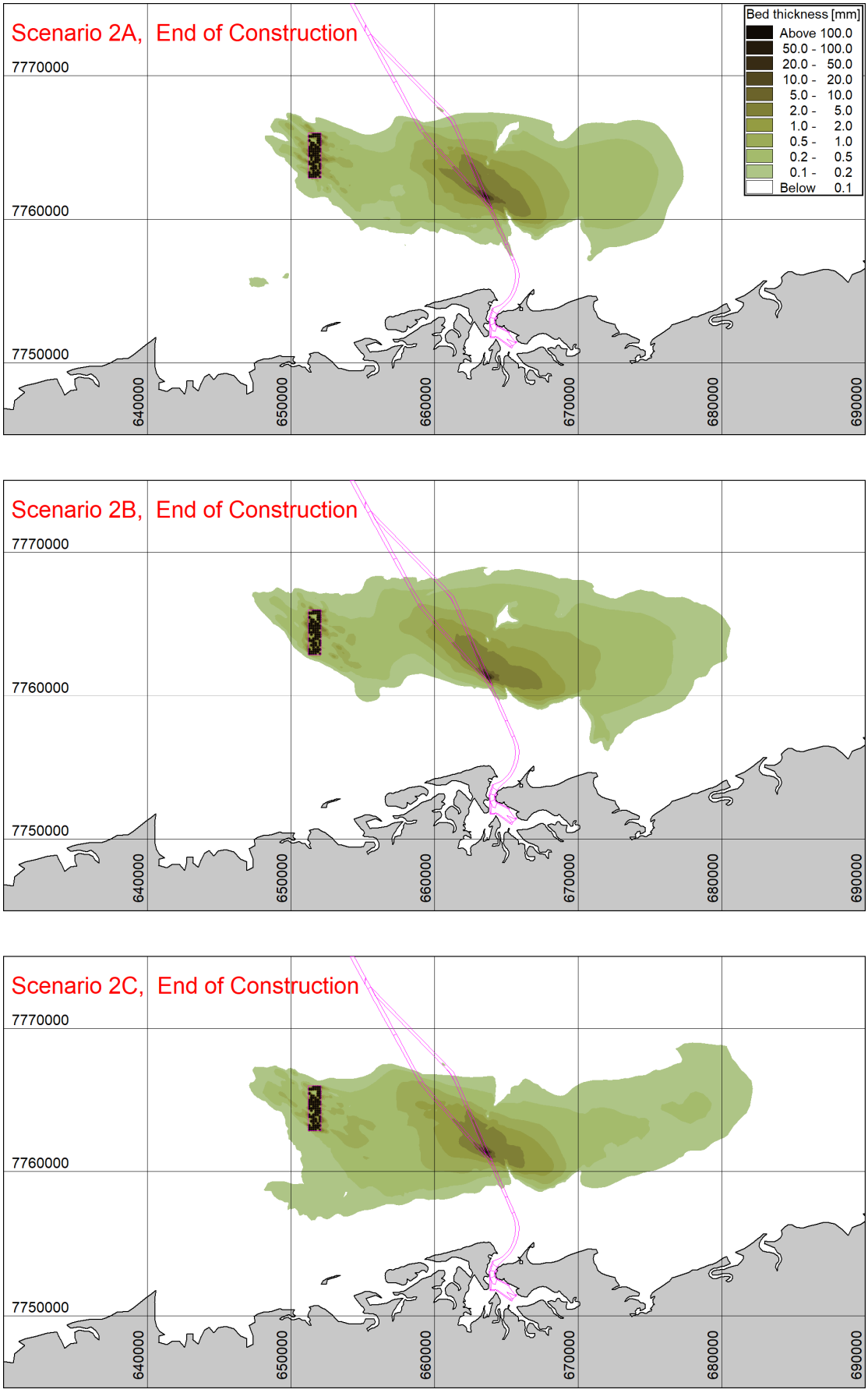

Figure 5-14 Net deposition fields at the completion of dredging operations for Scenario 2.

Regulatory Guidance

Supplementary post-processing of dredge spill results have been performed under direction from MScience in support of permitting efforts. The potential impacts of suspended spillage material from the construction operations has been assessed against the running mean criteria shown in Table 5-9 (WAMSI, 2019). Interrogation of the model results against the impact criteria includes the following steps:

1) The conversion of instantaneous 3D fields of total SSC into instantaneous 2D fields of total SSC, where the maximum concentration over the water column is retained at each location at each timestep.

2) The calculation of the running mean total SSC from the fields generated in 1), with calculation windows of 1, 3, 7, 14 and 28 days. This calculation includes the full 40-day simulation period for all scenarios.

3) Calculating the maximum envelope for each of the calculation windows and each scenario from the fields generated in 2).

4) For each scenario, plot the fields generated in 3) against the Possible and Probable Effect thresholds as indicated in Table 5-9 for each of the five running mean windows.

Table 5-9 Impact criteria, based upon running mean SSC fields (WAMSI, 2019). Applied here using depth-maximum SSC at each output timestep from the 3D model.

Window of Running Mean (days)	Possible Effect Threshold (mg/L)	Probable Effect Threshold (mg/L)
1	27.9	58.3
3	19.4	35.7
7	14.7	24.5
14	11.7	18.0
28	9.3	13.2

Results of the above analysis are shown in Figure 5-15 and Figure 5-16 for Scenarios 1 and 2, respectively. Shapefiles describing the Potential and Probable Effect mapping in Figure 5-15 and Figure 5-16 will be provided to MScience for use in subsequent reporting.

For Scenario 1 (Figure 5-15), the largest footprints for both the Possible and Probable Effect criteria are seen to occur for Scenario 1A, specifically for the 14-day running mean. Both the Possible and Probable Effect footprints are primarily arranged around the work area for the Zone 5 Channel, surrounded by an ellipse with the major axis aligned with the predominant tidal currents. The Possible Effect footprint is roughly 6km x 3km, while the Probably Effect footprint is roughly 4km x 2km. Secondary footprints are present within and immediately adjacent to SG7C. Dumping events feature localized and brief instances of high concentrations, which appear primarily within the shorter running mean windows.

For Scenario 2 (Figure 5-16), the footprints are indicative of the combined CSD and TSHD activities with the CSD work area showing a distinct signature to the south of that generated by the TSHD. Footprints from Scenario 2 are also generally larger than Scenario 1, which reflects both the larger total spillage and the shorter duration associated with Scenario 2. The largest Possible Effect criteria is again seen to occur for the 14-day running mean window, but here for Scenario 2B (Eastward residual current character).

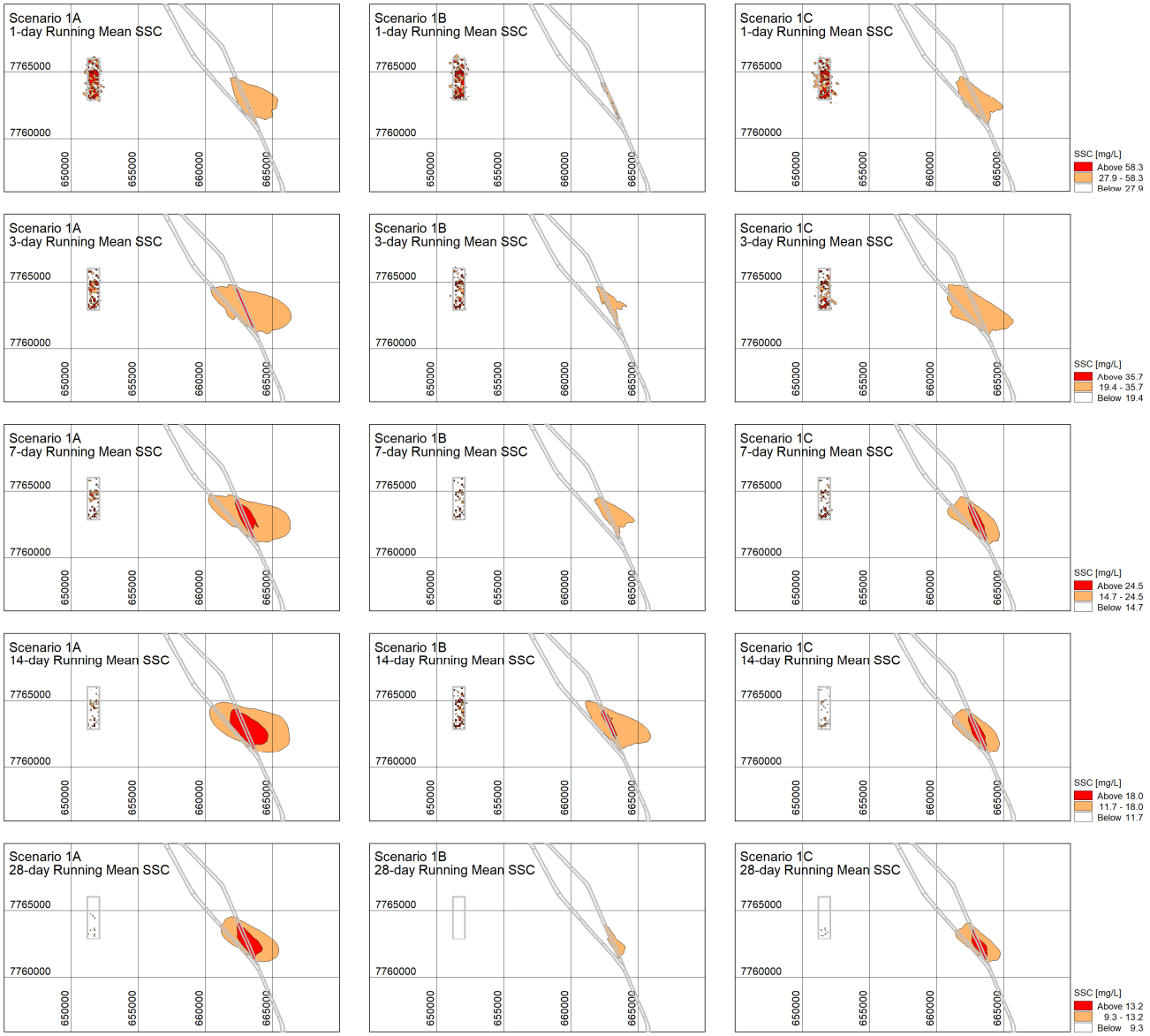

Figure 5-15 Scenario 1 impact mapping based upon running mean SSC fields, using the limits shown in Table 5-9. Orange = Possible Impact, Red = Probable Impact.

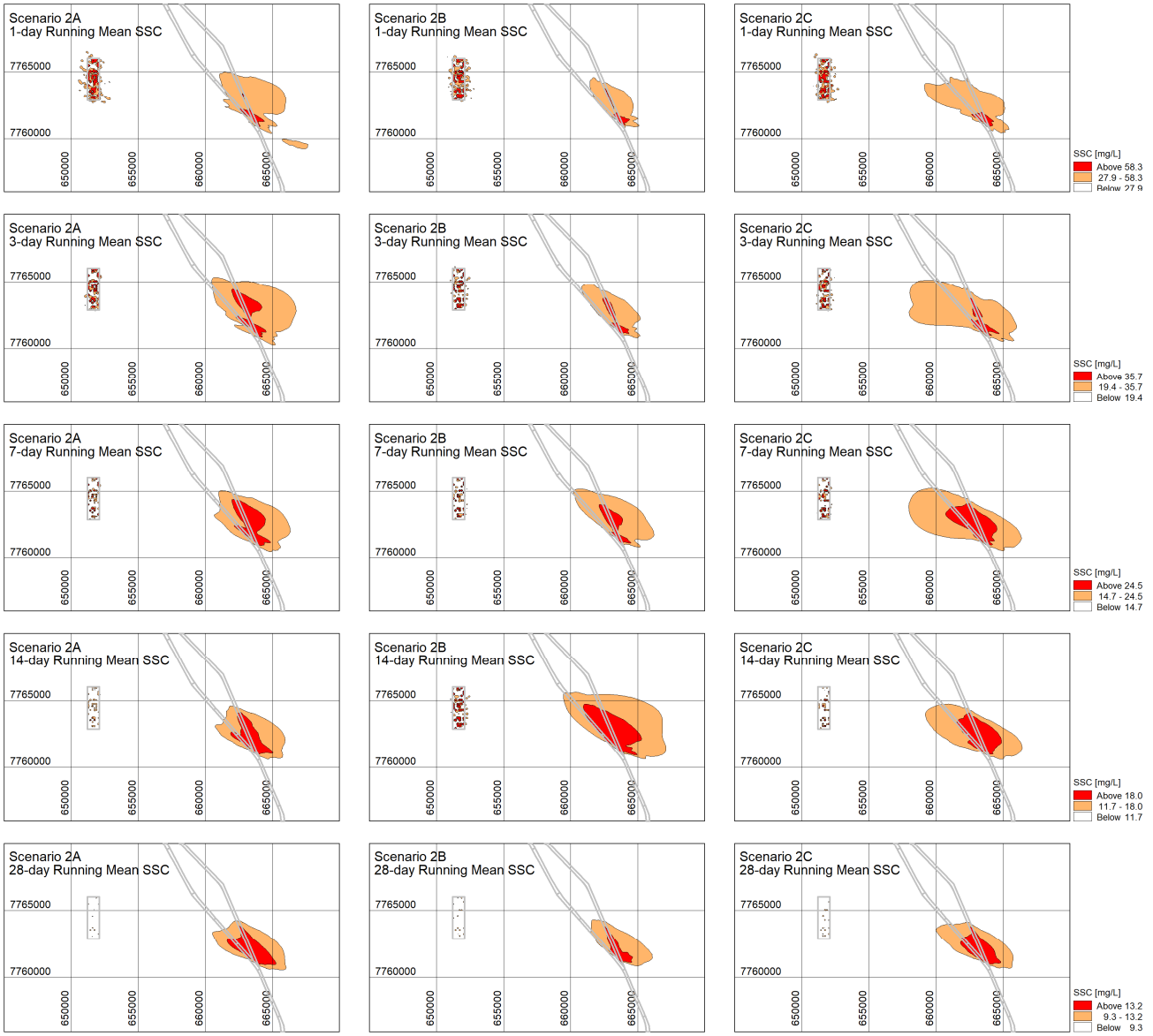

Figure 5-16 Scenario 2 impact mapping based upon running mean SSC fields, using the limits shown in Table 5-9. Orange = Possible Impact, Red = Probable Impact

6 References

AET (2016): “Fatal Accident on Board *Juan Sebastián de Elcano* on 3 November 2014”, Administration des enquêtes techniques (AET), Report N° AET/TM-2016/01, Luxembourg, 22 December 2016.

AHO (2025): AusTides v.2.1.1, tidal data version 2025.

Aviso (2014): https://www.aviso.altimetry.fr/en/data/products/auxiliary-products/global-tide-fes/description-fes2014.html (accessed 2024).

BHP (2011): Outer Harbour PER Appendix B4 (Quantum Project: Modelling of the Dredge and Disposal Programme).

Becker, J.B., E. van Eekelen, J. van Wiechen, W. de Lange, T. Damsma, T. Smolders and M. van Koningsveld (2015): “Estimating source terms for far-field dredge plume modelling”, Journal of Environmental Management, 149, 282-293.

CEDA/IADC (2018): “Dredging for Sustainable Infrastructure”, CEDA/IADC, The Hague.

Cheng, Y. and O.B. Andersen (2011): “Multimission empirical ocean tide modeling for shallow waters and polar seas”, JGR, Vol. 116, C11001.

de Wit, L., A.M. Talmon and C. van Rhee (2014): “3D CFD simulations of trailing suction hopper dredger plume mixing: A parameter study of near-field conditions influencing the suspended sediment source flux”, *Marine Pollution Bulletin*, 88 (2014) 47–61.

DHI (2013): “Browse LNG Precinct, Numerical Modelling in Support of Dredging Spoil Disposal Management Plan (DSDMP)”, Report prepared for Woodside Energy Ltd, Rev. 0, 19 April 2013.

DoT (2025): Gridded 1m LIDAR and multibeam surveys in vicinity of Spoilbank and Spoilbank Marina: HD20190512_Laser.bag, HD20190512_Mean, HD20250401_Mean.bag. Downloaded 21 May 2025.

Eliot, M. and C. Pattiaratchi (2010): “Remote forcing of water levels by tropical cyclones in southwest Australia”, *Continental Shelf Research,* 30 (2010), 1549–1561.

Foreman, M.G.G. (1977): “Manual for Tidal Heights Analysis and Prediction”, Pacific Marine Science Report 77-10, Institute of Ocean Sciences, Dept. of Fisheries and Oceans (Canada).

GA (2020): North West Shelf Bathymetry 2020 30m, Geosciences Australia, http://pid.geoscience.gov.au/dataset/ga/144600.

GA (2024): Geosciences Australia AusBathyTopo (Australia) 250m 2024. https://pid.geoscience.gov.au/dataset/ga/150050.

GEBCO (2024): GEBCO 2024 Grid (doi:10.5285/1c44ce99-0a0d-5f4f-e063-7086abc0ea0f), GEBCO Compilation Group.

GHD (2022): “Channel Entry Geotechnical Investigation, Factual Geotechnical Report”, Report prepared for PPA, 21 March 2022.

JdN (2025): “*Juan Sebastián de Elcano*”, Jan de Nul vessel factsheet, https://www.jandenul.com/fleet/trailing-suction-hopper-dredgers.

JdN (2025b): "*J.F.J. de Nul*", vessel factsheet, https://www.jandenul.com/fleet/cutter-suction-dredgers

Jeppesen (2024): C-MAP Global Chart Database.

Johnson, B.H. and Fong, M.T. (1995): "Development and Verification of Numerical Models for Predicting the Initial Fate of Dredged Material Disposed in Open Water. Report 2. Theoretical Developments and Verification Results", Technical Report DRP-93-1 USACE Waterways Experiment Station, Vicksburg, MS.

Krone, R.B. (1962): "Flume Studies of the Transport of Sediment in Estuarial Processes" Hydraulic Engineering Laboratory and Sanitary Engineering Research Laboratory, Univ. of California, Berkeley, California.

MScience (2019): "CROP 2 2019 Phase 2 Water Quality Monitoring", Report prepared for Pilbara Ports Authority, 18 October 2019.

MScience (2018): "CROP 2 2018 (TSHD) Water Quality Monitoring", Report prepared for Pilbara Ports Authority, 26 November 2018.

Partheniades, E. (1965). "Erosion and deposition of cohesive soils", Proc. Am. Soc. Civ. Engrs, 91 (HYI) 105-139.

Pilbara Ports (2025): "Port of Port Hedland Handbook", rev13, 20 February 2025.

Pilbara Ports (2024): "Port Development Guidelines, Appendix C: Hydrographic Survey Technical Standards", rev12.0, 05 July 2024.

Pugh, D.T. (1987): *Tides, Surges and Mean Sea Level*, John Wiley & Sons.

RPS (2023): "Santos Barossa DPD Studies, Sediment Dispersion Modelling", Rev. 2, 23 Feb 2023.

Smith. G., E. Yesilnacar, J. Jiang and C. Taylor (2015): "Marine Habitat Mapping Incorporating Both Derivatives of LiDAR Data and Hydrodynamic Conditions", J. Mar. Sci. Eng. 2015, 3, 492-508.

Schlack, F. and N. Hewitt (2015): "Accurate Determination of Chart Depths by Establishing a Hydroid as a Port's true Chart Datum", 22nd Australasian Coasts & Ports Conference.

Smith, S.J. and C.T. Friedrichs (2011): "Size and settling velocities of cohesive flocs and suspended sediment aggregates in a trailing suction hopper dredge plume", *Continental Shelf Research*, 31, S50-S63.

Su, C.-H. et al.(2023): "Preliminary assessment of local moderate resolution atmospheric reanalysis for Australia," in "Bureau Research Report – BRR084," Bureau of Meteorology, Australia, 2023.

van Eekelen, E., J. van Wiechen and M. van Koningsveld (2015): "Practical use of dredge plume source terms", CEDA Dredging Days 2015.

Vlasbom, W.J. (2005): "Dredging Equipment and Technology, Chapter 3: Cutter Suction Dredger", Delft University of Technology Lecture notes, Central Dredging Association (CEDA).

WAMSI (2020): "Guideline on dredge plume modelling for environmental impact assessment", WAMSI Dredging Science Node Themes 2/3, Western Australian Marine Science Institution, November 2020.

WAMSI (2019): “Synthesis Report: Defining thresholds and indicators of coral response to dredging-related pressures”, WAMSI Dredging Science Node Theme 4, Western Australian Marine Science Institution, March 2019.

Whitehouse, R., R. Soulsby, W. Roberts and H. Mitchener (2000): *Dynamics of Estuarine Muds*, Thomas Telford Publishing.

Worley (2025): “Pilbara Ports Authority, Zone 5 Bypass Channel Geotechnical Report”, Report prepared for Pilbara Ports, Rev B, Document no: 311012-02609-GEO-RPT-00001, 04 December 2025.

APPENDIX A

Hydrodynamic Model Validation

A Hydrodynamic Model Validation

This appendix contains supplementary graphics and statistics related to validation of the 2D and 3D hydrodynamic models. Both have been validated against long-term measured water levels and currents within the extensive network of metocean instrumentation maintained by Pilbara Ports (Figure 2-1).

Figures are presented in pairs, with each pair representing validation from 2021 and 2022 for a given combination of measurement station and measured quantity. Results from 2021 are in oddly numbered figure, 2022 evenly numbered.

Figures A-1 through A-8 present composite graphics of water level time series plots and performance statistics for year-long simulations of the 2D Regional Hydrodynamic Model for stations C1, E3, B17 and B31.

Figures A-9 through A-16 present composite graphics of water level time series plots and performance statistics within the seasonal window of 15 Aug – 31 Oct from the 3D Local Hydrodynamic Model for the same stations C1, E3, B17 and B31.

Figures A-17 through A-22 present composite graphics of current speed time series plots and performance statistics within the seasonal window of 15 Aug – 31 Oct from the 3D Local Hydrodynamic Model for the AWACs at stations E3 (depth-averaged), B16 (depth-averaged) and B31 (bottom AWAC bin, which is the only data available for these periods).

Figures A-23 through A-28 present time series comparisons of (u,v) current velocity components within the seasonal window of 15 Aug – 31 Oct from the 3D Local Hydrodynamic Model for the AWACs at stations E3 (depth-averaged), B16 (depth-averaged) and B31 (bottom AWAC bin, which is the only data available for these periods).

Figures A-29 and A-30 present scatter plots of (u,v) current velocity components within the seasonal window of 15 Aug – 31 Oct from the 3D Local Hydrodynamic Model for the AWACs at stations E3 (depth-averaged), B16 (depth-averaged) and B31 (bottom AWAC bin, which is the only data available for these periods).

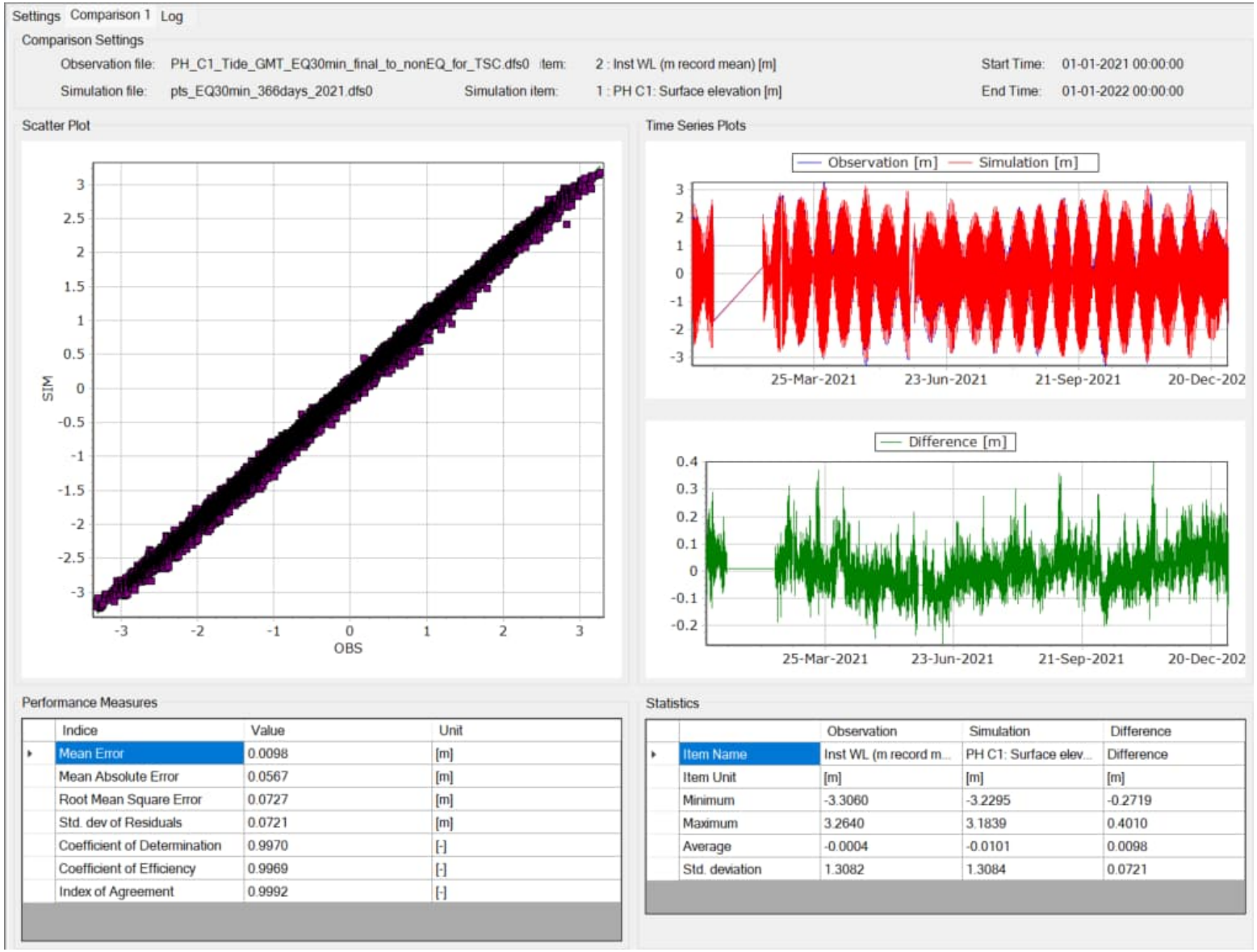

Figure A-1 Performance statistics for 2D Regional Hydrodynamic model vs. water level measurements. Station C1, year 2021.

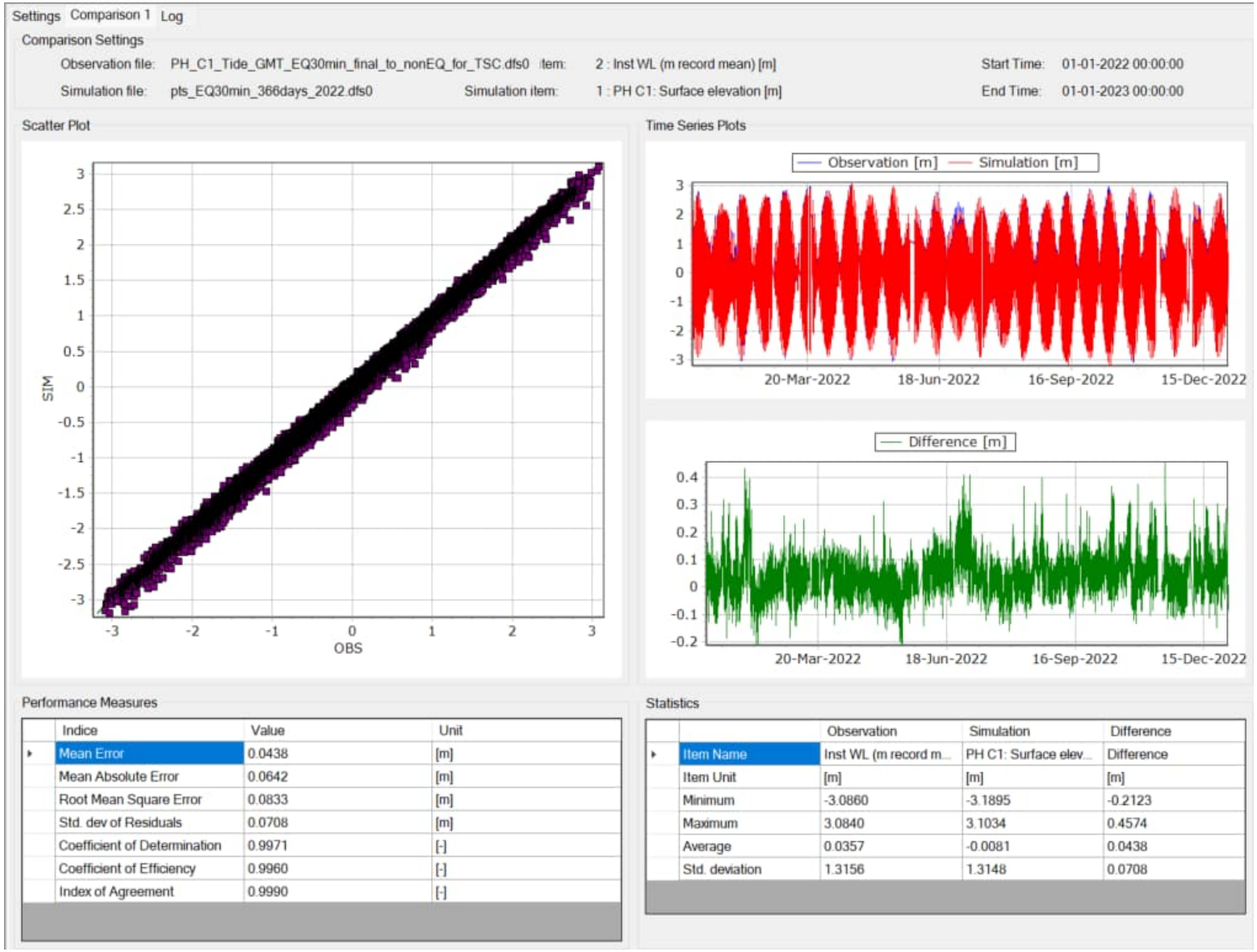

Figure A-2 Performance statistics for 2D Regional Hydrodynamic model vs. water level measurements. Station C1, year 2022.

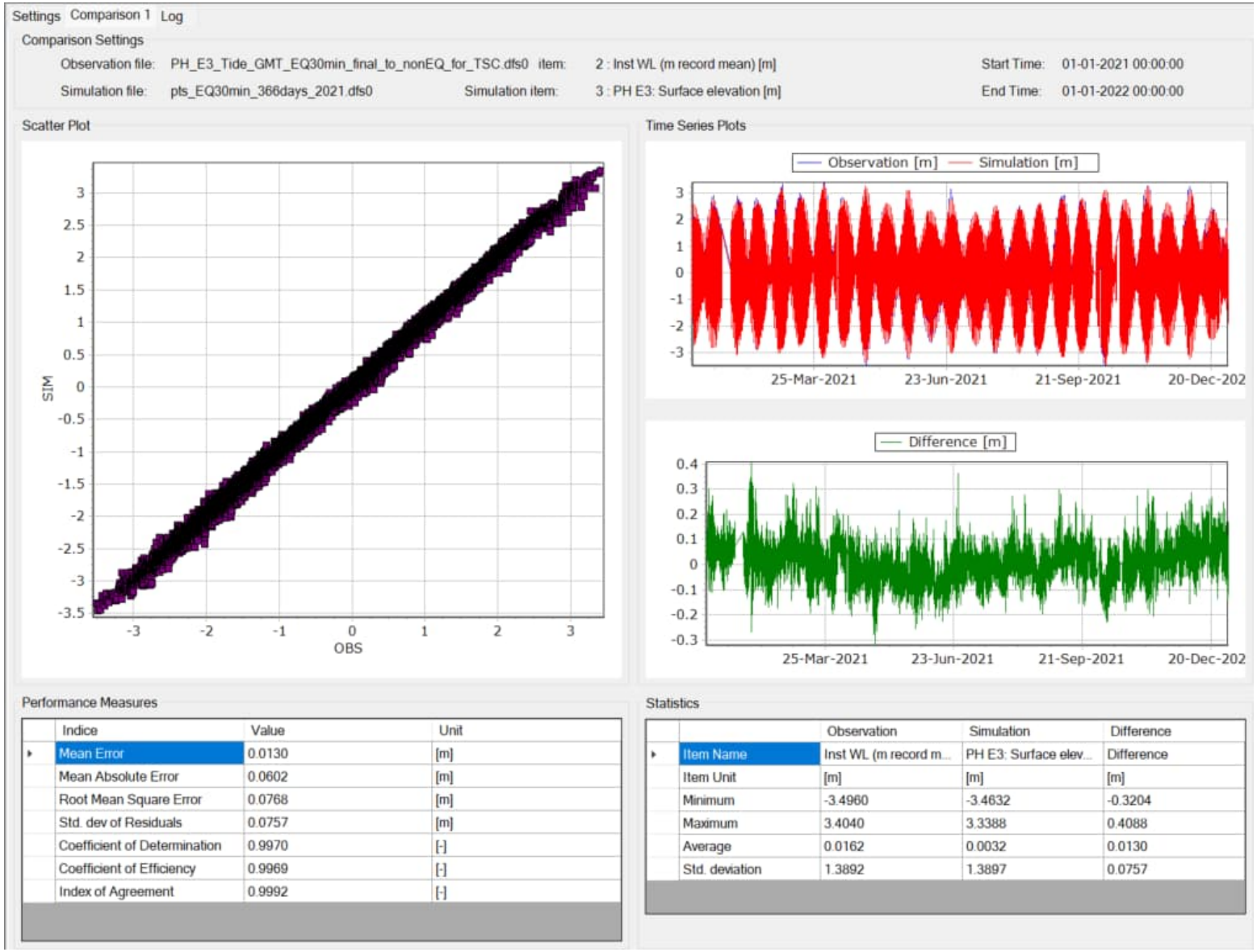

Figure A-3 Performance statistics for 2D Regional Hydrodynamic model vs. water level measurements. Station E3, year 2021.

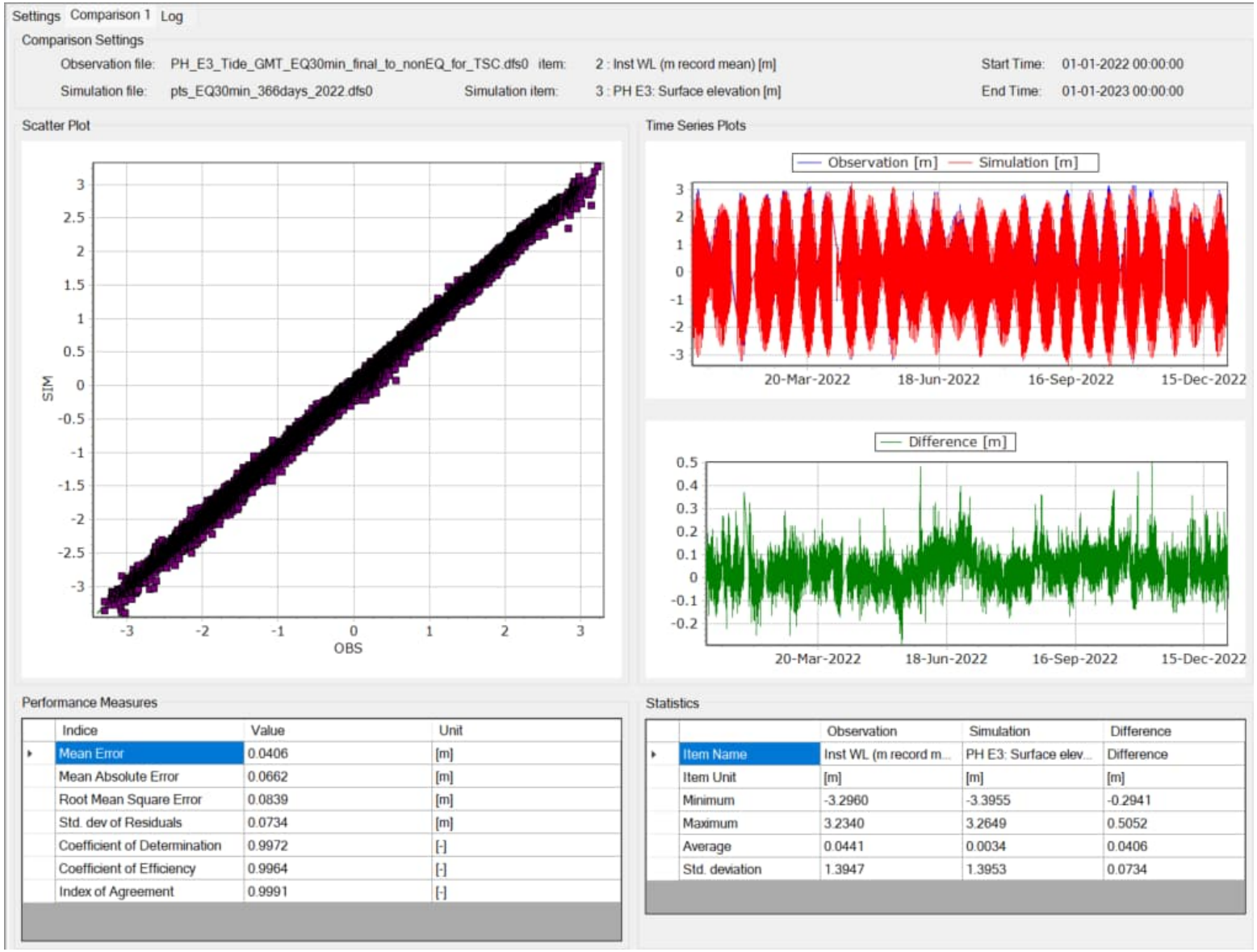

Figure A-4 Performance statistics for 2D Regional Hydrodynamic model vs. water level measurements. Station E3, year 2022.

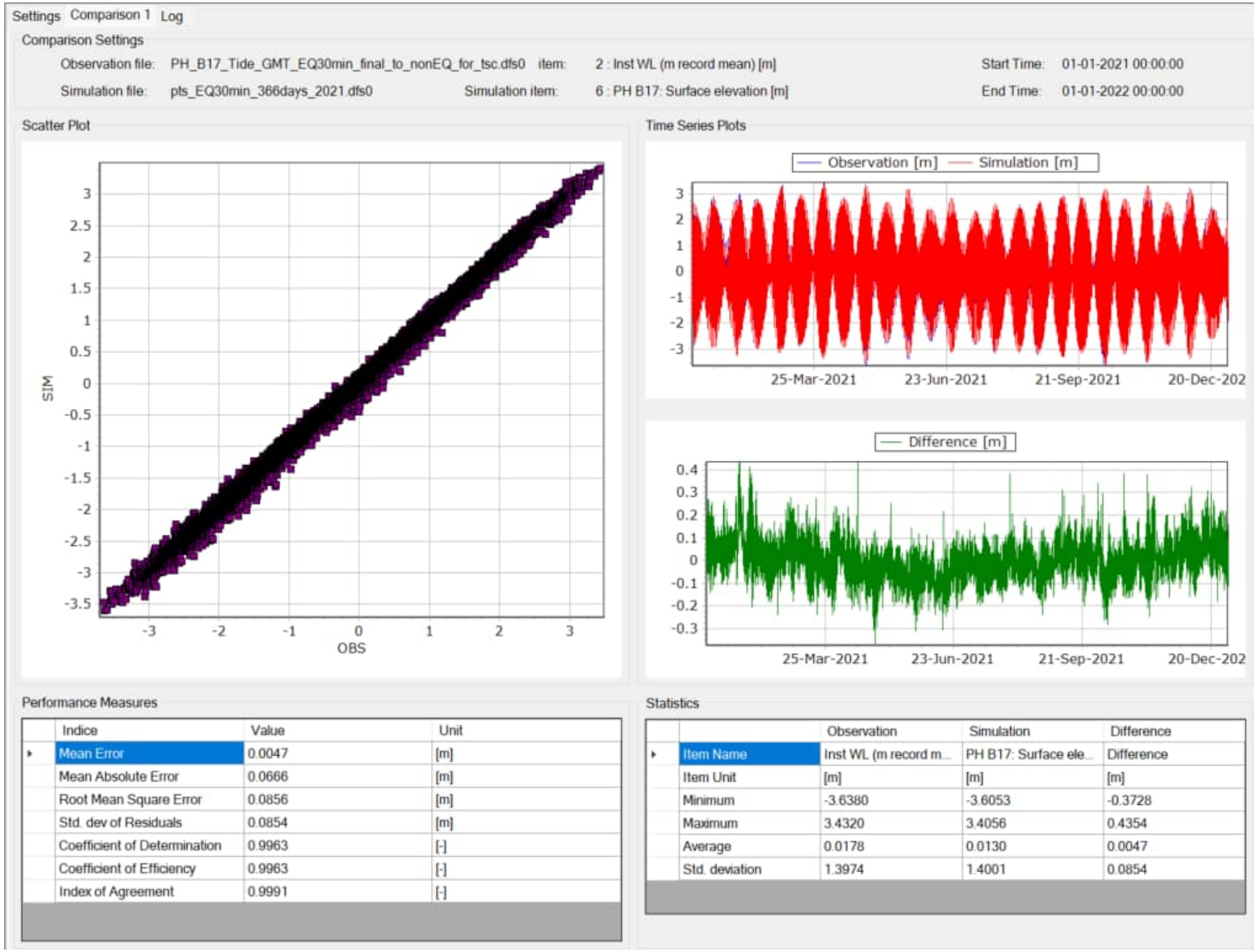

Figure A-5 Performance statistics for 2D Regional Hydrodynamic model vs. water level measurements. Station B17, year 2021.

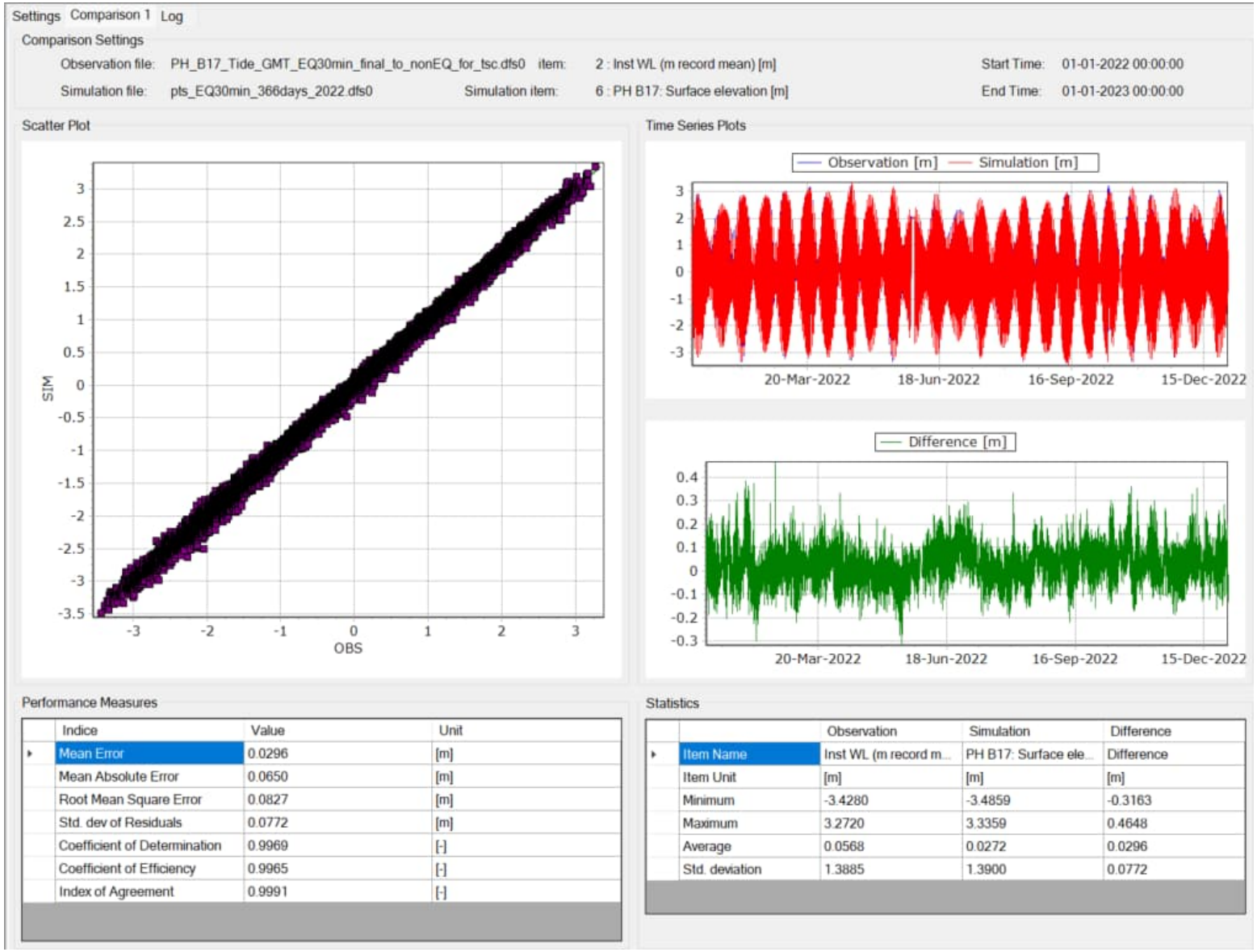

Figure A-6 Performance statistics for 2D Regional Hydrodynamic model vs. water level measurements. Station B17, year 2022.

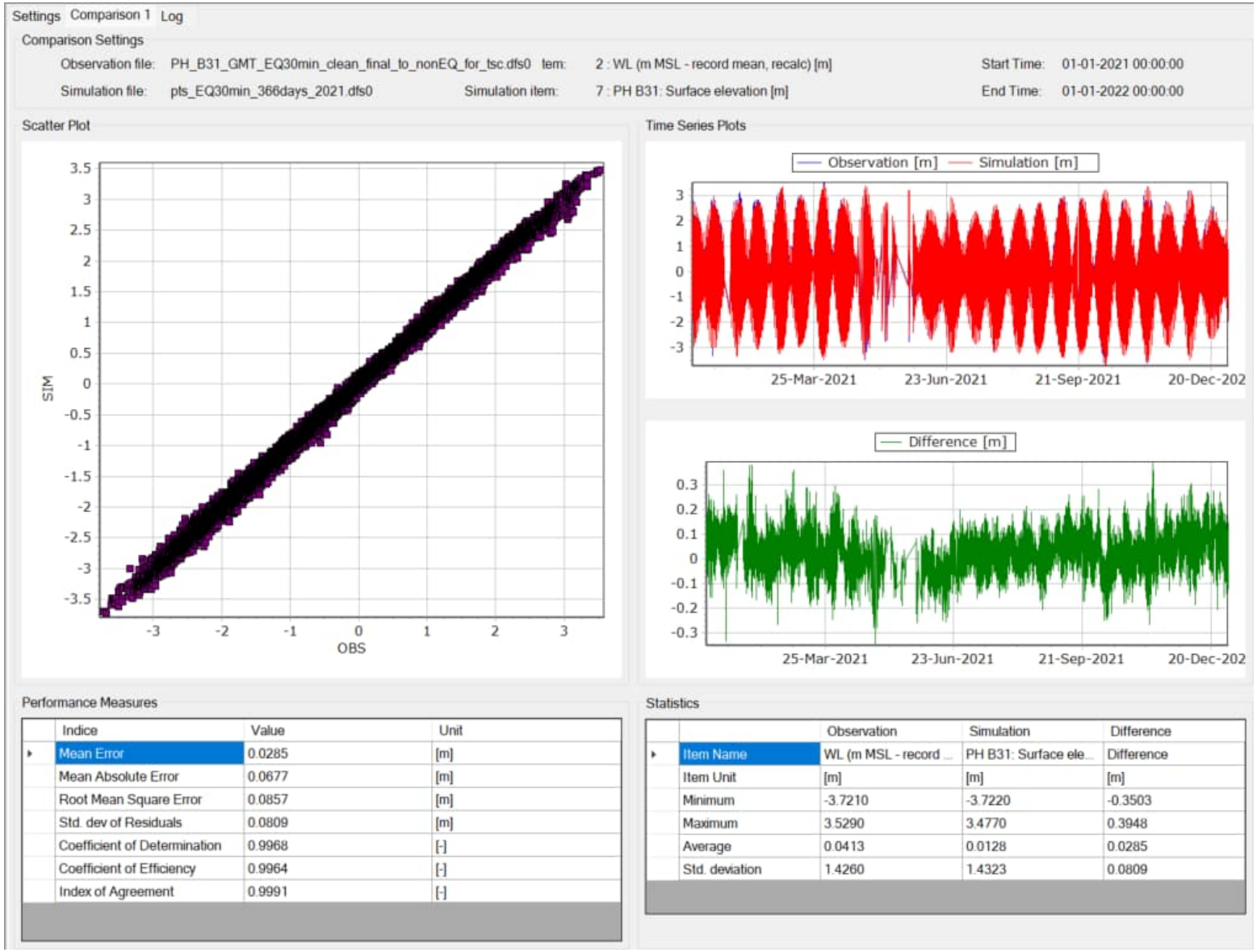

Figure A-7 Performance statistics for 2D Regional Hydrodynamic model vs. water level measurements. Station B31, year 2021.

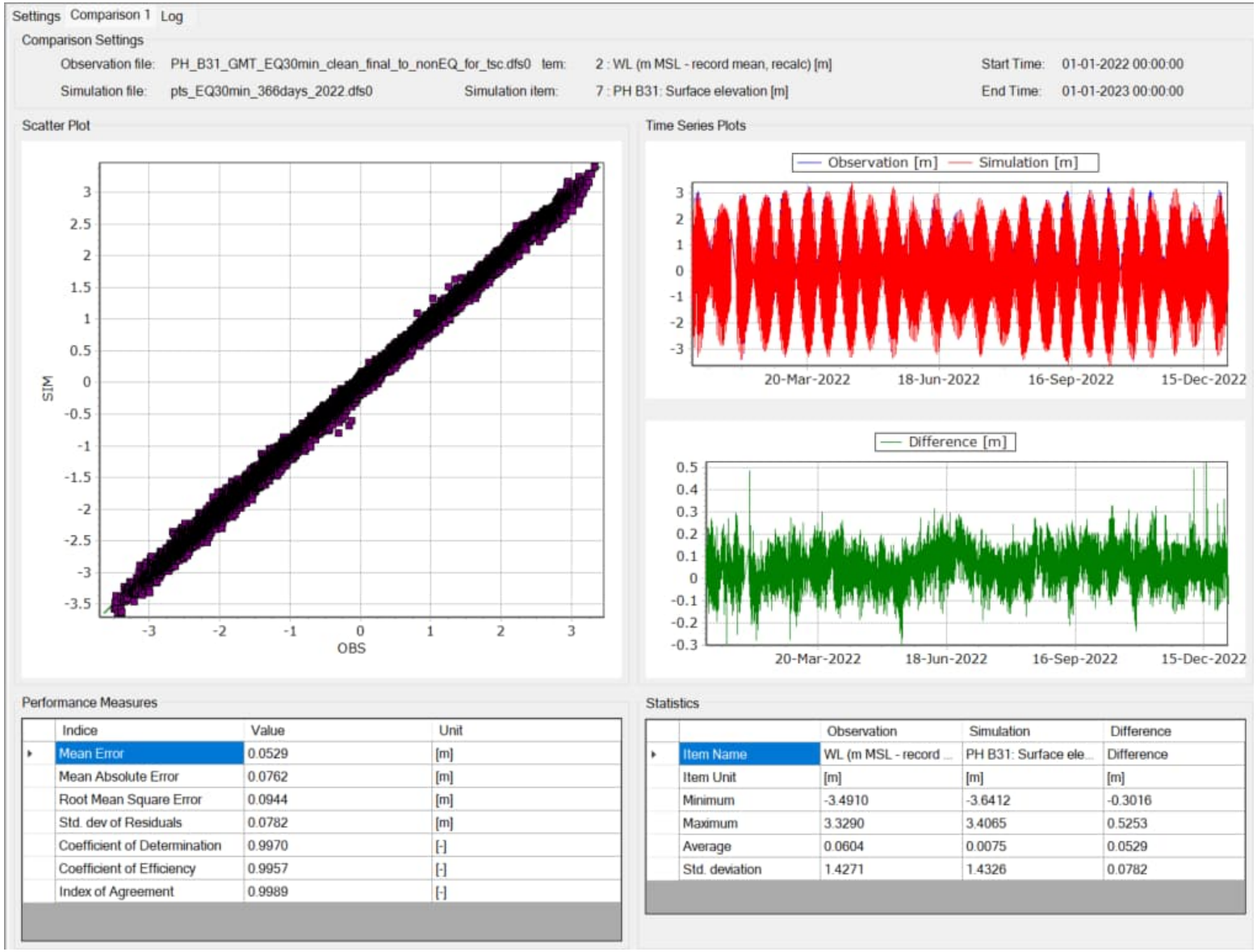

Figure A-8 Performance statistics for 2D Regional Hydrodynamic model vs. water level measurements. Station B31, year 2022.

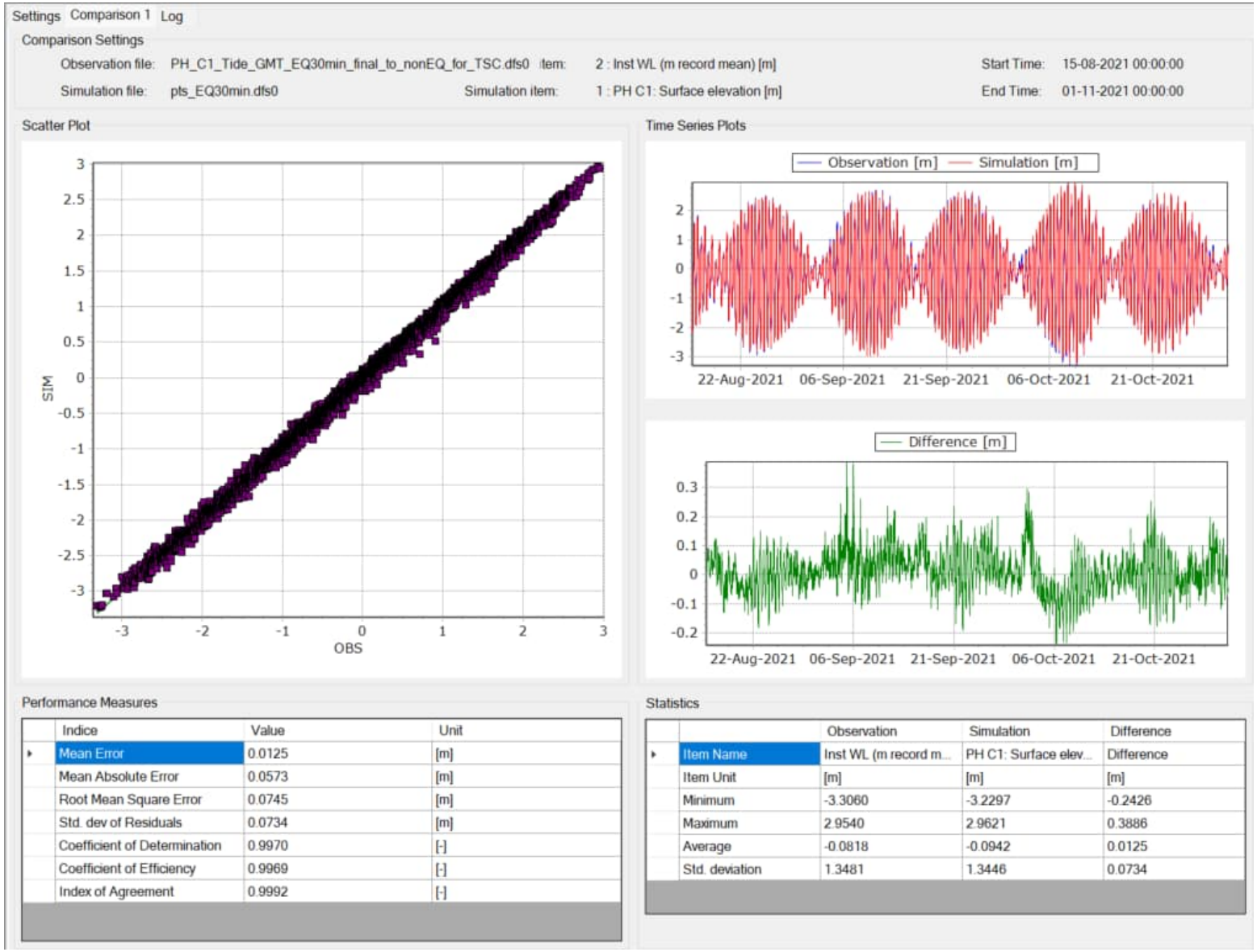

Indice	Value	Unit
Mean Error	0.0125	[m]
Mean Absolute Error	0.0573	[m]
Root Mean Square Error	0.0745	[m]
Std. dev of Residuals	0.0734	[m]
Coefficient of Determination	0.9970	[-]
Coefficient of Efficiency	0.9969	[-]
Index of Agreement	0.9992	[-]

	Observation	Simulation	Difference
Item Name	Inst WL (m record m...	PH C1: Surface elev...	Difference
Item Unit	[m]	[m]	[m]
Minimum	-3.3060	-3.2297	-0.2426
Maximum	2.9540	2.9621	0.3886
Average	-0.0818	-0.0942	0.0125
Std. deviation	1.3481	1.3446	0.0734

Figure A-9 Performance statistics for 3D Local Hydrodynamic model vs. water level measurements. Station C1, 15Aug – 31 Oct 2021.

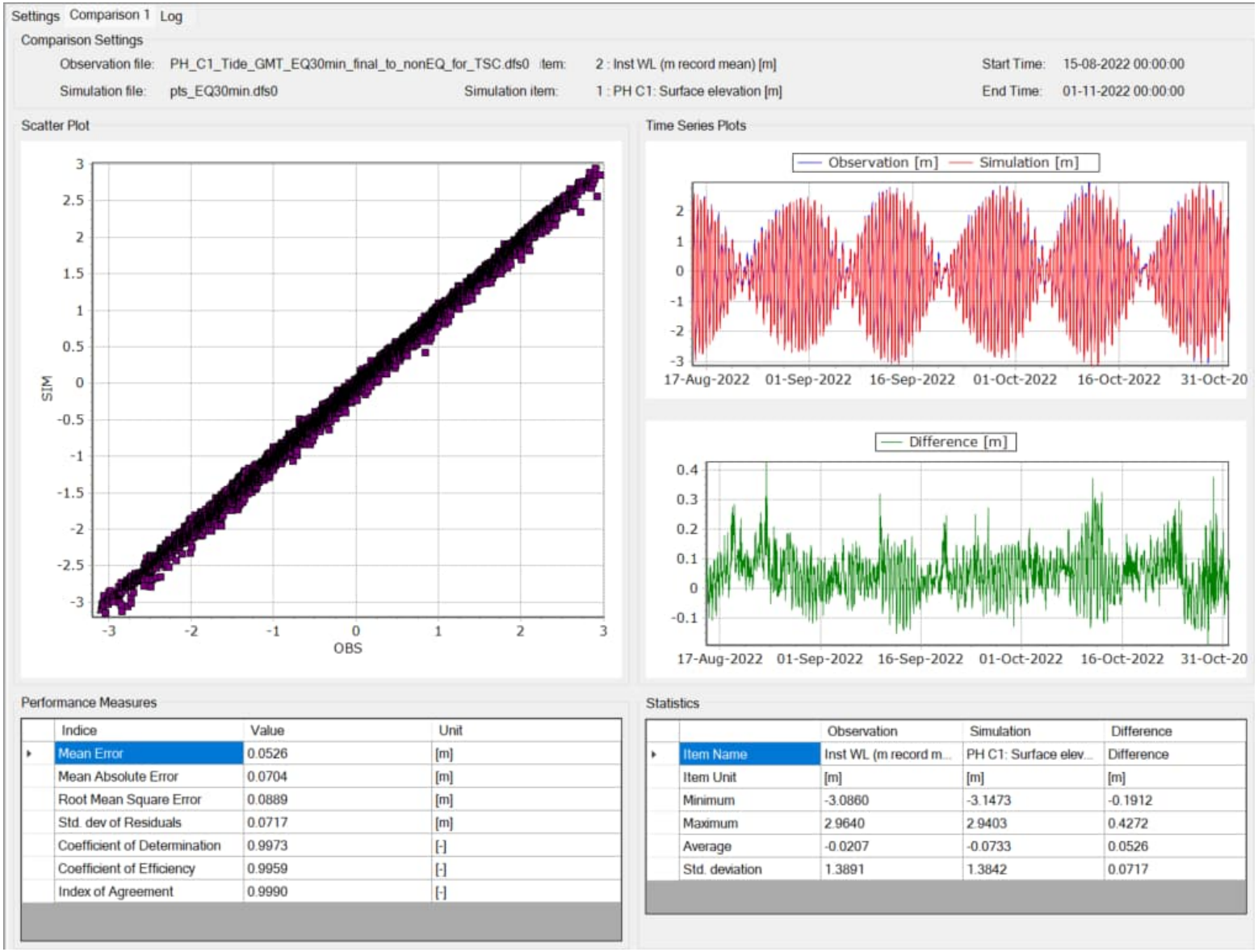

Figure A-10 Performance statistics for 3D Local Hydrodynamic model vs. water level measurements. Station C1, 15Aug – 31 Oct 2022.

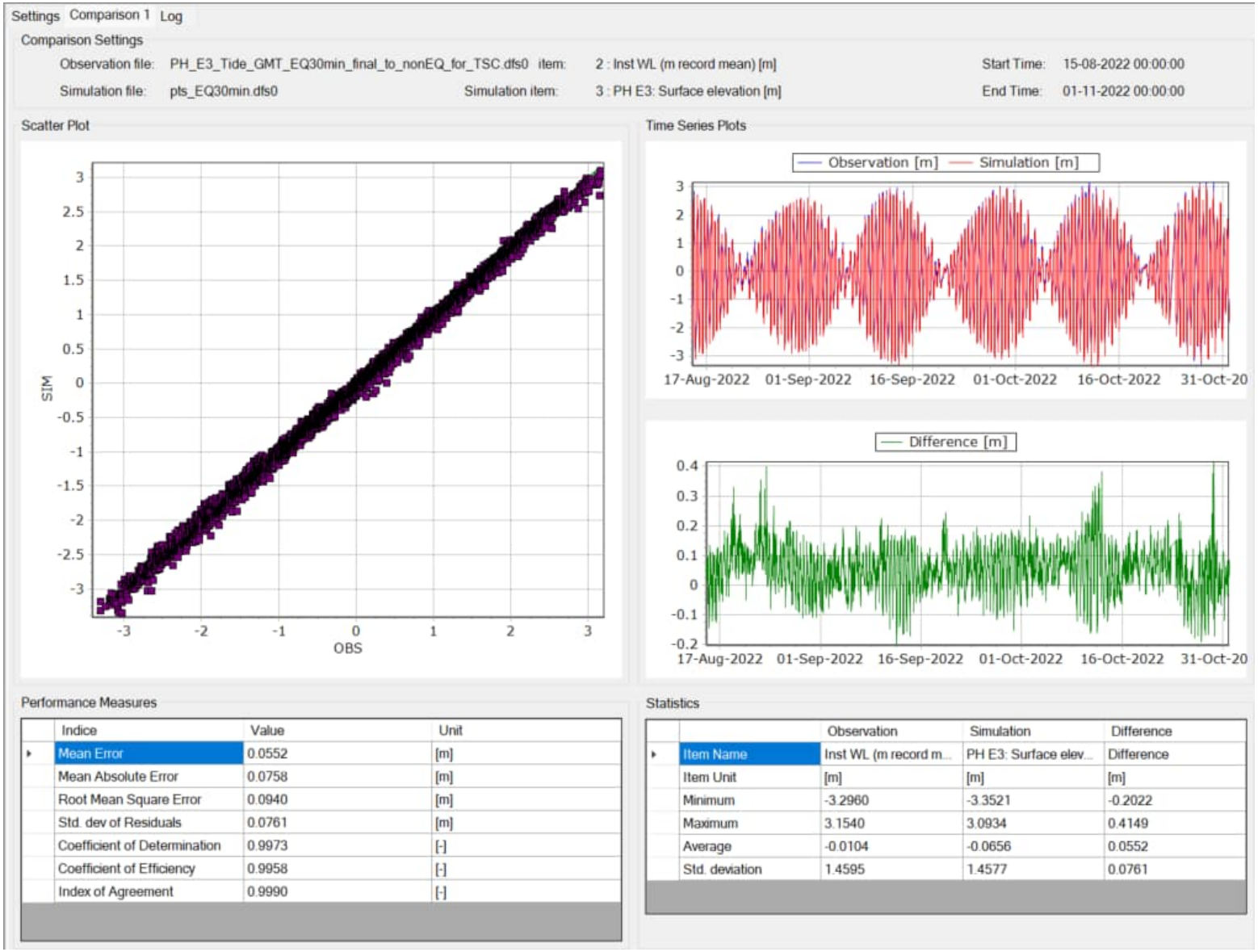

Figure A-11 Performance statistics for 3D Local Hydrodynamic model vs. water level measurements. Station E3, 15Aug – 31 Oct 2022.

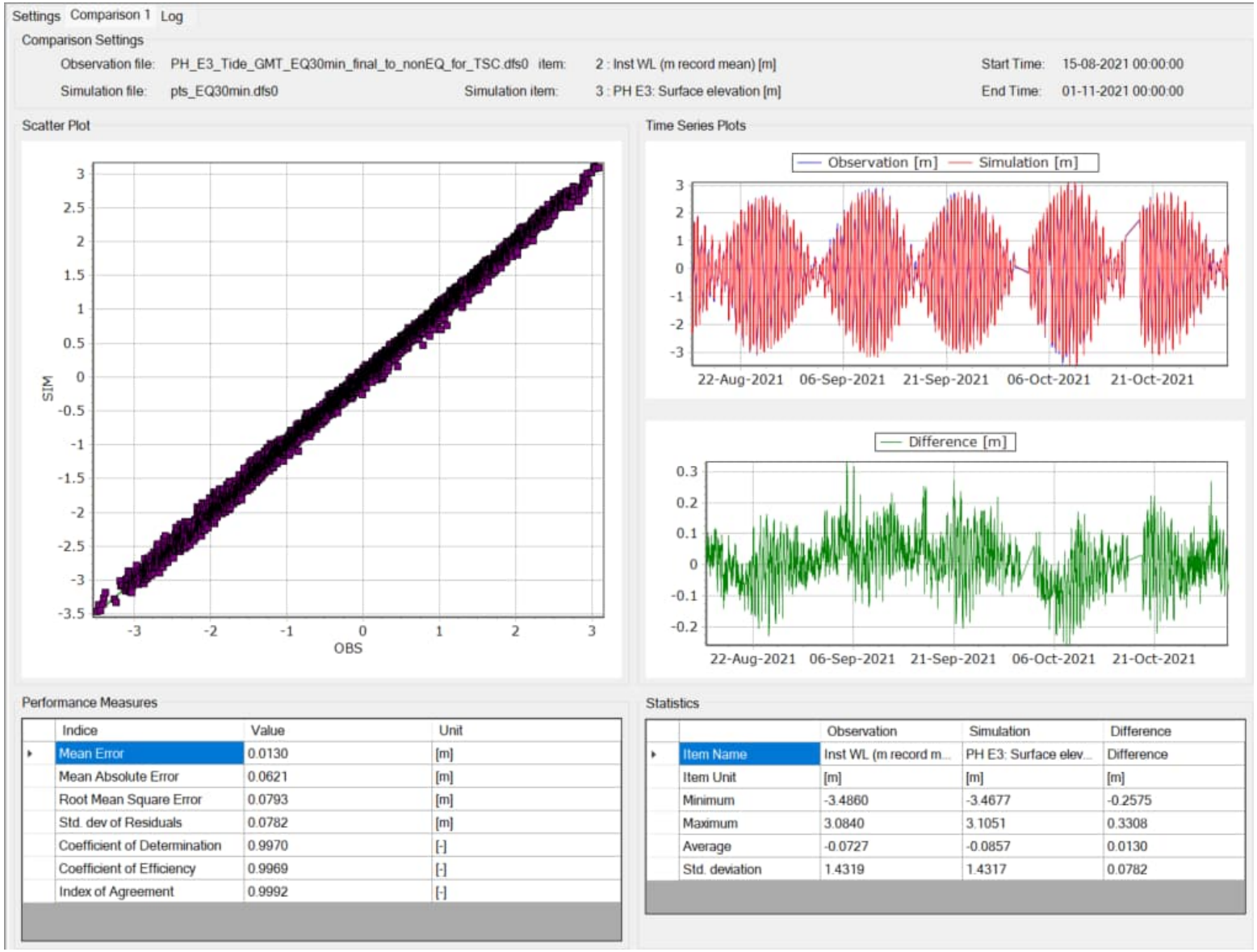

Figure A-12 Performance statistics for 3D Local Hydrodynamic model vs. water level measurements. Station E3, 15Aug – 31 Oct 2021.

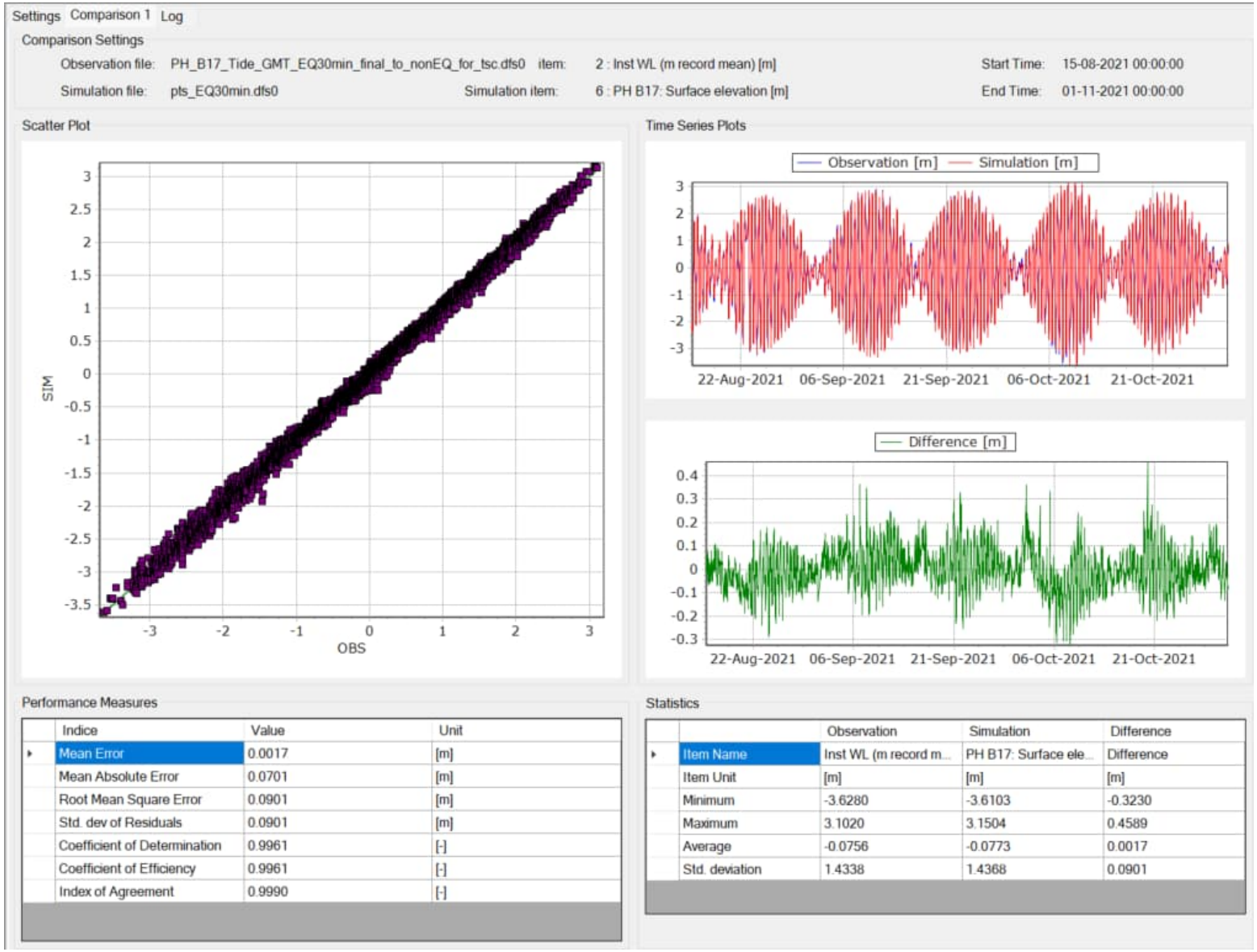

Figure A-13 Performance statistics for 3D Local Hydrodynamic model vs. water level measurements. Station B17, 15Aug – 31 Oct 2021.

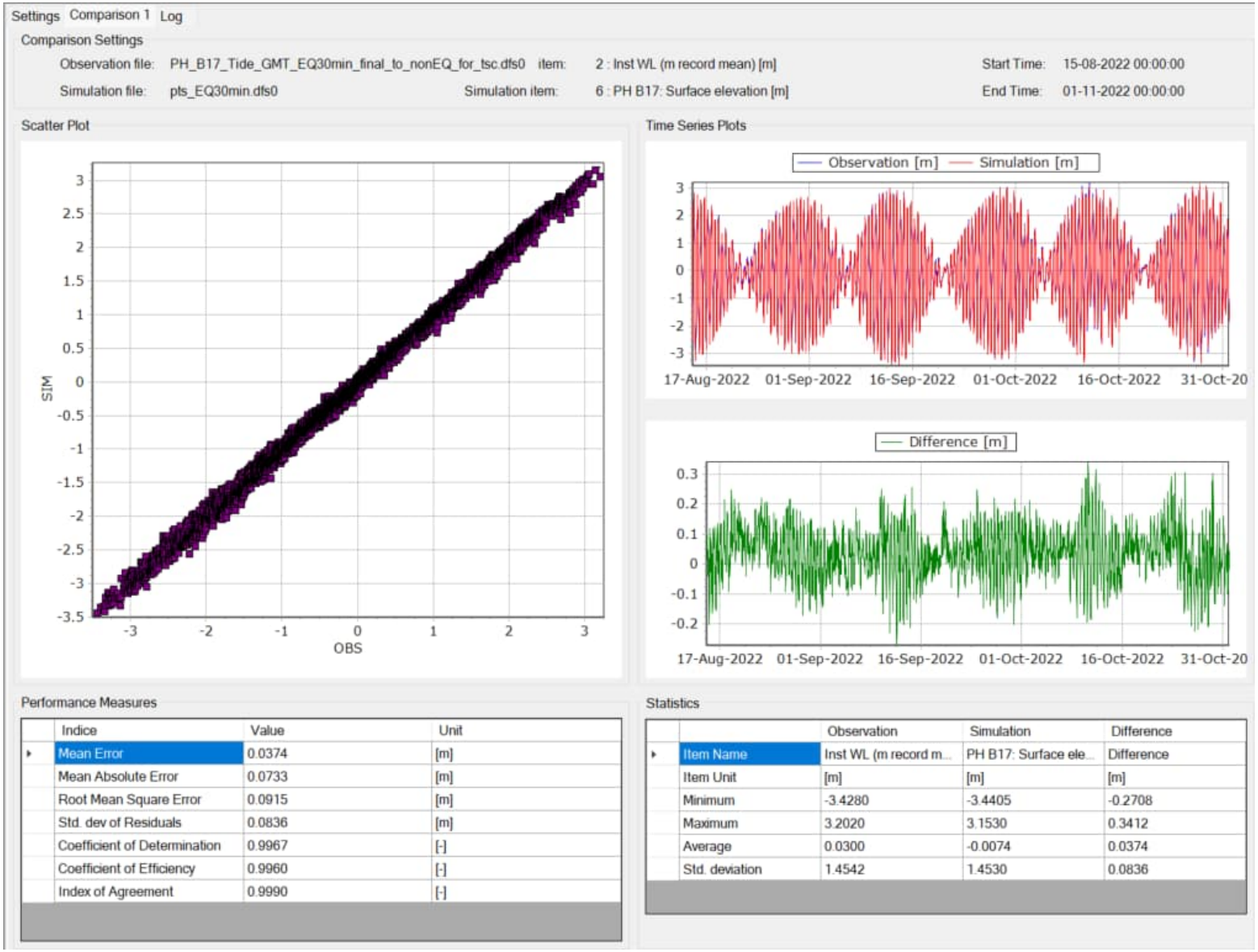

Figure A-14 Performance statistics for 3D Local Hydrodynamic model vs. water level measurements. Station B17, 15Aug – 31 Oct 2022.

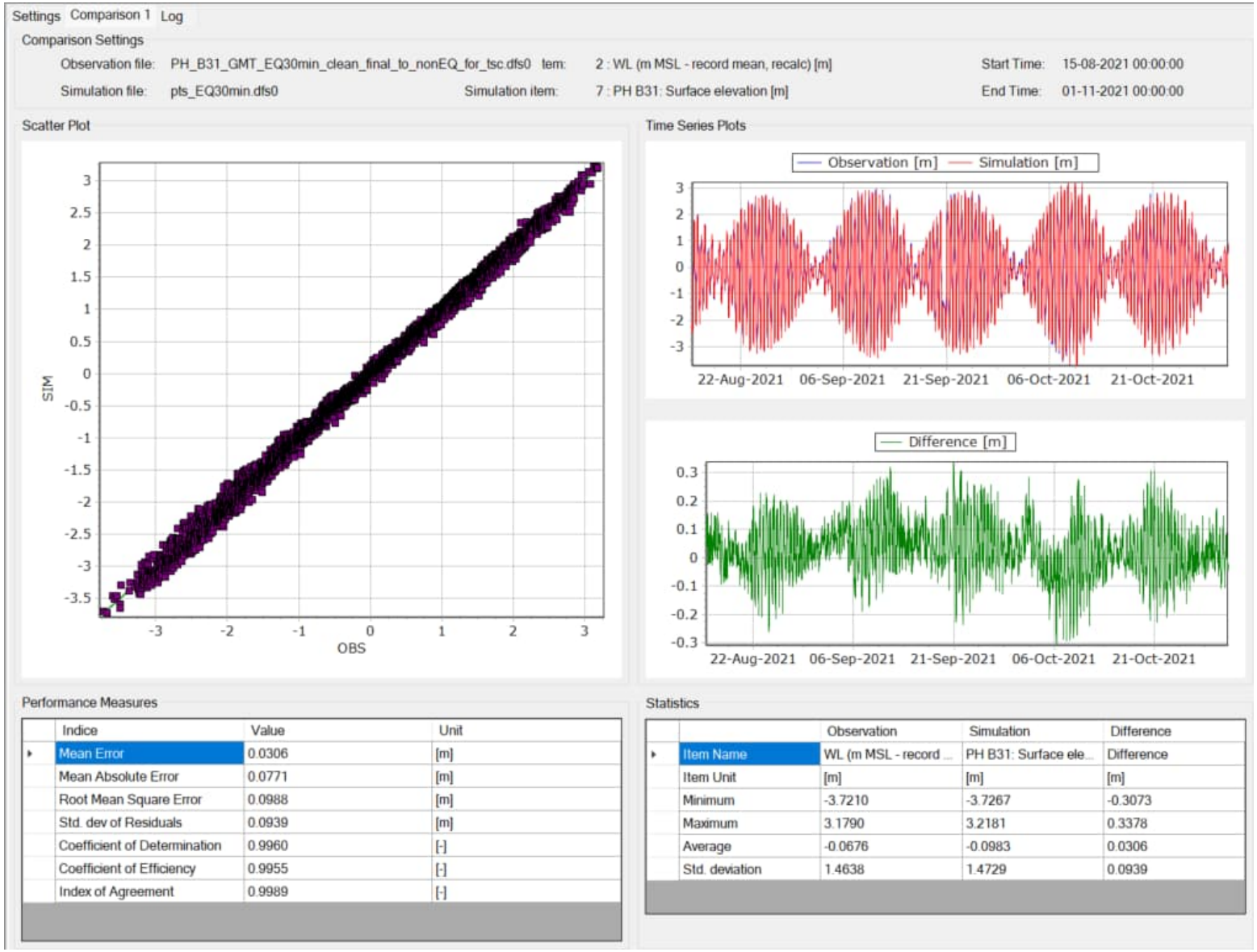

Figure A-15 Performance statistics for 3D Local Hydrodynamic model vs. water level measurements. Station B31, 15Aug – 31 Oct 2021.

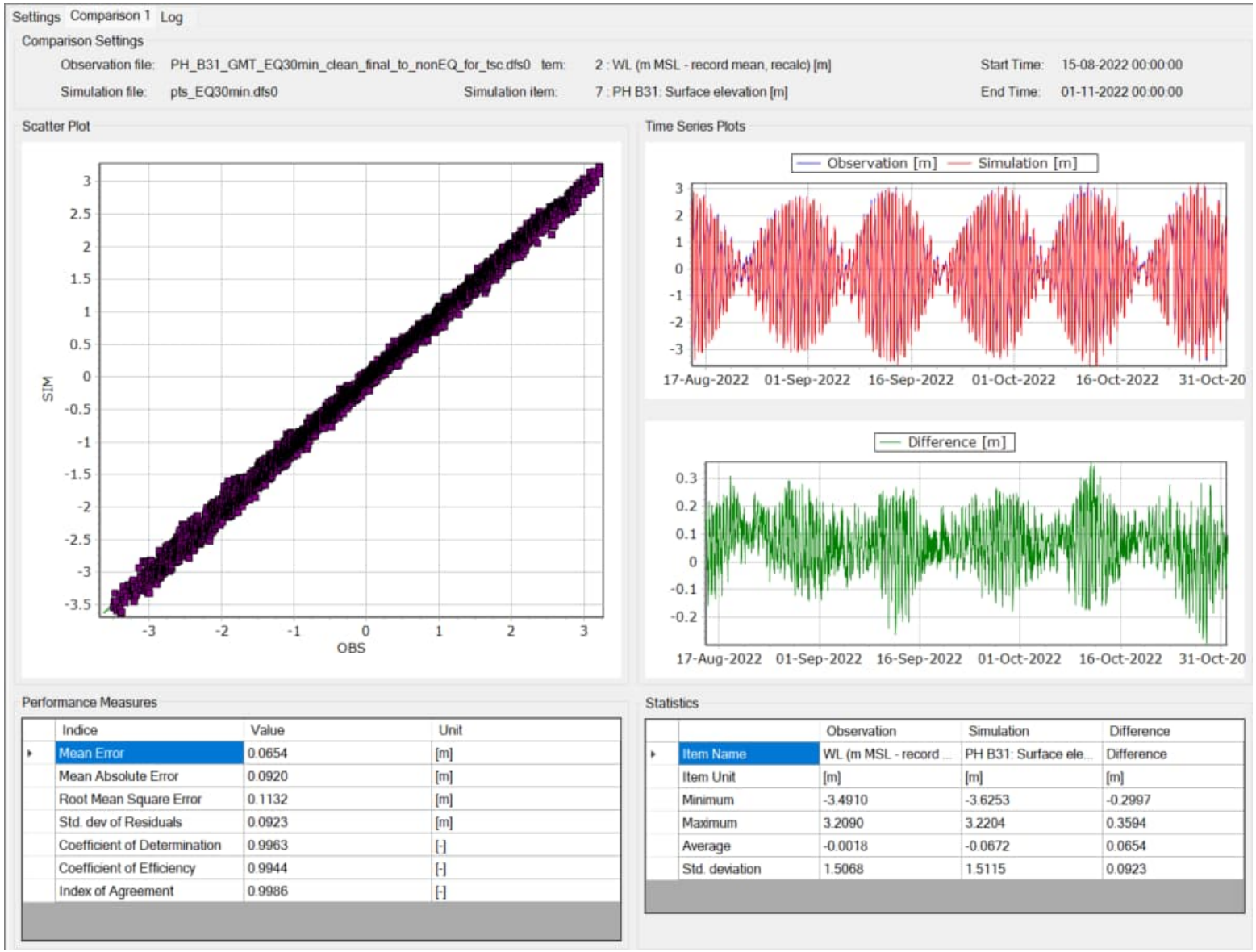

Indice	Value	Unit
Mean Error	0.0654	[m]
Mean Absolute Error	0.0920	[m]
Root Mean Square Error	0.1132	[m]
Std. dev of Residuals	0.0923	[m]
Coefficient of Determination	0.9963	[-]
Coefficient of Efficiency	0.9944	[-]
Index of Agreement	0.9986	[-]

	Observation	Simulation	Difference
Item Name	WL (m MSL - record ...	PH B31: Surface ele...	Difference
Item Unit	[m]	[m]	[m]
Minimum	-3.4910	-3.6253	-0.2997
Maximum	3.2090	3.2204	0.3594
Average	-0.0018	-0.0672	0.0654
Std. deviation	1.5068	1.5115	0.0923

Figure A-16 Performance statistics for 3D Local Hydrodynamic model vs. water level measurements. Station B31, 15Aug – 31 Oct 2022.

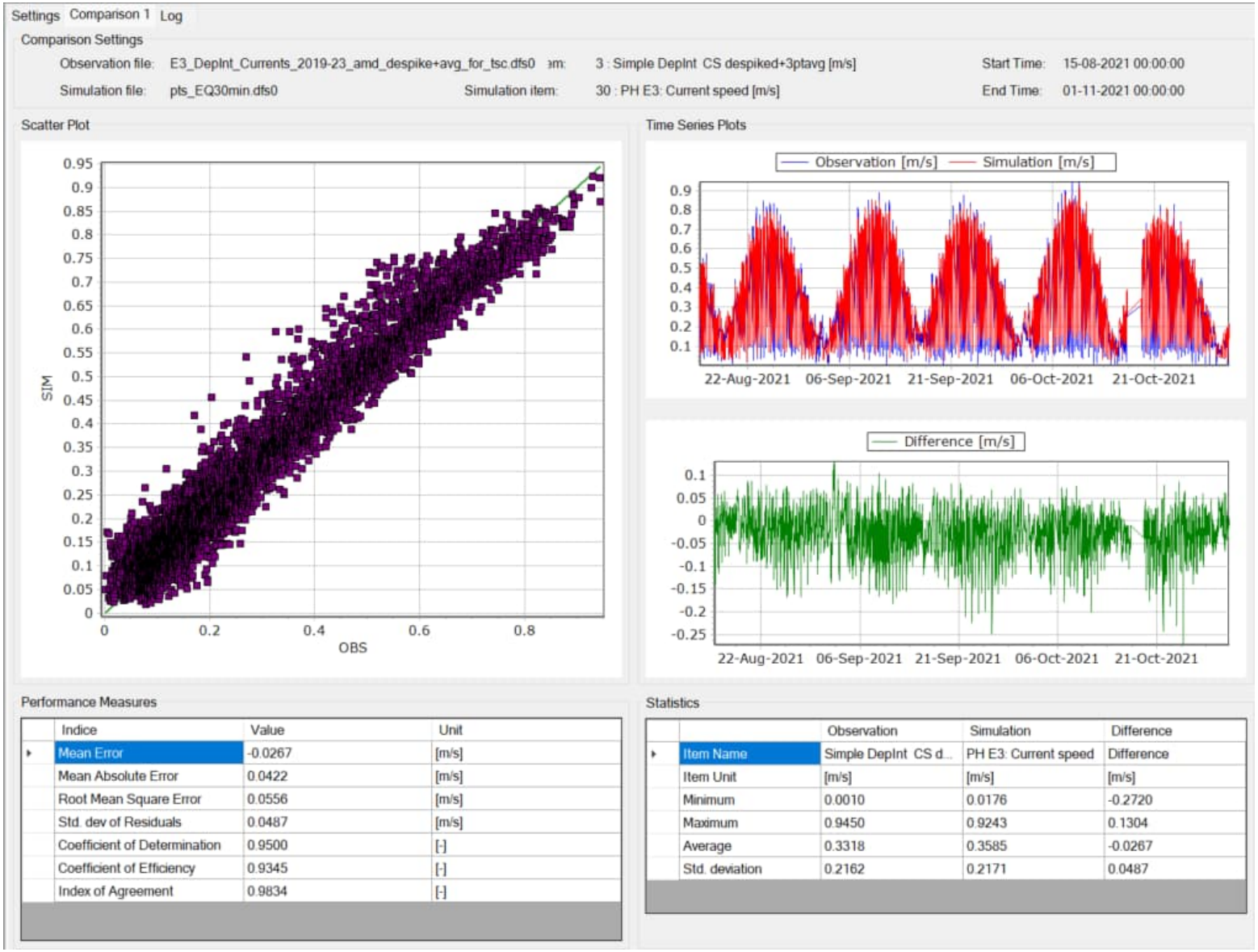

Figure A-17 Performance statistics for 3D Local Hydrodynamic model vs. depth-integrated current speed measurements. Station E3 AWAC, 15Aug – 31 Oct 2021.

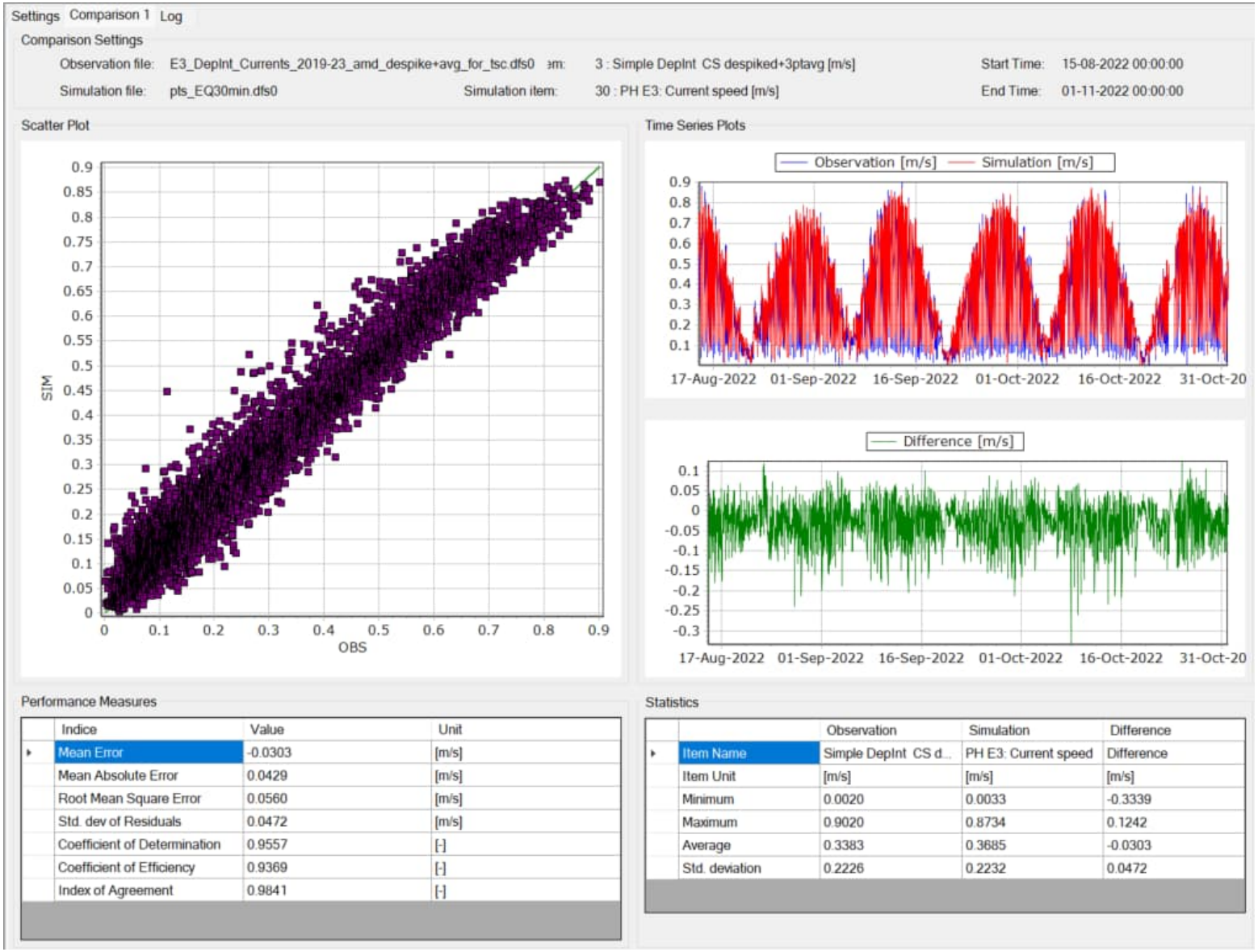

Figure A-18 Performance statistics for 3D Local Hydrodynamic model vs. depth-integrated current speed measurements. Station E3 AWAC, 15Aug – 31 Oct 2022.

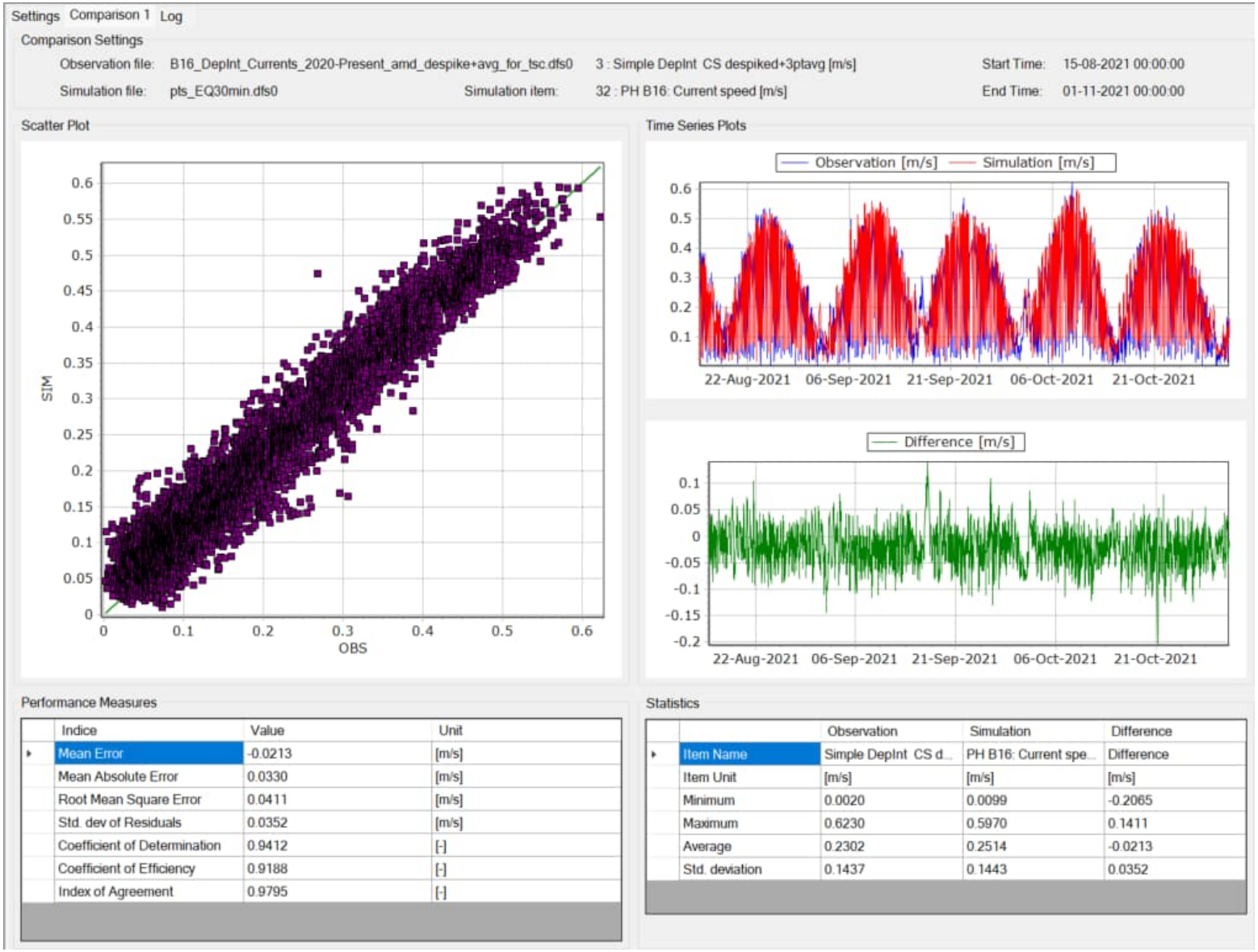

Indice	Value	Unit
Mean Error	-0.0213	[m/s]
Mean Absolute Error	0.0330	[m/s]
Root Mean Square Error	0.0411	[m/s]
Std. dev of Residuals	0.0352	[m/s]
Coefficient of Determination	0.9412	[-]
Coefficient of Efficiency	0.9188	[-]
Index of Agreement	0.9795	[-]

	Observation	Simulation	Difference
Item Name	Simple DepInt CS d...	PH B16: Current spe...	Difference
Item Unit	[m/s]	[m/s]	[m/s]
Minimum	0.0020	0.0099	-0.2065
Maximum	0.6230	0.5970	0.1411
Average	0.2302	0.2514	-0.0213
Std. deviation	0.1437	0.1443	0.0352

Figure A-19 Performance statistics for 3D Local Hydrodynamic model vs. depth-integrated current speed measurements. Station B16 AWAC, 15Aug – 31 Oct 2021.

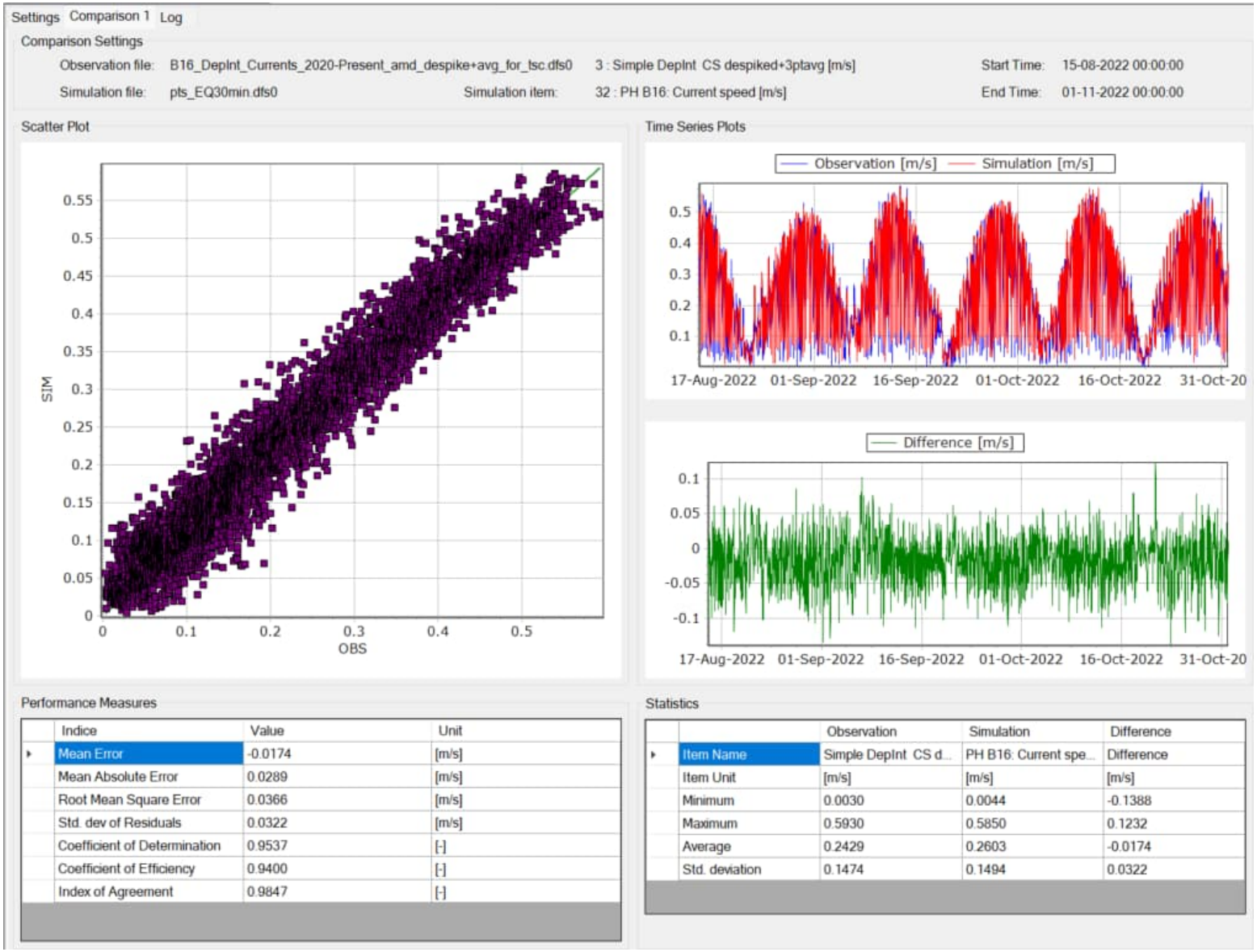

Indice	Value	Unit
Mean Error	-0.0174	[m/s]
Mean Absolute Error	0.0289	[m/s]
Root Mean Square Error	0.0366	[m/s]
Std. dev of Residuals	0.0322	[m/s]
Coefficient of Determination	0.9537	[-]
Coefficient of Efficiency	0.9400	[-]
Index of Agreement	0.9847	[-]

	Observation	Simulation	Difference
Item Name	Simple DepInt CS d...	PH B16: Current spe...	Difference
Item Unit	[m/s]	[m/s]	[m/s]
Minimum	0.0030	0.0044	-0.1388
Maximum	0.5930	0.5850	0.1232
Average	0.2429	0.2603	-0.0174
Std. deviation	0.1474	0.1494	0.0322

Figure A-20 Performance statistics for 3D Local Hydrodynamic model vs. depth-integrated current speed measurements. Station B16 AWAC, 15Aug – 31 Oct 2022.

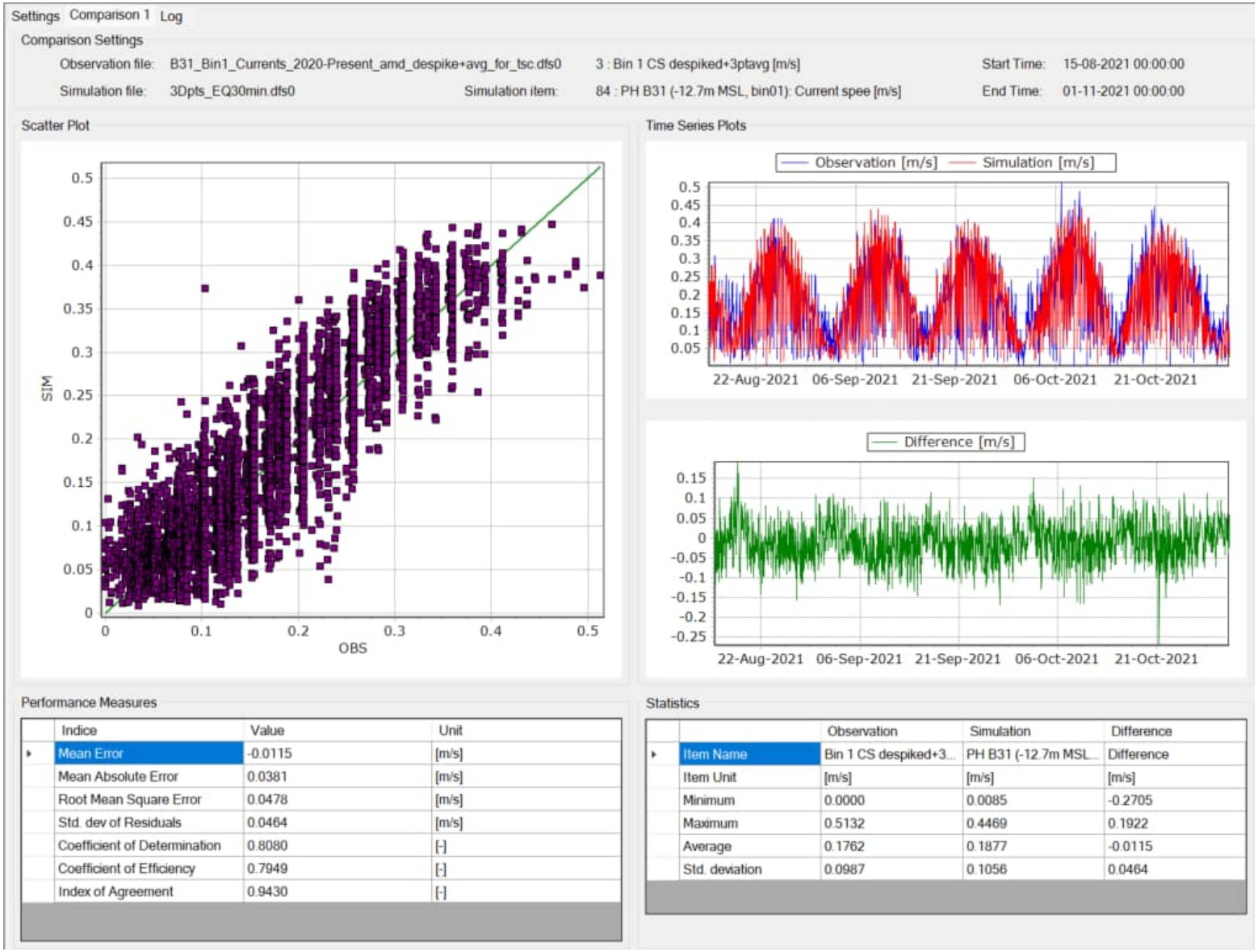

Figure A-21 Performance statistics for 3D Local Hydrodynamic model vs. bottom bin current speed measurements. Station B31 AWAC, 15Aug – 31 Oct 2021.

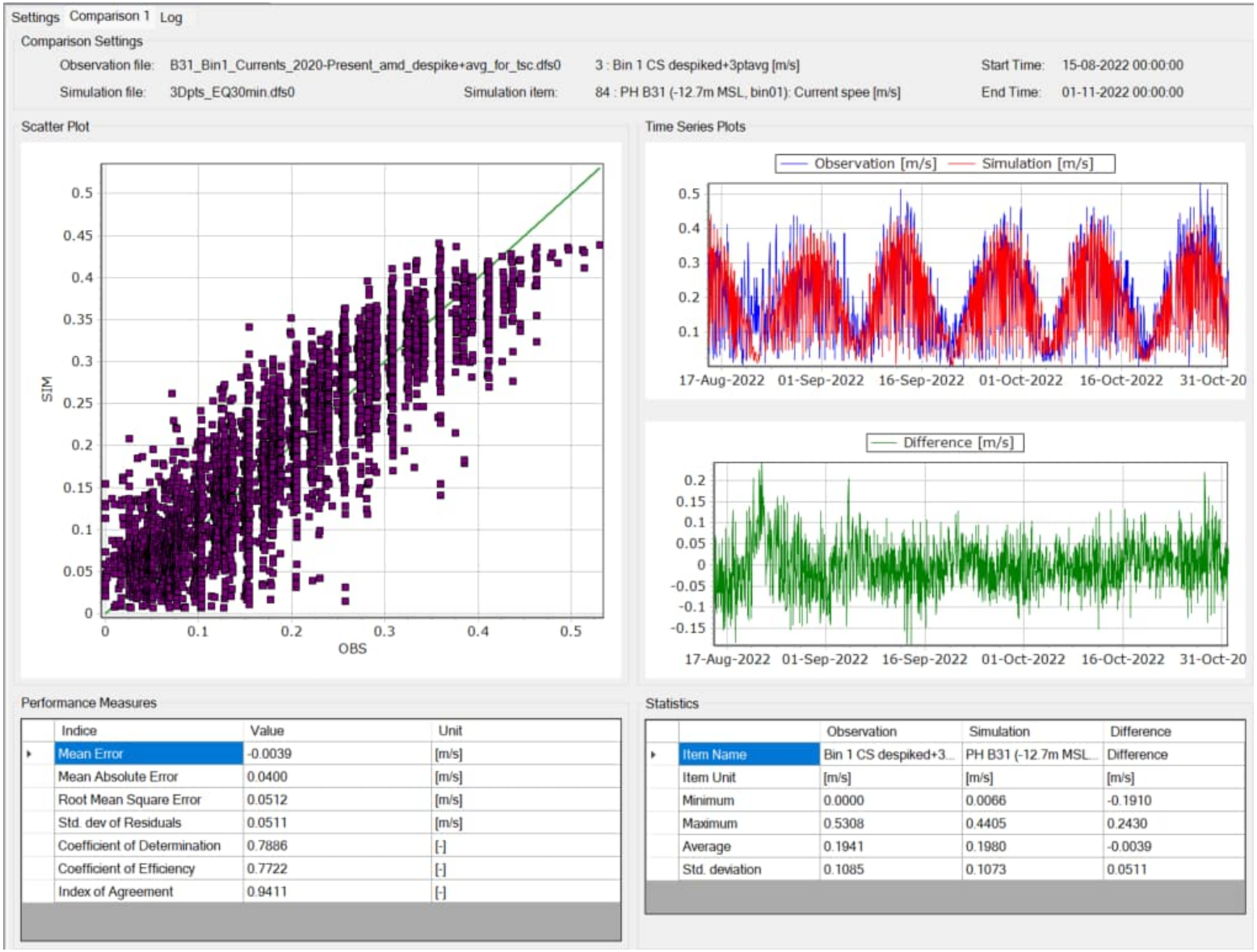

Figure A-22 Performance statistics for 3D Local Hydrodynamic model vs. bottom bin current speed measurements. Station B31 AWAC, 15Aug – 31 Oct 2022.

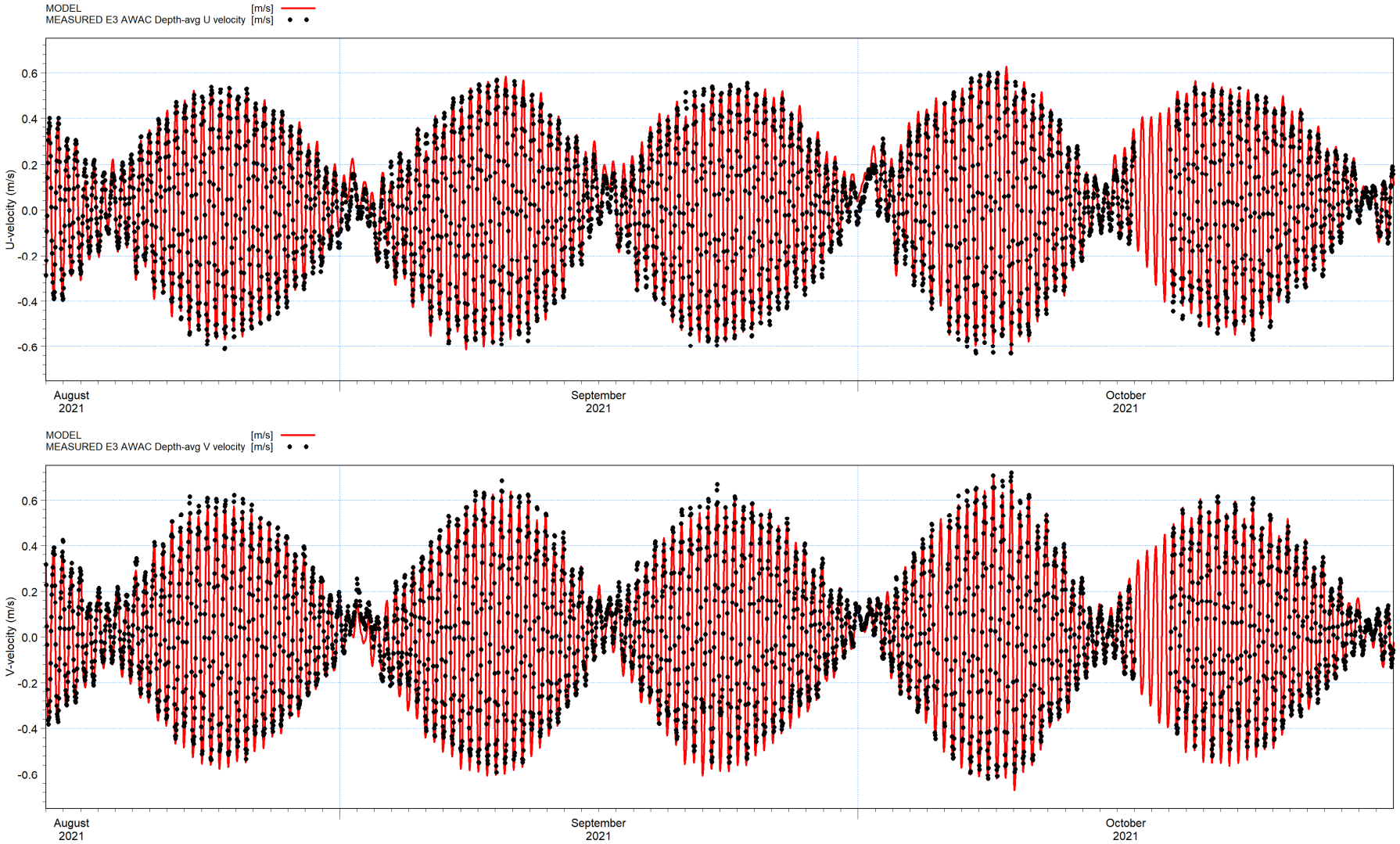

Figure A-23 Validation plots of modelled vs. measured depth-averaged velocity components at the E3 AWAC from 3D Local Hydrodynamic Model. 15Aug – 01Nov 2021.

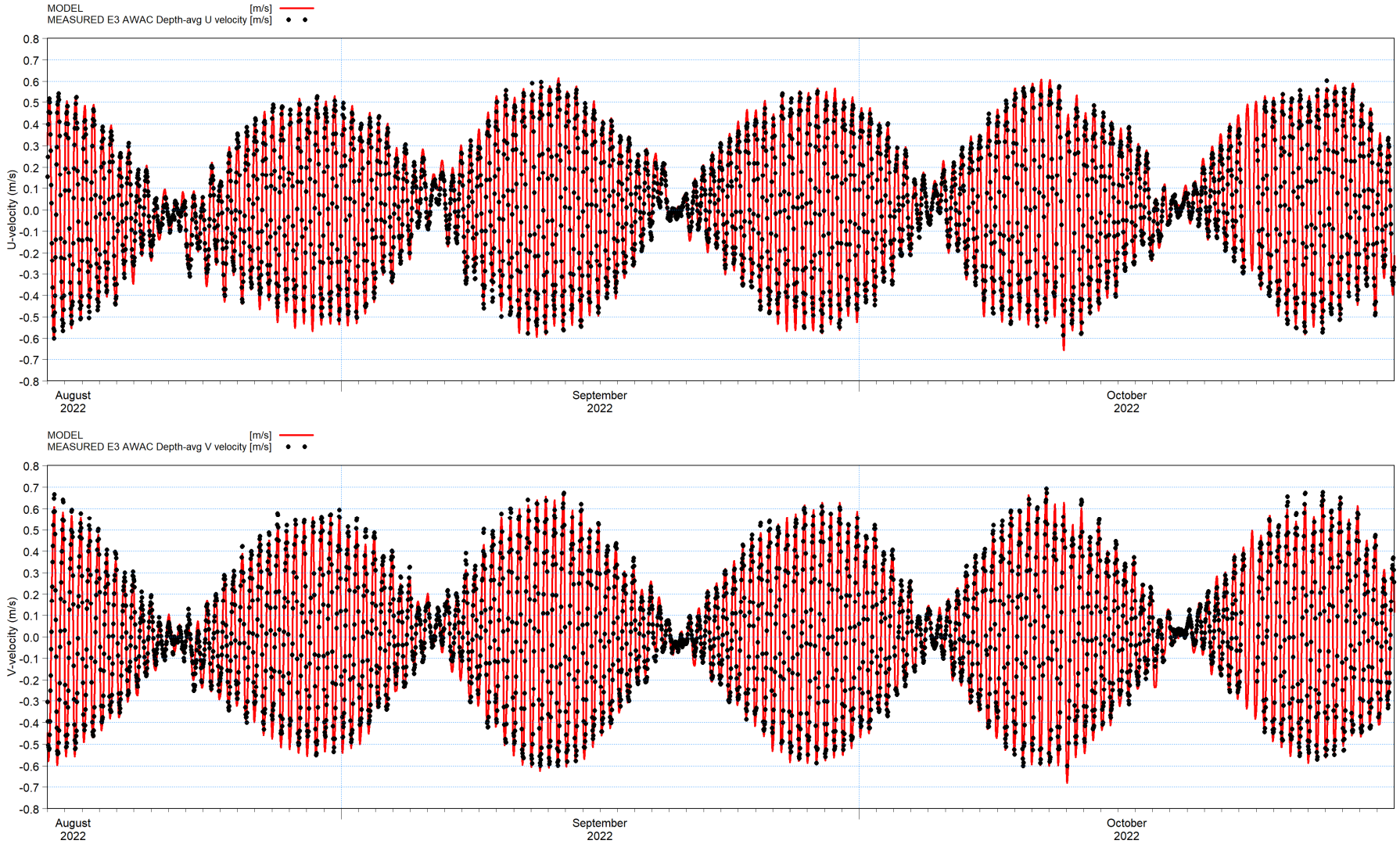

Figure A-24 Validation plots of modelled vs. measured depth-averaged velocity components at the E3 AWAC from 3D Local Hydrodynamic Model. 15Aug – 01Nov 2022.

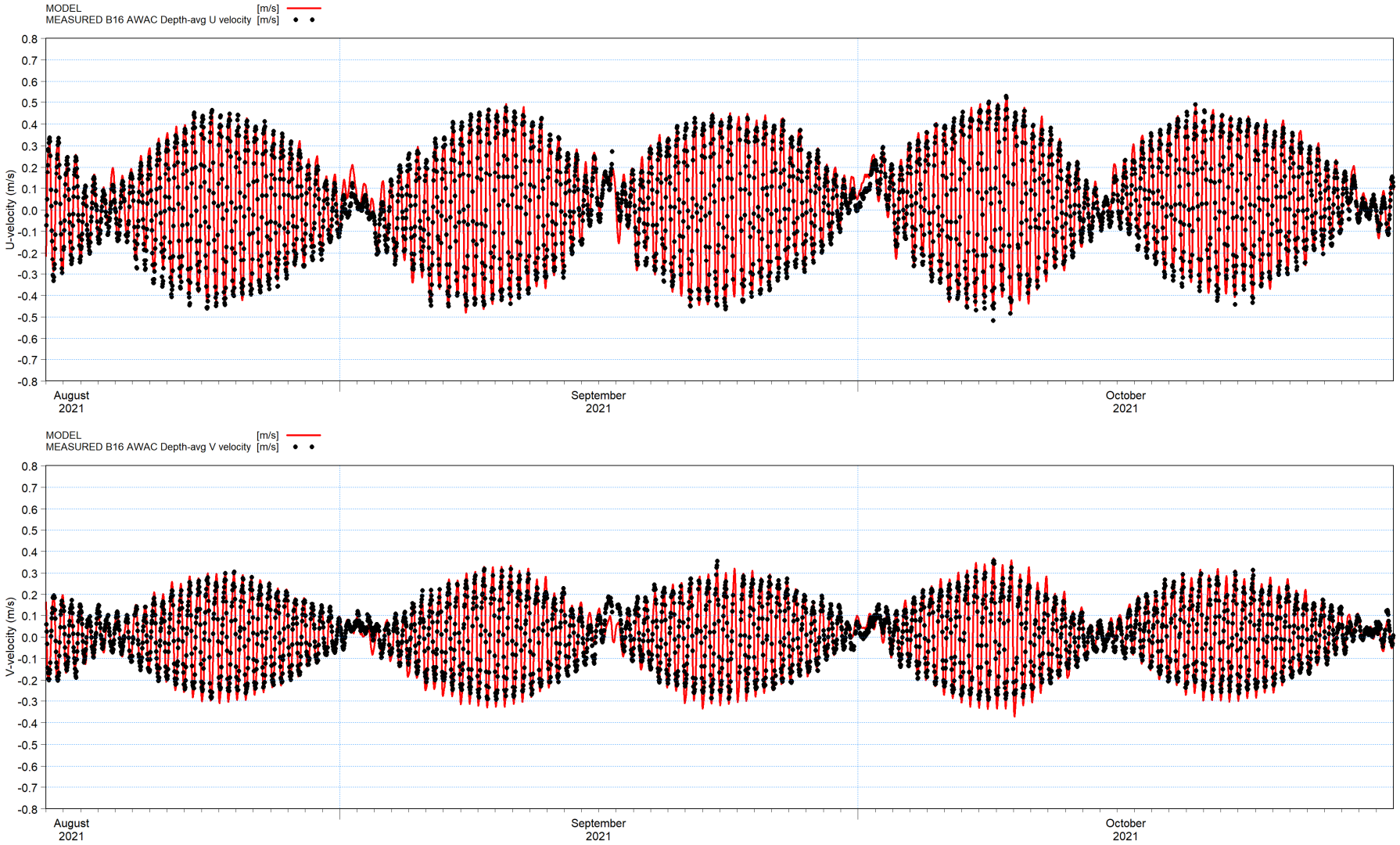

Figure A-25 Validation plots of modelled vs. measured depth-averaged velocity components at the B16 AWAC from 3D Local Hydrodynamic Model. 15Aug – 01Nov 2021.

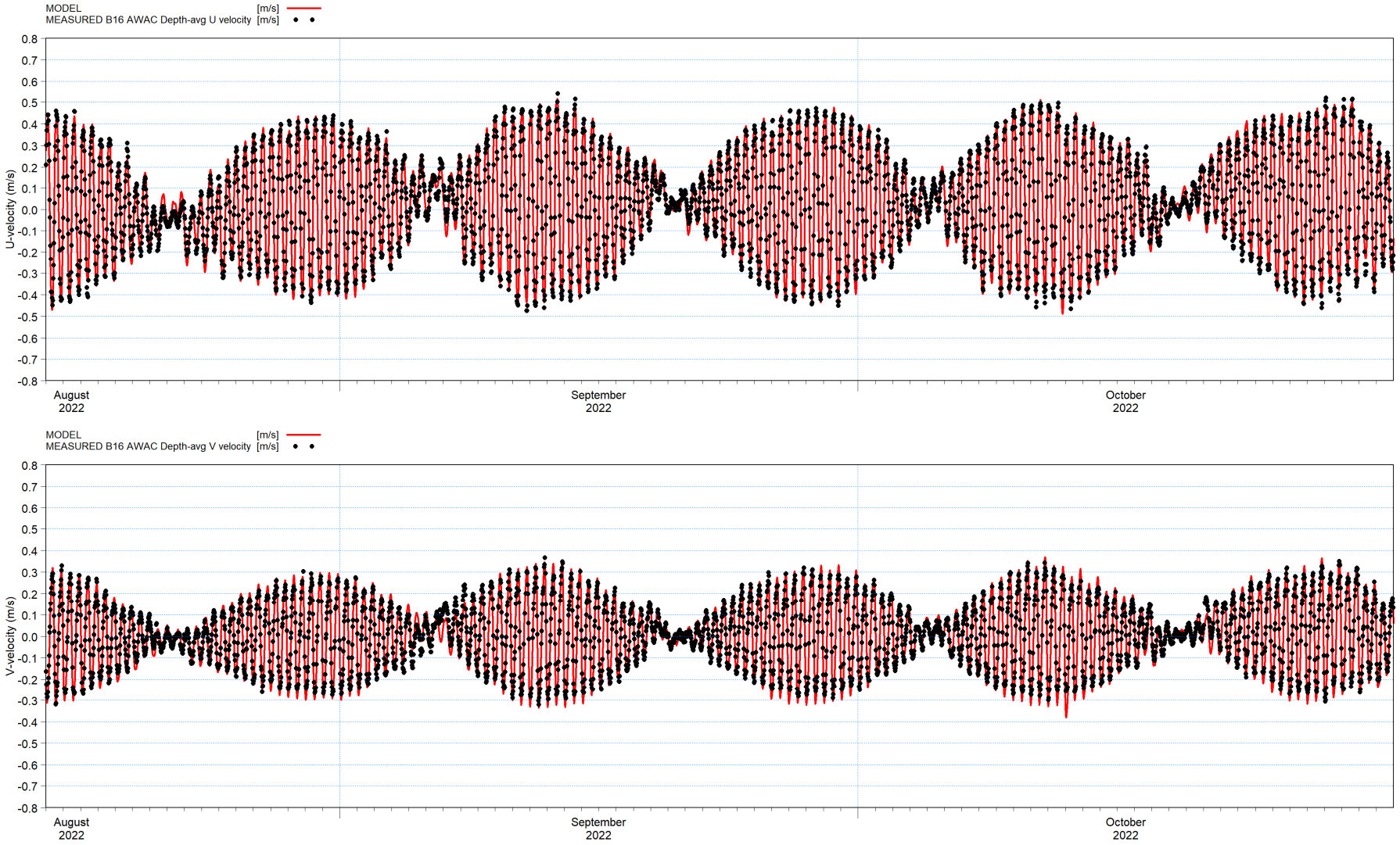

Figure A-26 Validation plots of modelled vs. measured depth-averaged velocity components at the B16 AWAC from 3D Local Hydrodynamic Model. 15Aug – 01Nov 2022.

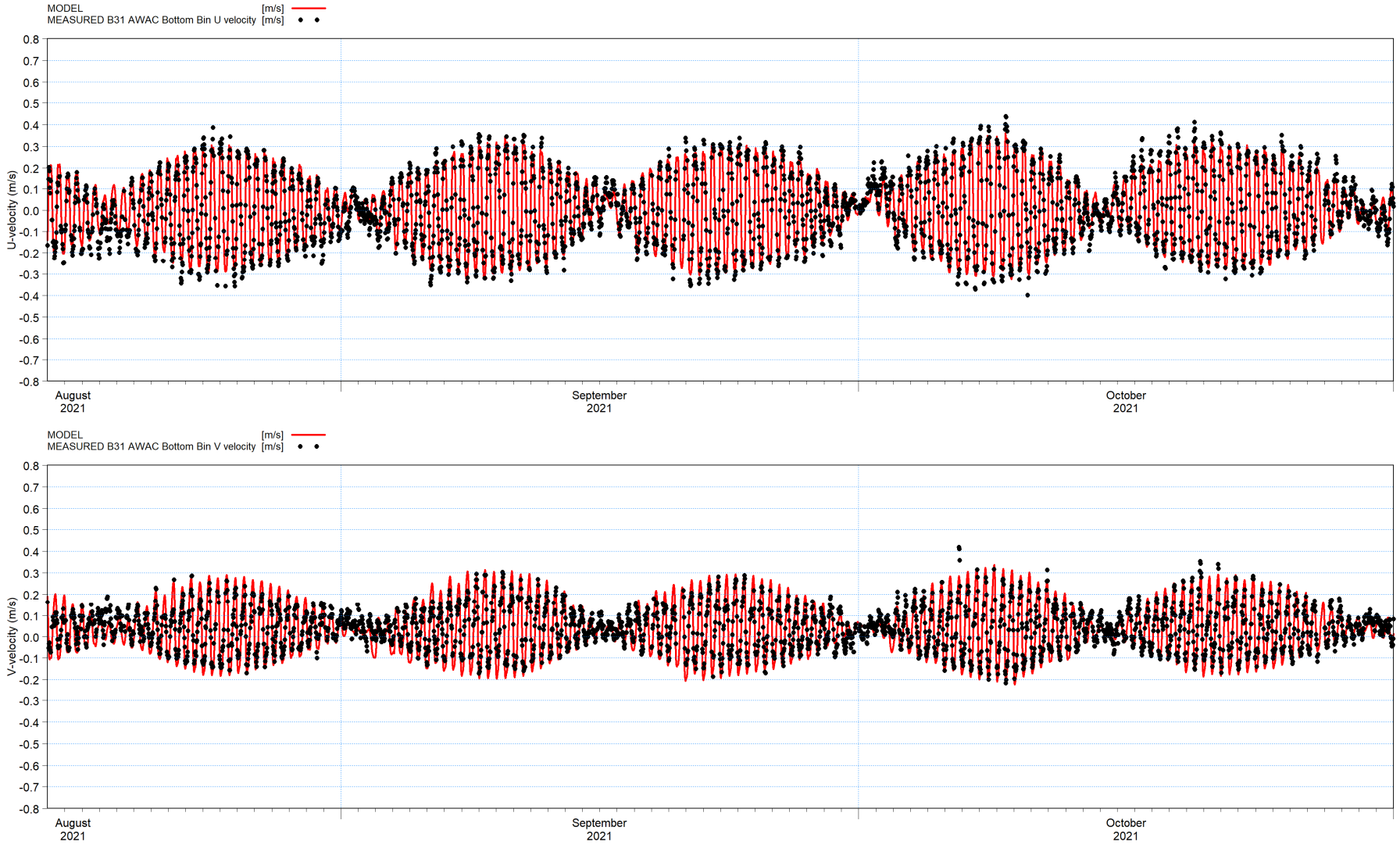

Figure A-27 Validation plots of modelled vs. measured bottom bin velocity components at the B31 AWAC from 3D Local Hydrodynamic Model. 15Aug – 01Nov 2021.

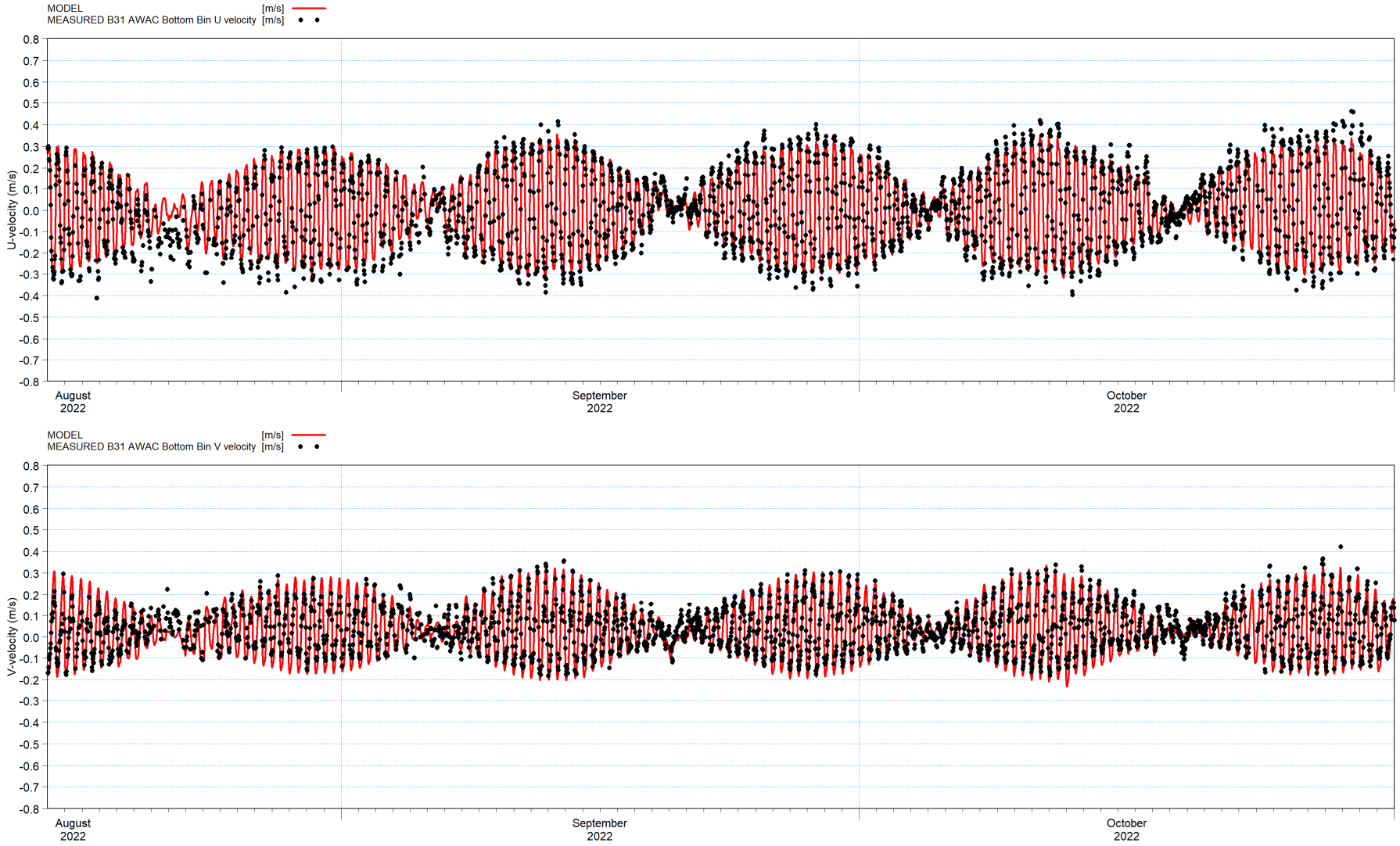

Figure A-28 Validation plots of modelled vs. measured bottom bin velocity components at the B31 AWAC from 3D Local Hydrodynamic Model. 15Aug – 01Nov 2022.

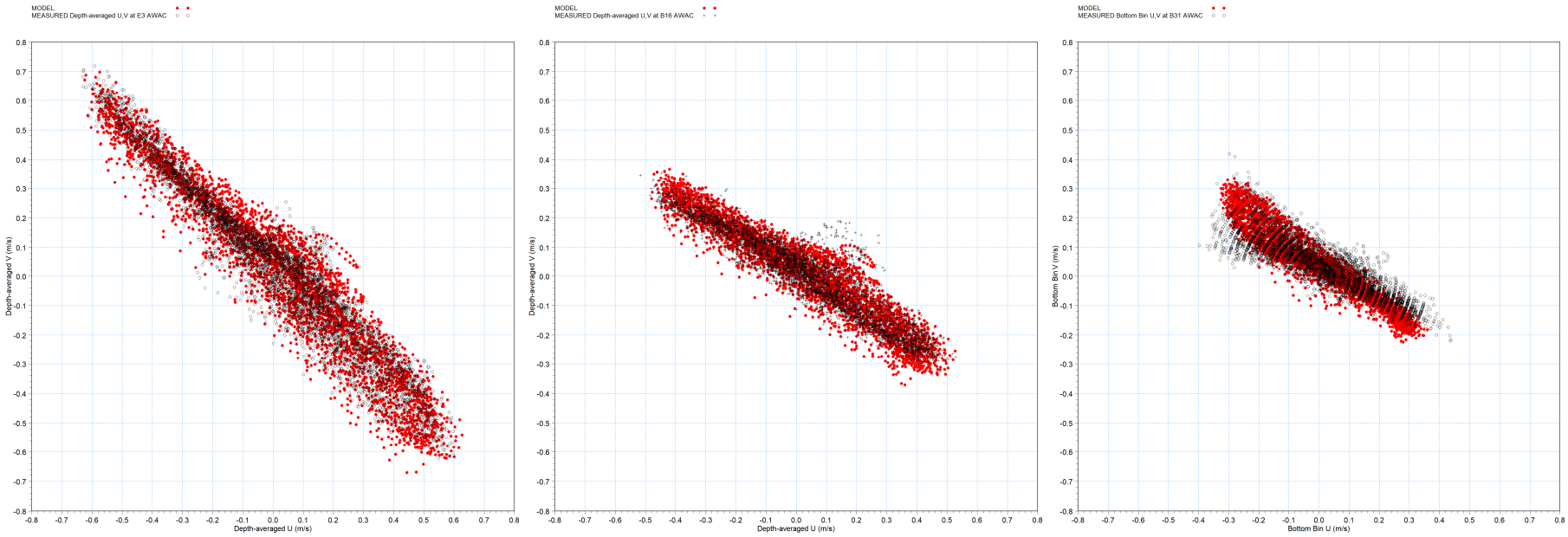

Figure A-29 Validation plots of modelled (red) vs. measured depth-averaged velocity components (black) at the E3 AWAC (left), B16 AWAC (middle) and bottom-bin velocity components at B31 AWAC (right) from 3D Local Hydrodynamic Model. 15Aug – 01Nov 2021. Pattern in right image caused by limited decimals (0.1kt) present in native measured record.

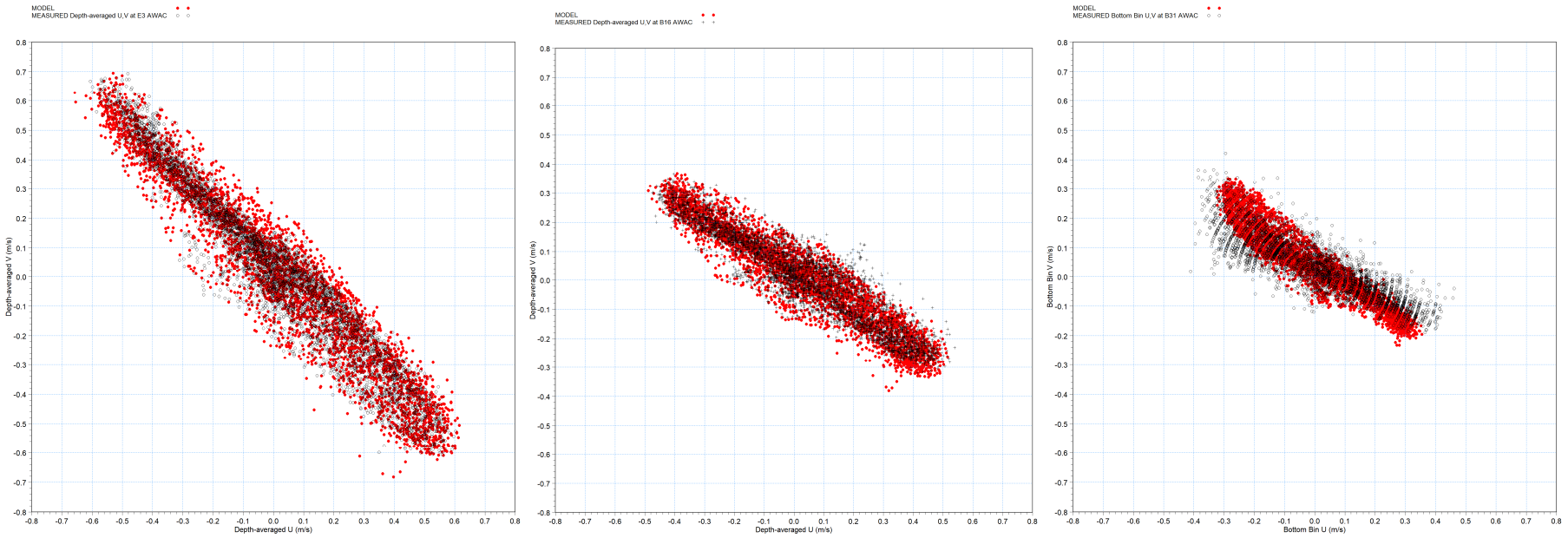

Figure A-30 Validation plots of modelled (red) vs. measured depth-averaged velocity components (black) at the E3 AWAC (left), B16 AWAC (middle) and bottom-bin velocity components at B31 AWAC (right) from 3D Local Hydrodynamic Model. 15Aug – 01Nov 2022. Pattern in right image caused by limited decimals (0.1kt) present in native measured record.

APPENDIX B

Wave Model Validation

B Wave Model Validation

This appendix contains supplementary graphics and statistics related to validation of the Local Wave Model, which has been validated against measurements within the extensive network of metocean instrumentation maintained by Pilbara Ports (Figure 2-1).

Figures are presented in pairs, with each pair representing validation from 2021 and 2022 for a given combination of measurement station and measured quantity. Results from 2021 are in oddly numbered figure, 2022 evenly numbered.

Figures B-1 and B-2 present time series plots of $Hm0_{TOT}$, $Hm0_{SEA}$ and $Hm0_{SWELL}$ for the waverider buoy at station C2. For 2021, the sea/swell split in the measurements was applied at 9s, while in 2022 it was applied at 7s. The model extractions follow this convention.

Figures B-3 and B-4 present time series plots of $Hm0_{TOT}$, $Hm0_{SEA}$ and $Hm0_{SWELL}$ for the AWAC at station E3. The sea/swell split in the measurements was applied at 7s for both years. The model extractions follow this convention.

Figures B-5 and B-6 present time series plots of $Hm0_{TOT}$, $Hm0_{SEA}$ and $Hm0_{SWELL}$ for the waverider buoy at station B15. For 2021, the sea/swell split in the measurements was applied at 9s, while in 2022 it was applied at 7s. The model extractions follow this convention.

Figures B-7 and B-8 present time series plots of $Hm0_{TOT}$, $Hm0_{SEA}$ and $Hm0_{SWELL}$ for the AWAC at station B16. The sea/swell split in the measurements was applied at 7s for both years. The model extractions follow this convention.

Figures B-9 and B-10 present time series plots of $Hm0_{TOT}$, $Hm0_{SEA}$ and $Hm0_{SWELL}$ for the AWAC at station B31. The sea/swell split in the measurements was applied at 7s for both years. The model extractions follow this convention.

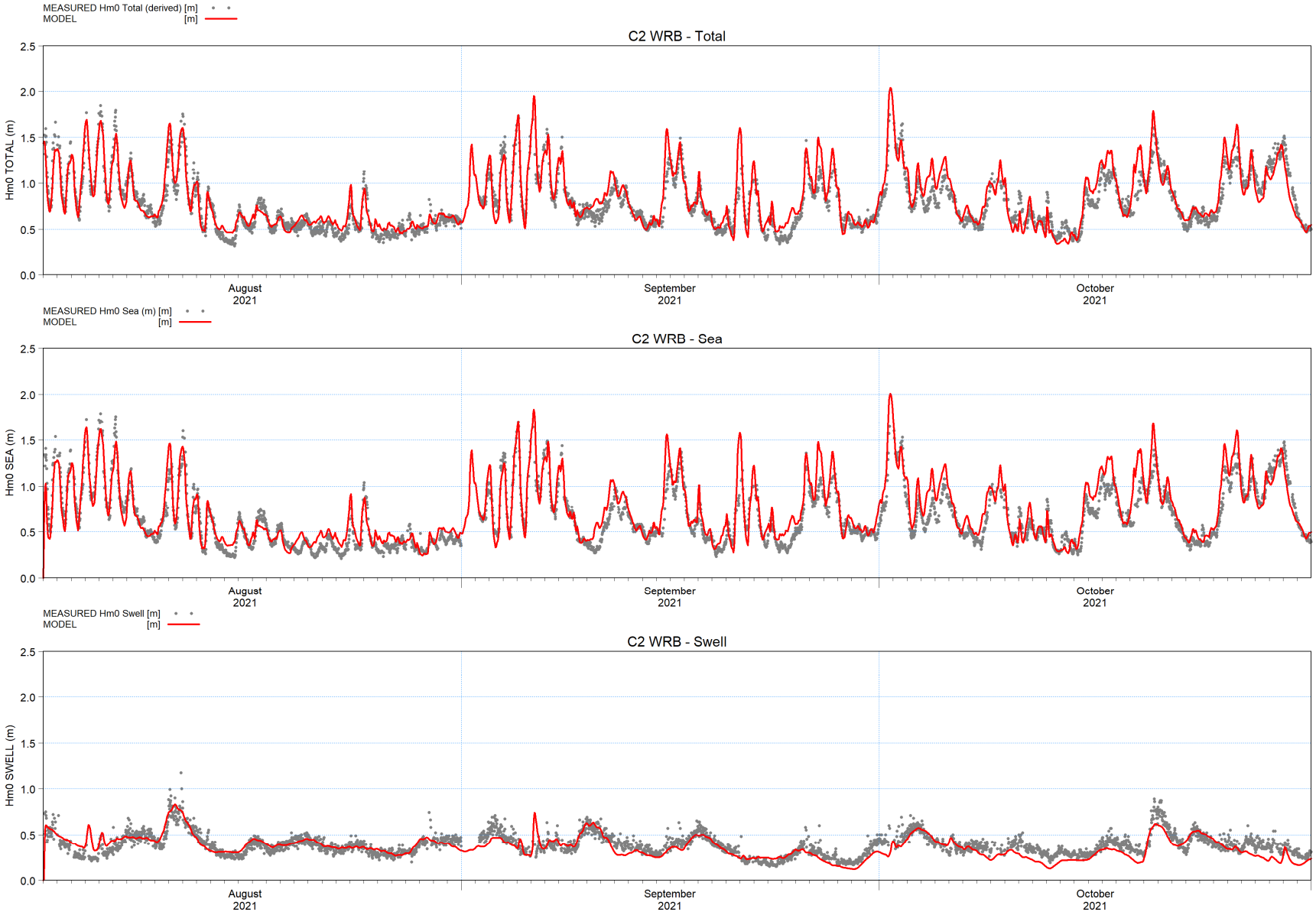

Figure B-1 Time series comparison for Local Wave Model hindcast vs. measured Hm0 (Total, Sea, Swell). Station C2 WRB, 2021.

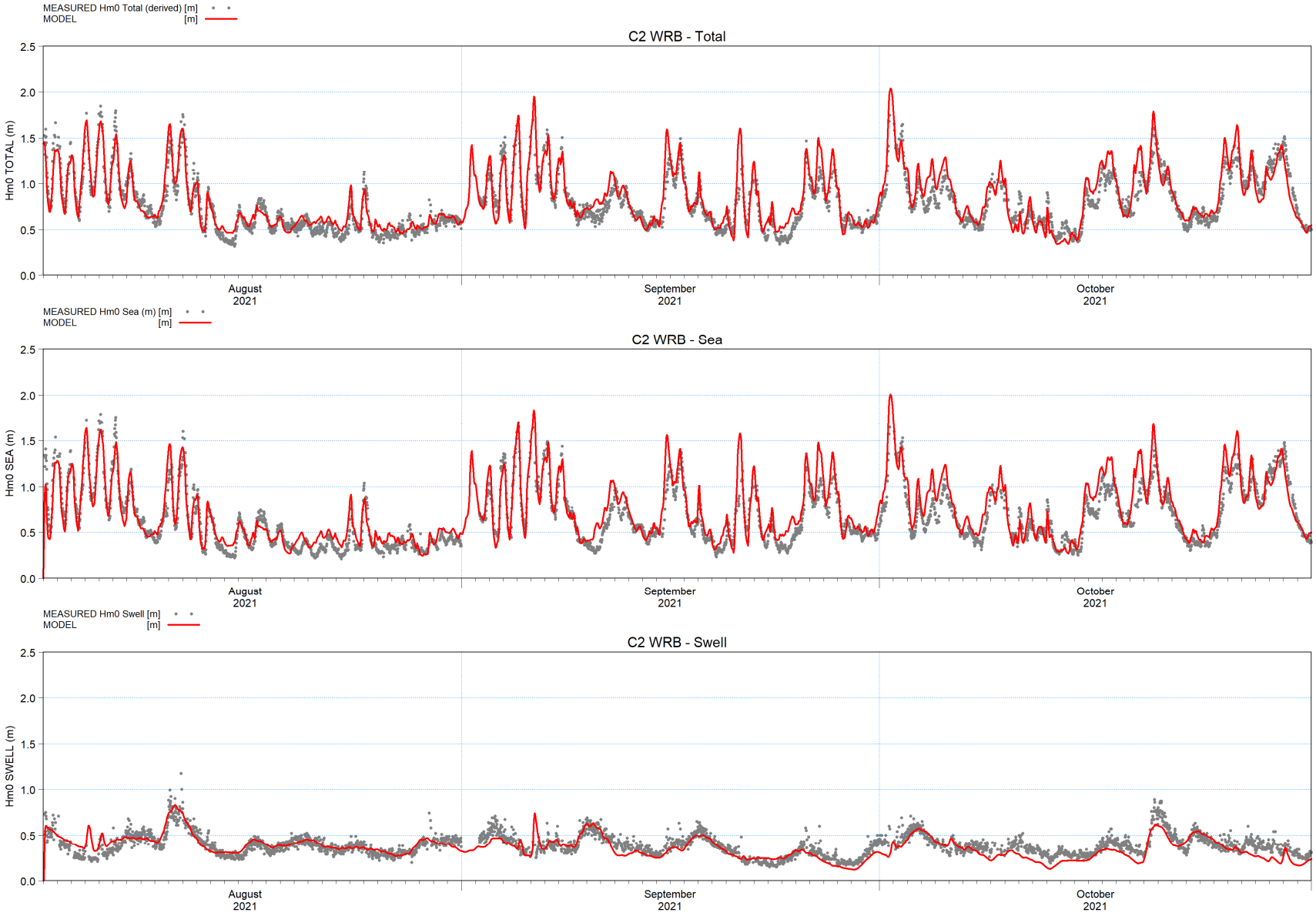

Figure B-2 Time series comparison for Local Wave Model hindcast vs. measured Hm0 (Total, Sea, Swell). Station C2 WRB, 2022.

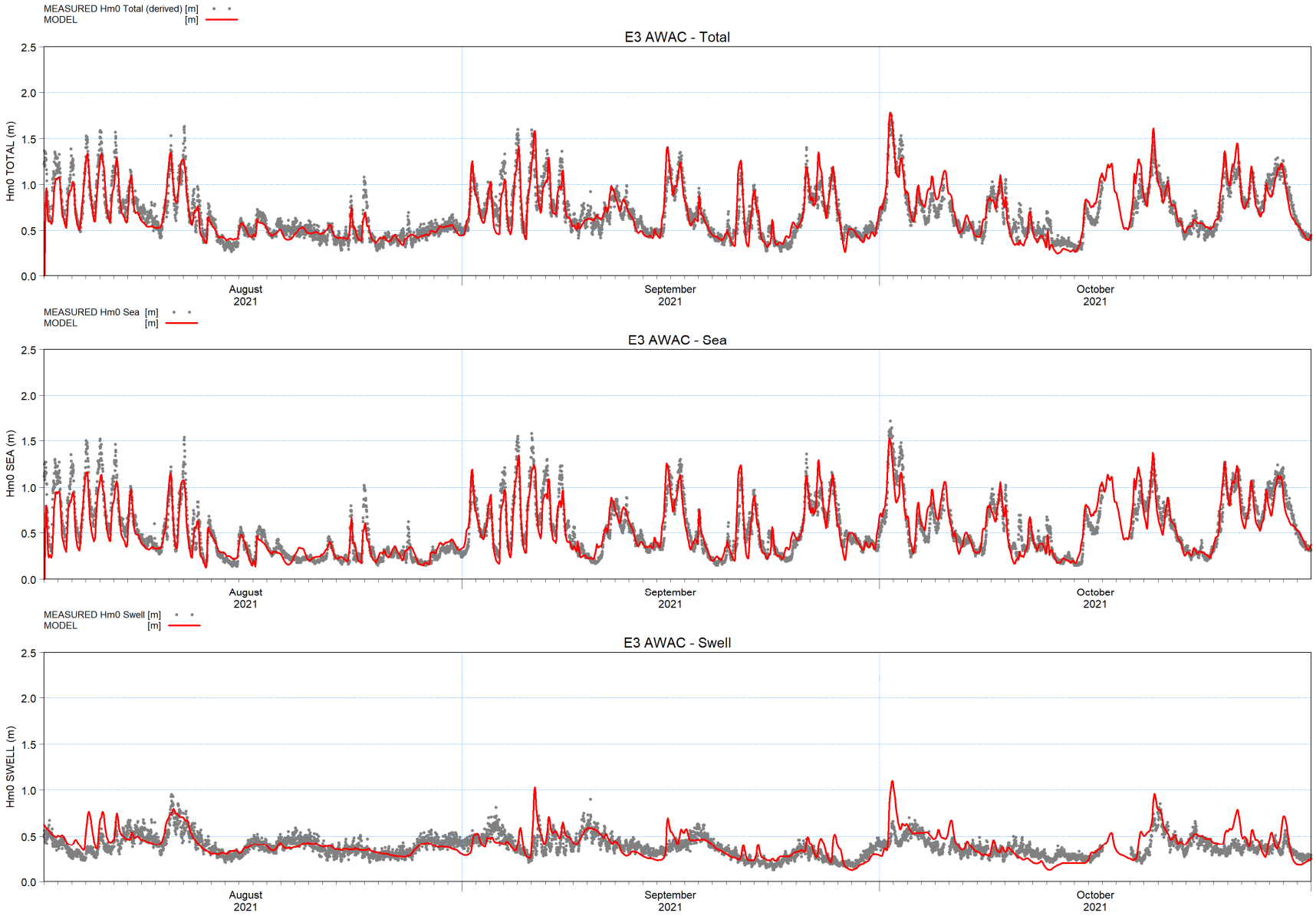

Figure B-3 Time series comparison for Local Wave Model hindcast vs. measured Hm0 (Total, Sea, Swell). Station E3 AWAC, 2021.

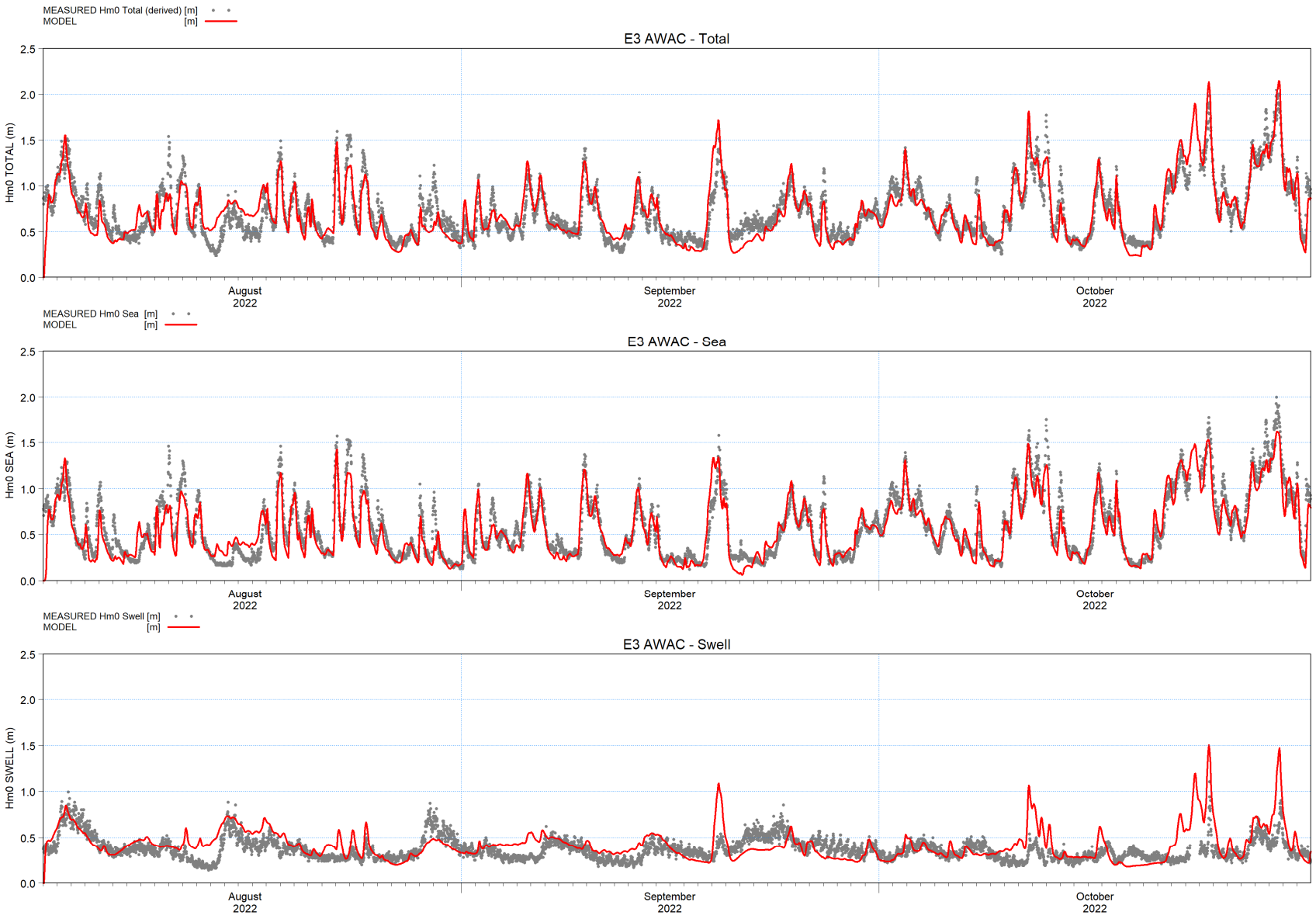

Figure B-4 Time series comparison for Local Wave Model hindcast vs. measured Hm0 (Total, Sea, Swell). Station E3 AWAC, 2022.

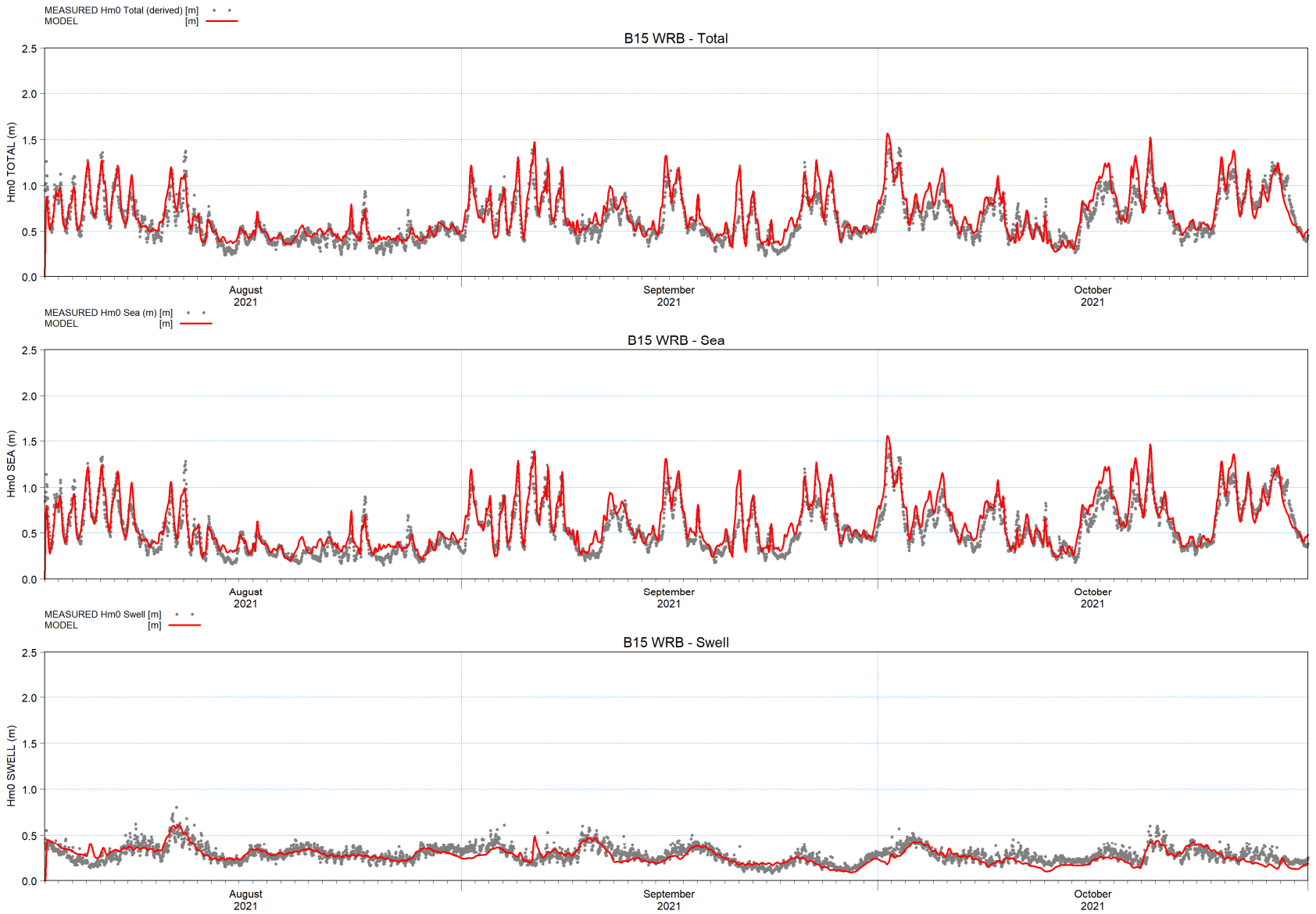

Figure B-5 Time series comparison for Local Wave Model hindcast vs. measured Hm0 (Total, Sea, Swell). Station B15 WRB, 2021.

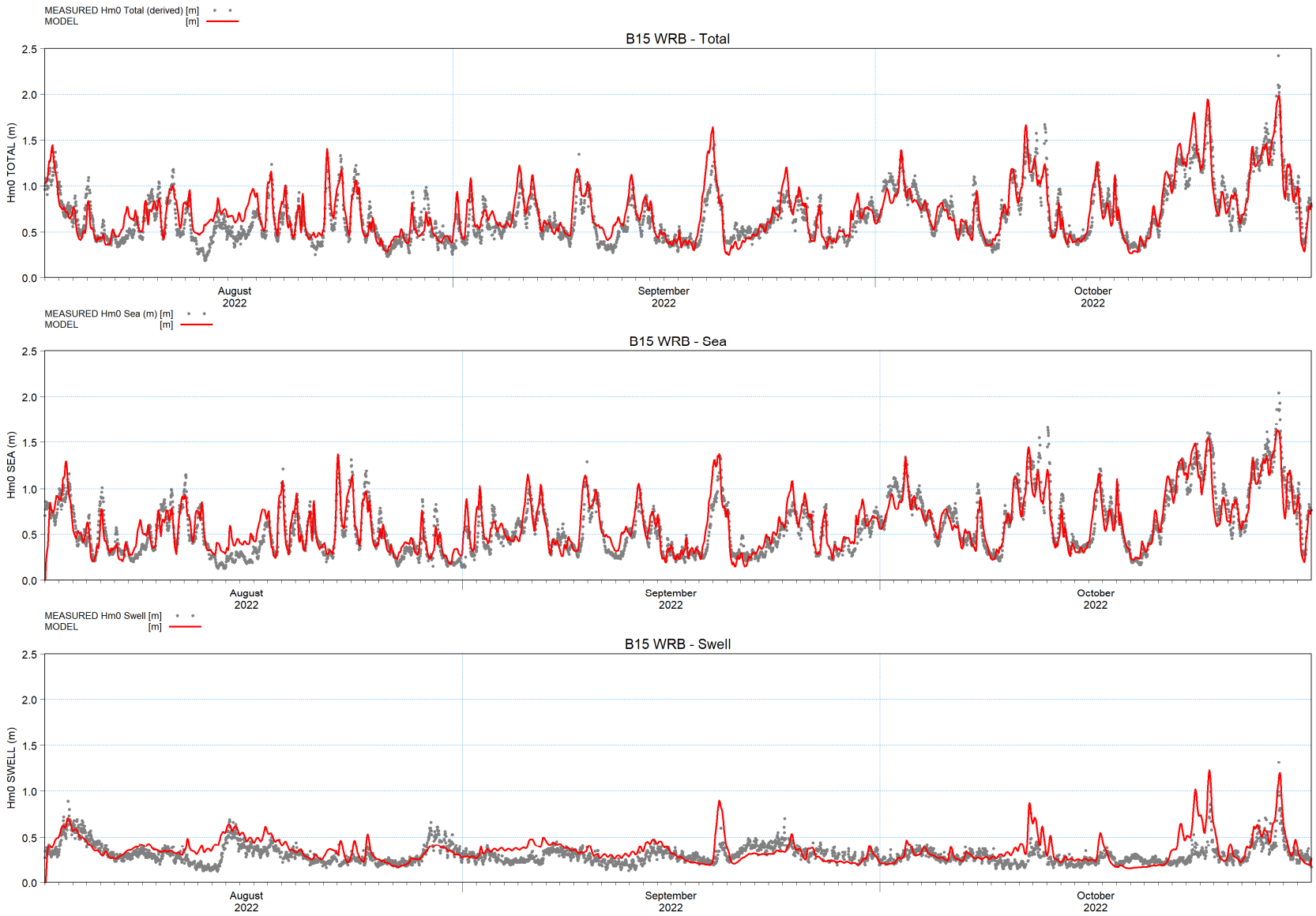

Figure B-6 Time series comparison for Local Wave Model hindcast vs. measured Hm0 (Total, Sea, Swell). Station B15 WRB, 2022.

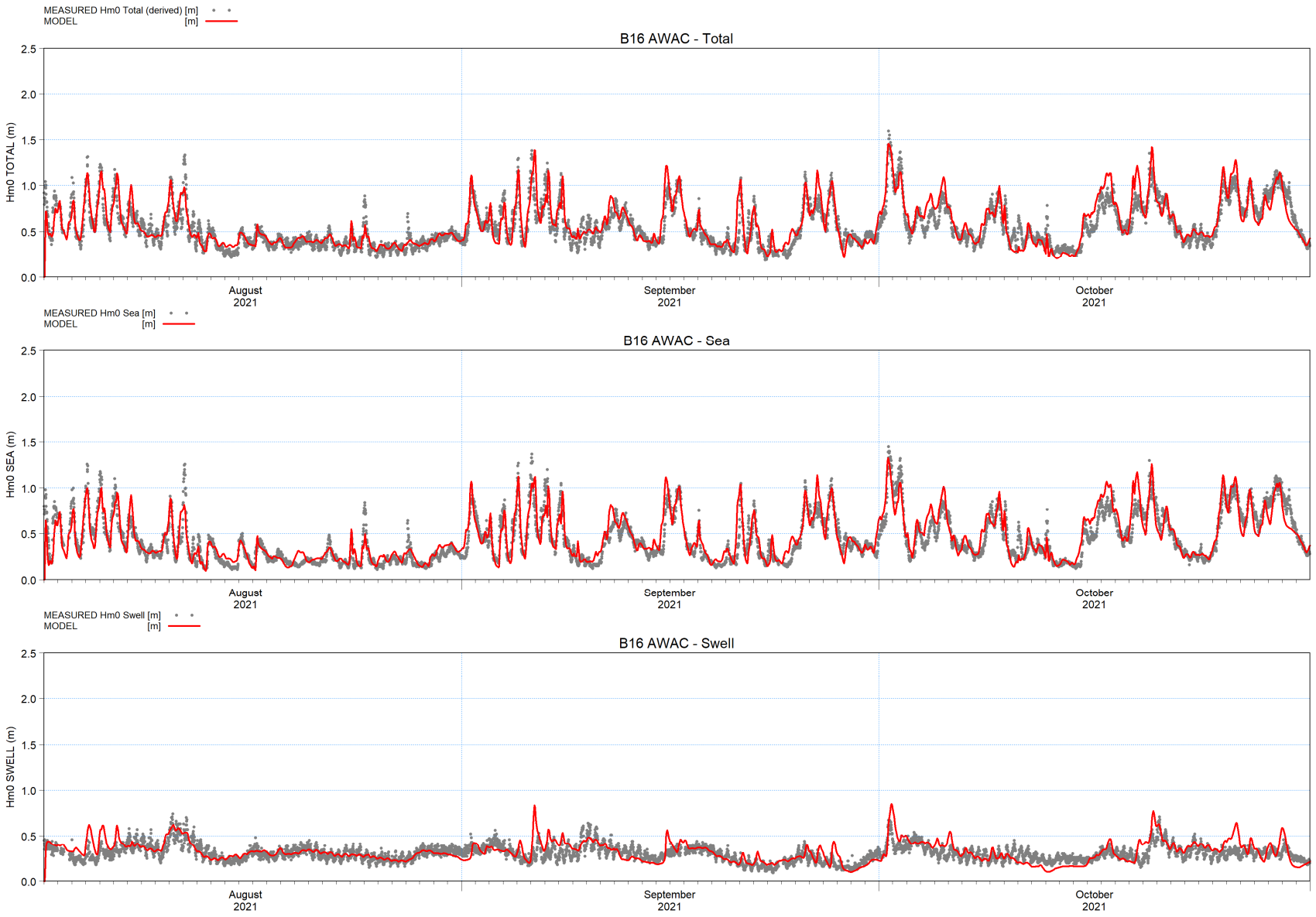

Figure B-7 Time series comparison for Local Wave Model hindcast vs. measured Hm0 (Total, Sea, Swell). Station B16 AWAC, 2021.

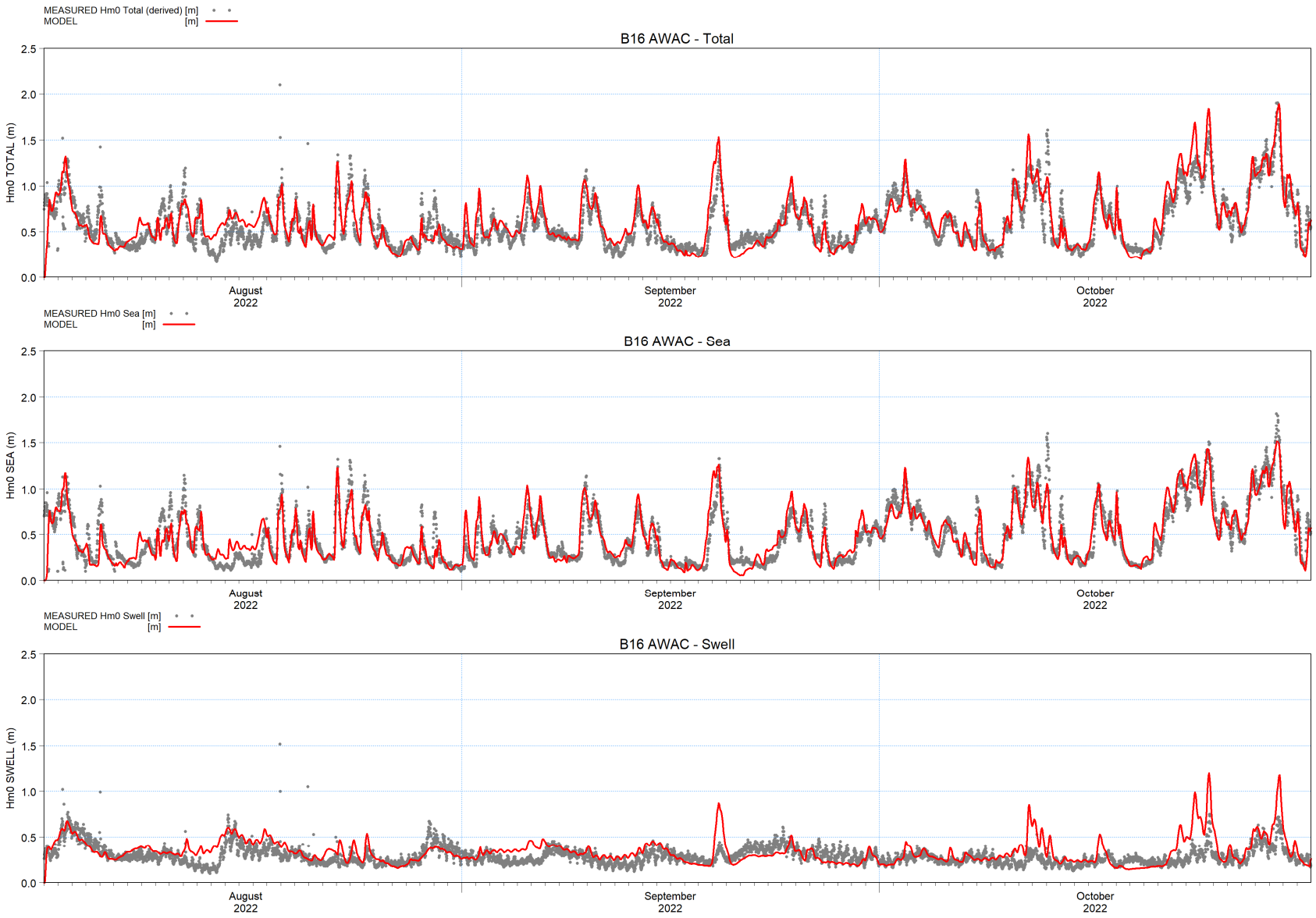

Figure B-8 Time series comparison for Local Wave Model hindcast vs. measured Hm0 (Total, Sea, Swell). Station B16 AWAC, 2022.

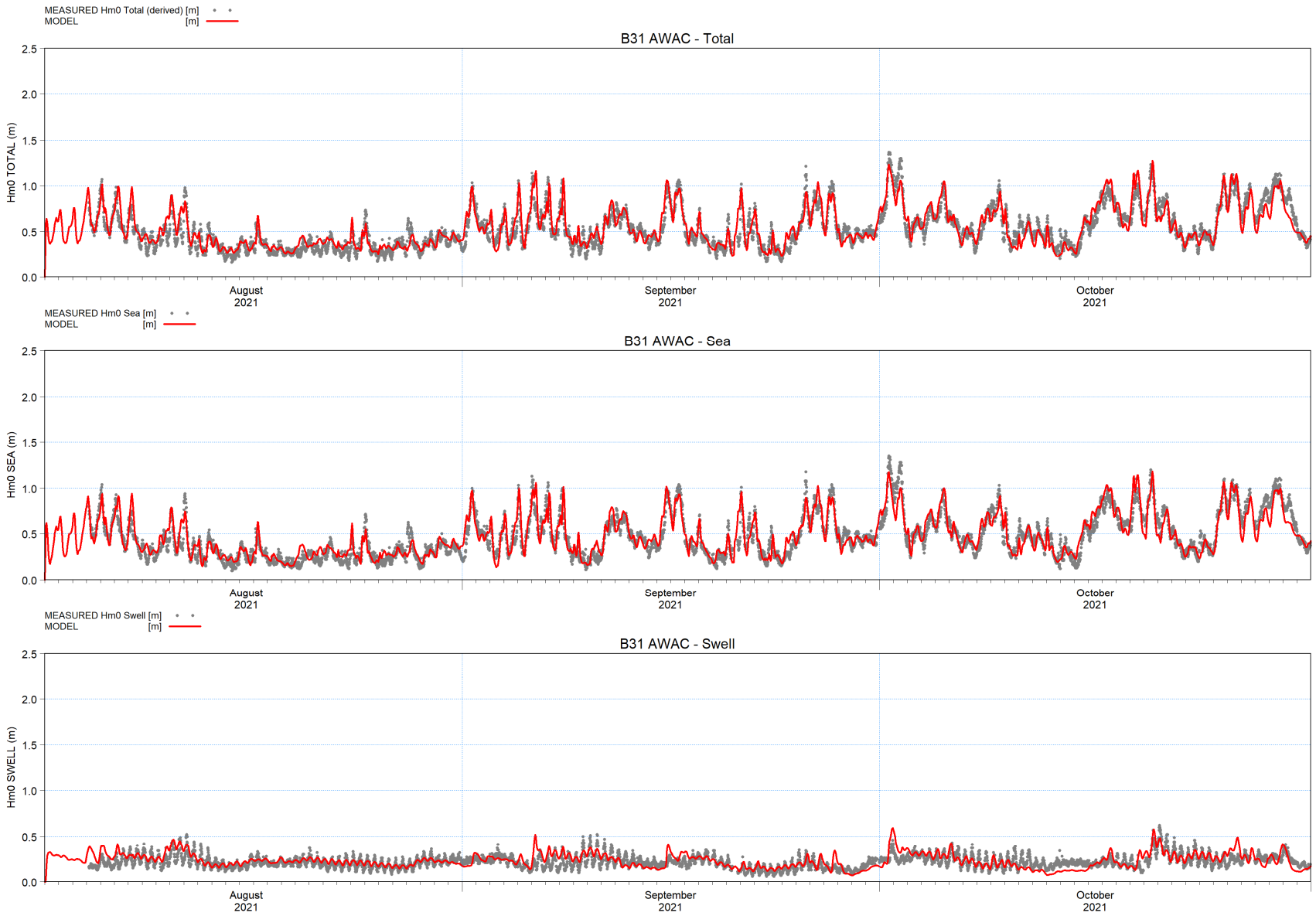

Figure B-9 Time series comparison for Local Wave Model hindcast vs. measured Hm0 (Total, Sea, Swell). Station B31 AWAC, 2021.

Figure B-10 Time series comparison for Local Wave Model hindcast vs. measured Hm0 (Total, Sea, Swell). Station B31 AWAC, 2022.

APPENDIX C

Instantaneous Depth-Maximum SSC Fields

C Instantaneous Depth-Maximum SSC Fields

This appendix contains sample instantaneous output suspended sediment concentration (SSC) fields from the MT model. Each figure presents a chronology of sediment plumes from a given scenario, where the fields plotted represent the instantaneous maximum SSC (as the sum from all modelled fractions) over depth at each location within the 3D model domain. Each pane advances by half of a simulation week. For Scenario 2 (2A, 2B, 2C), spillage from dredging operations has already ceased prior to the final pane at T = t0 + 5.0 weeks.

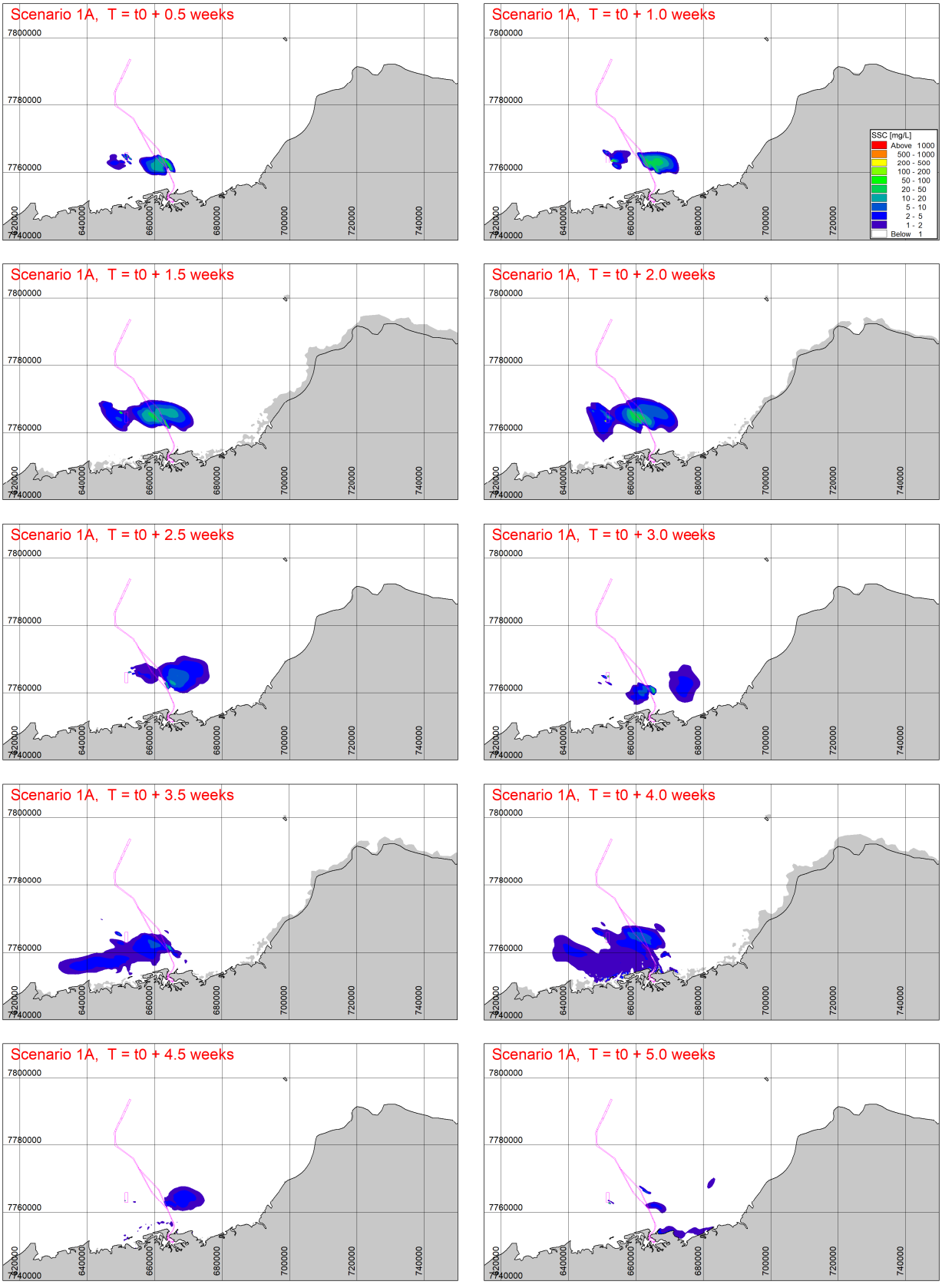

Figure C-1 Chronology of sediment plumes from Scenario 1A (TSHD only, neutral residual character). Contours represent the depth-maximum SSC at each timestep, with each pane advancing by half of a simulation week.

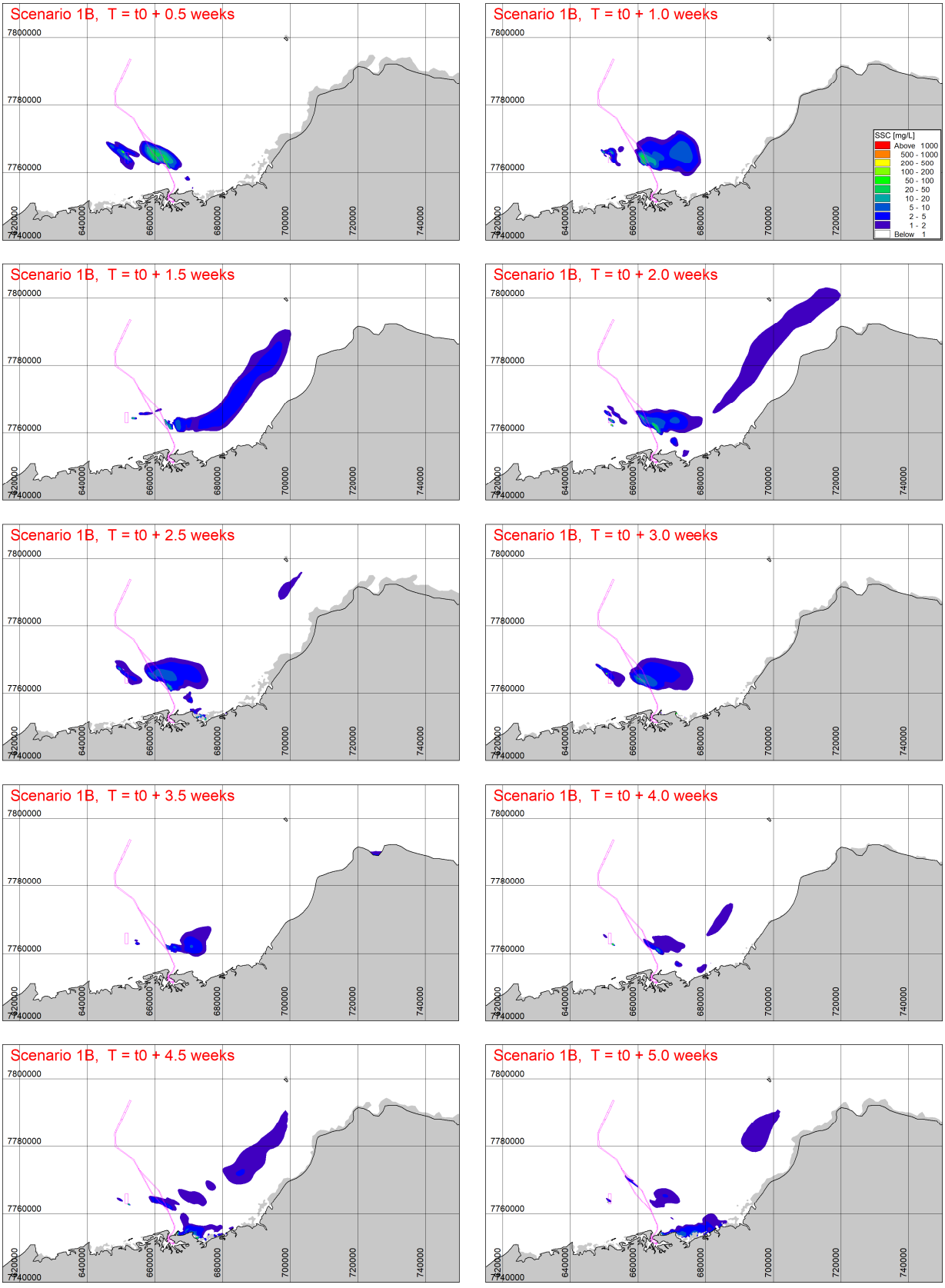

Figure C-2 Chronology of sediment plumes from Scenario 1B (TSHD only, eastward residual character). Contours represent the depth-maximum SSC at each timestep, with each pane advancing by half of a simulation week.

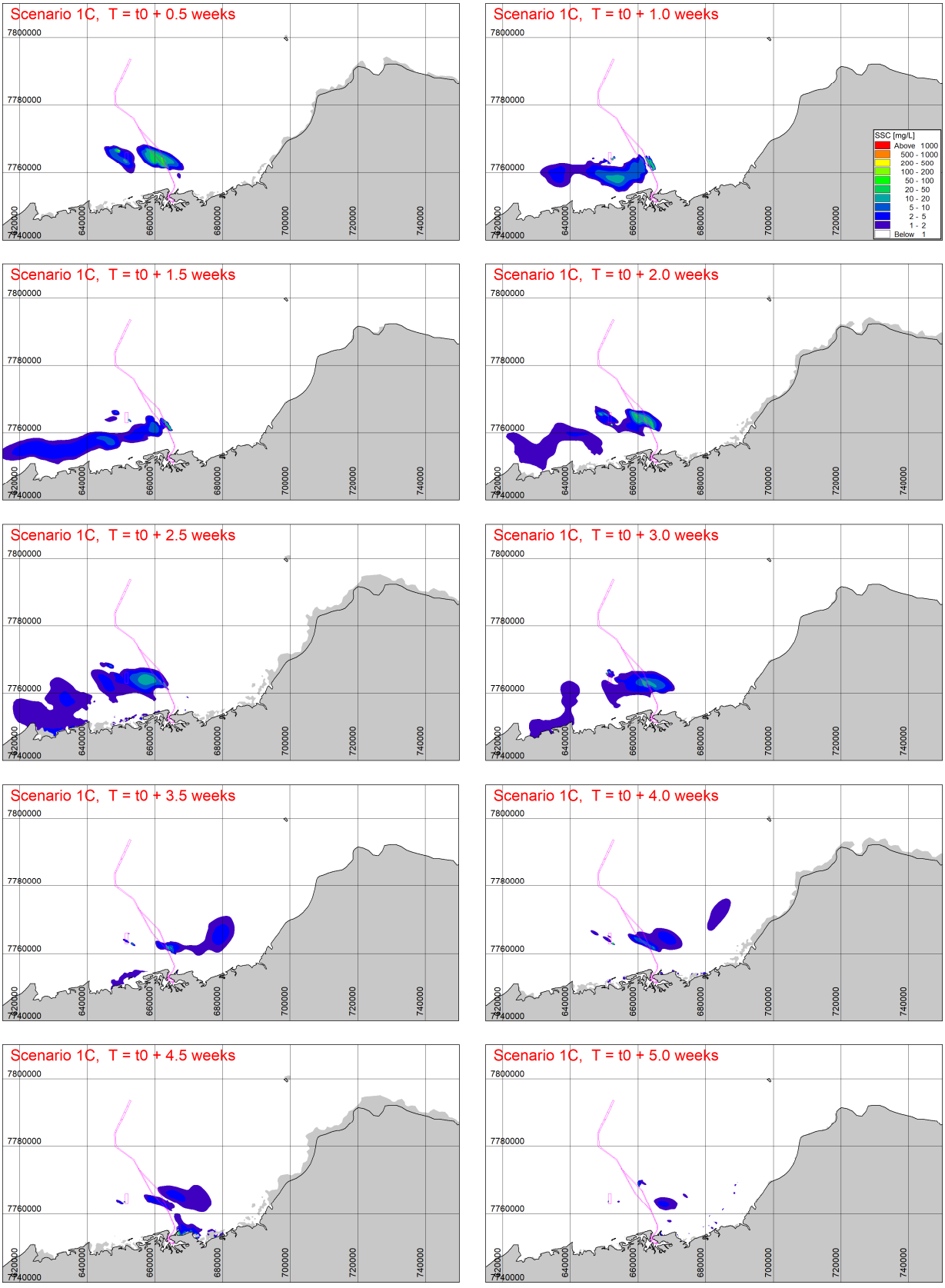

Figure C-3 Chronology of sediment plumes from Scenario 1C (TSHD only, westward residual character). Contours represent the depth-maximum SSC at each timestep, with each pane advancing by half of a simulation week.

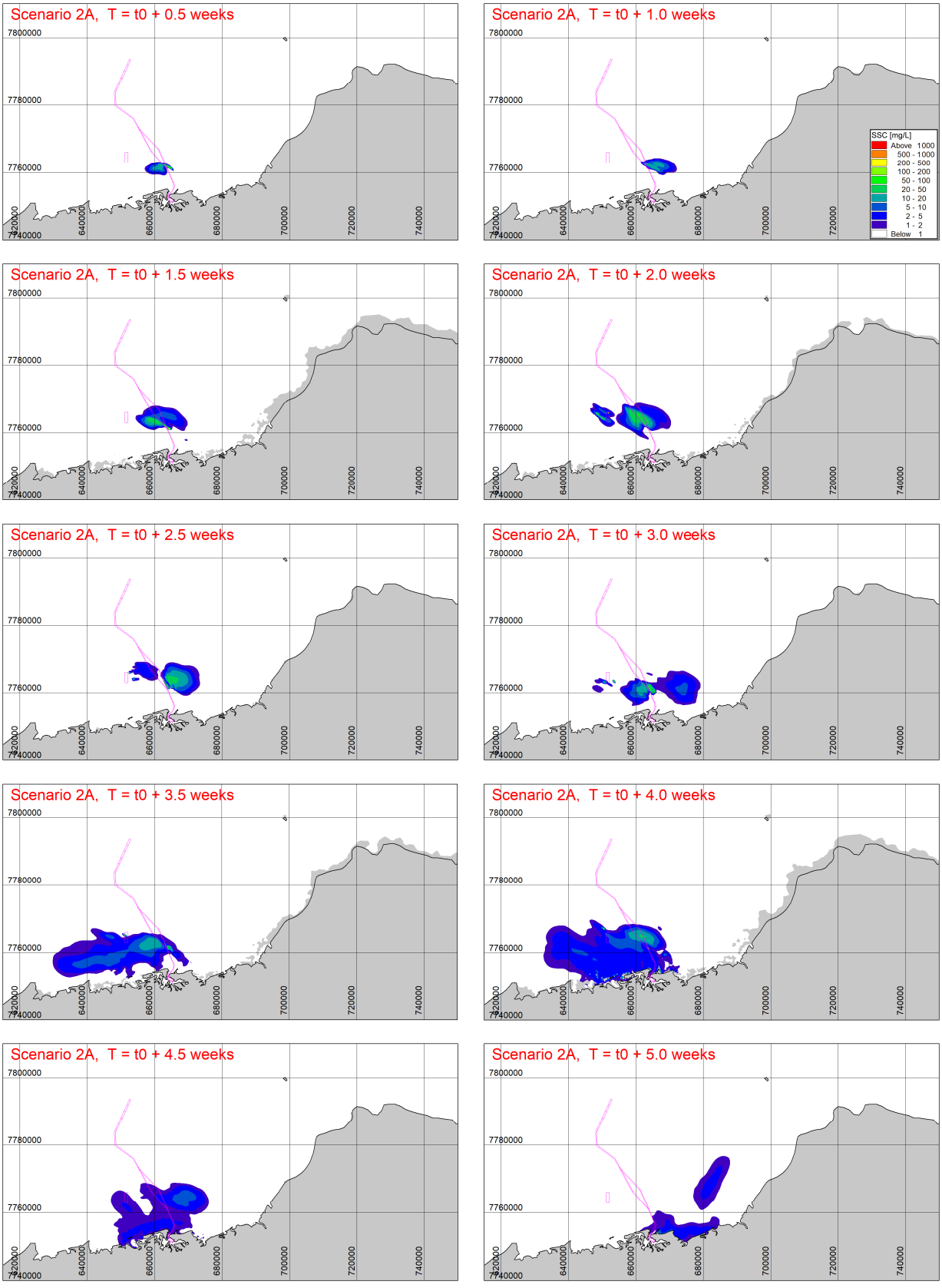

Figure C-4 Chronology of sediment plumes from Scenario 2A (CSD/TSHD, neutral residual character). Contours represent the depth-maximum SSC at each timestep, with each pane advancing by half of a simulation week.

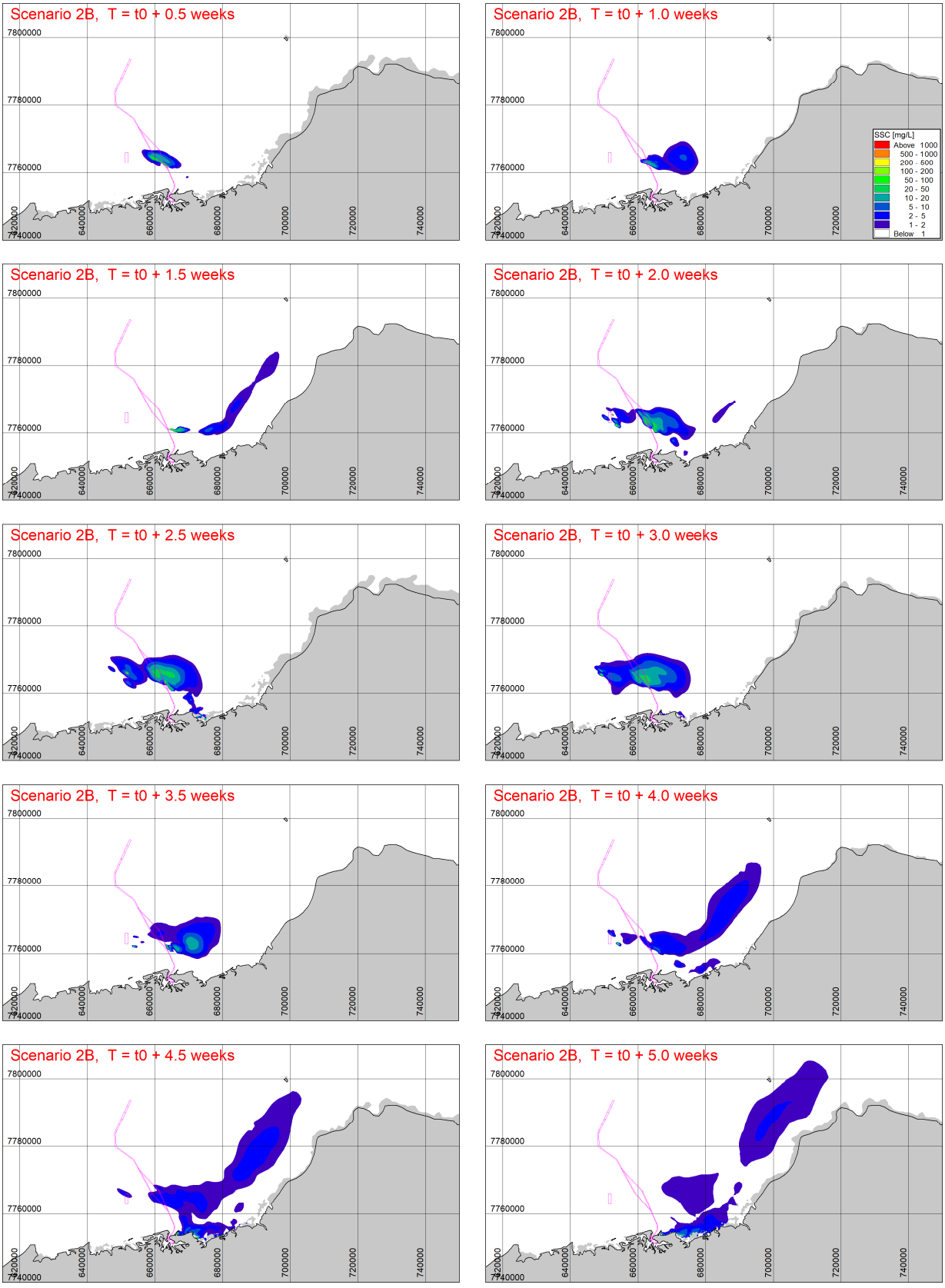

Figure C-5 Chronology of sediment plumes from Scenario 2B (CSD/TSHD, eastward residual character). Contours represent the depth-maximum SSC at each timestep, with each pane advancing by half of a simulation week.

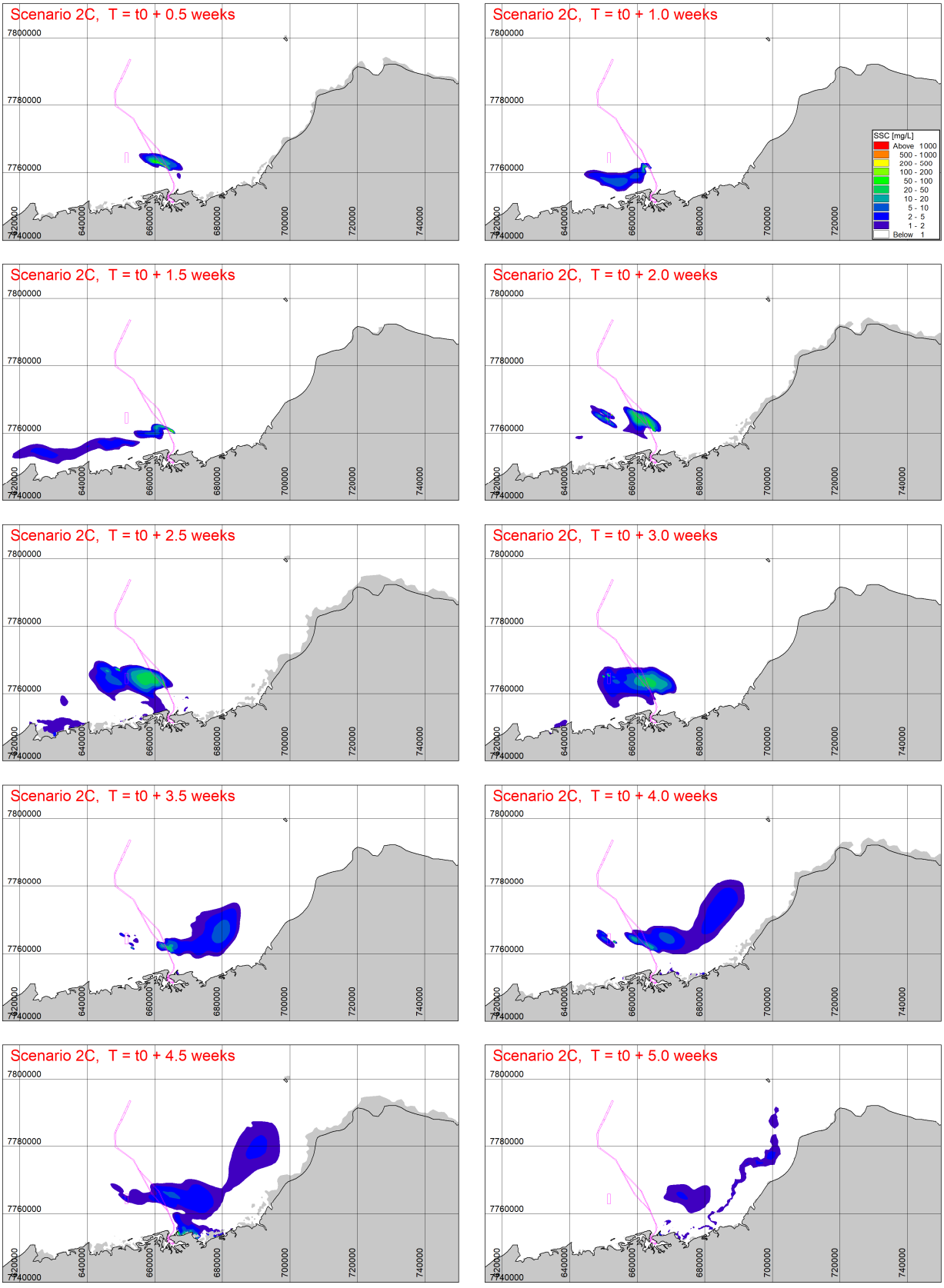

Figure C-6 Chronology of sediment plumes from Scenario 2C (CSD/TSHD, westward residual character). Contours represent the depth-maximum SSC at each timestep, with each pane advancing by half of a simulation week.

APPENDIX D

Statistical Depth-Maximum SSC Fields

D Statistical Depth-Maximum SSC Fields

This appendix contains sample statistical fields of output suspended sediment concentration (SSC) fields from the MT model. Each figure presents median, 95th percentile and maximum envelopes of SSC from a given scenario. The input basis for each statistical field is the instantaneous maximum SSC (as the sum from all modelled fractions) over depth at each location within the 3D model domain, saved every 30 minutes. Statistics are generated over the portion of the simulation duration during which construction is active (Table 5-6).

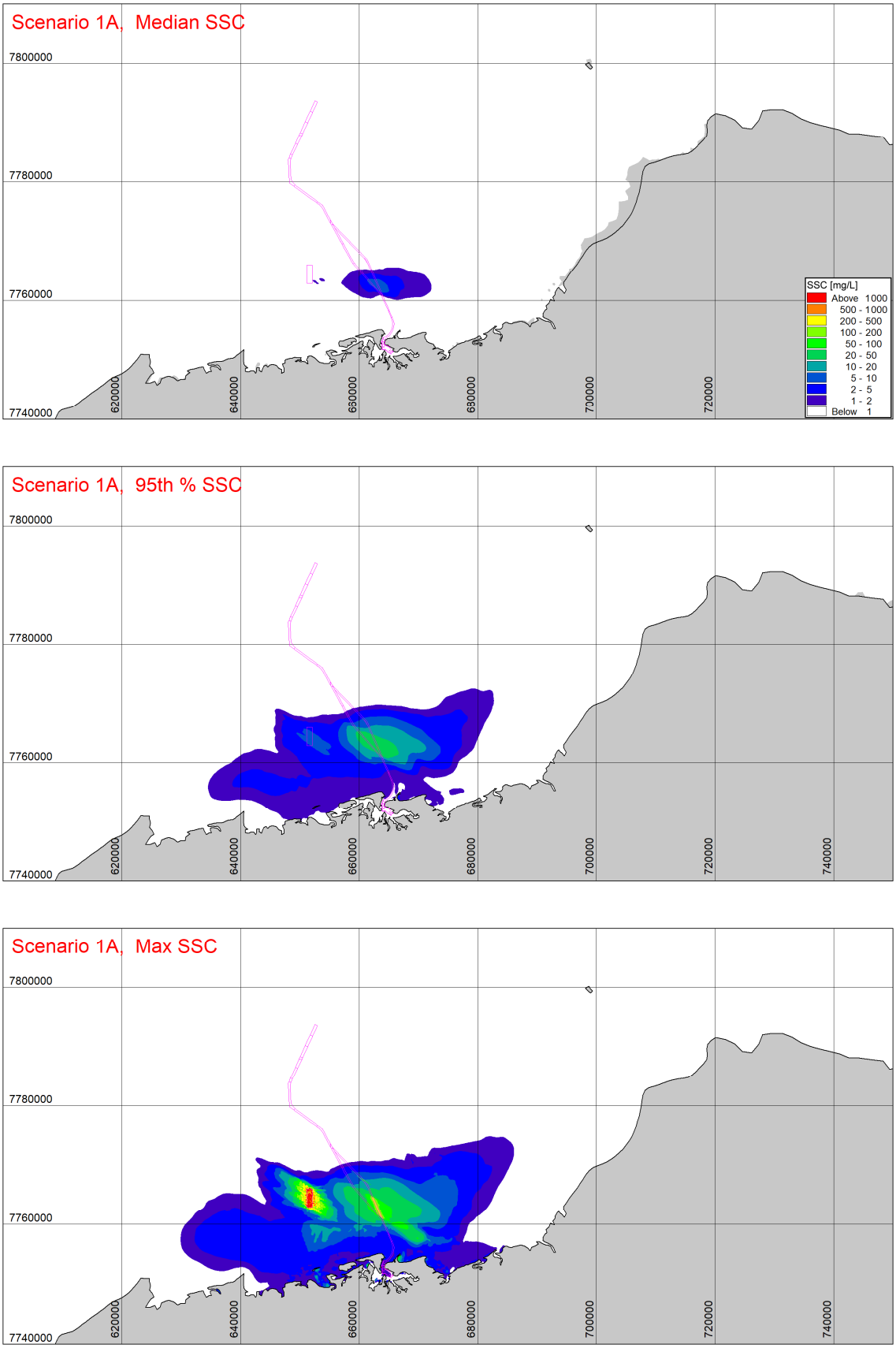

Figure D-1 Statistical SSC fields of sediment plumes from Scenario 1A (TSHD only, neutral residual character). Derived from the depth-maximum total SSC at each output timestep.

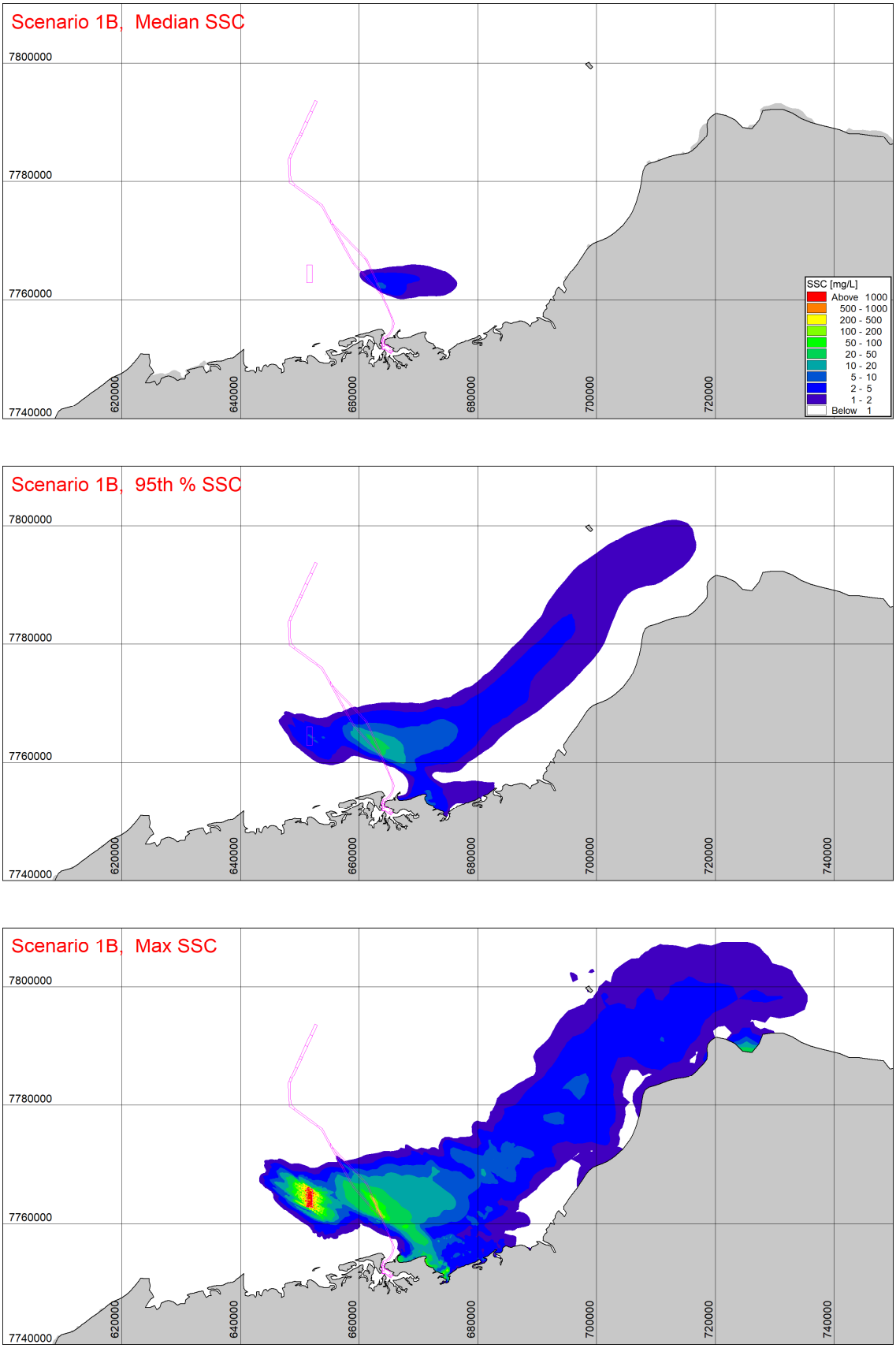

Figure D-2 Statistical SSC fields of sediment plumes from Scenario 1B (TSHD only, eastward residual character). Derived from the depth-maximum total SSC at each output timestep.

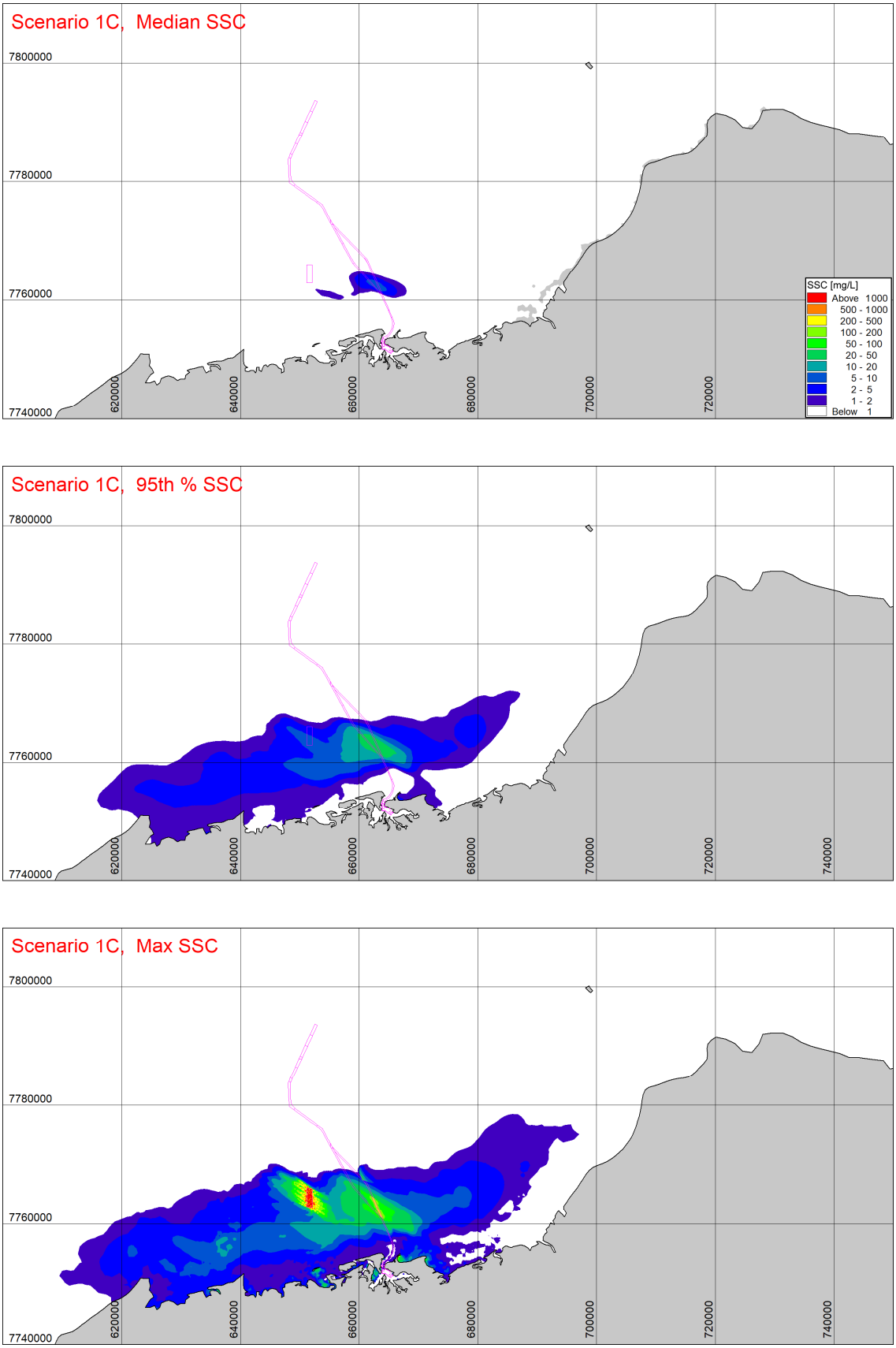

Figure D-3 Statistical SSC fields of sediment plumes from Scenario 1C (TSHD only, westward residual character). Derived from the depth-maximum total SSC at each output timestep.

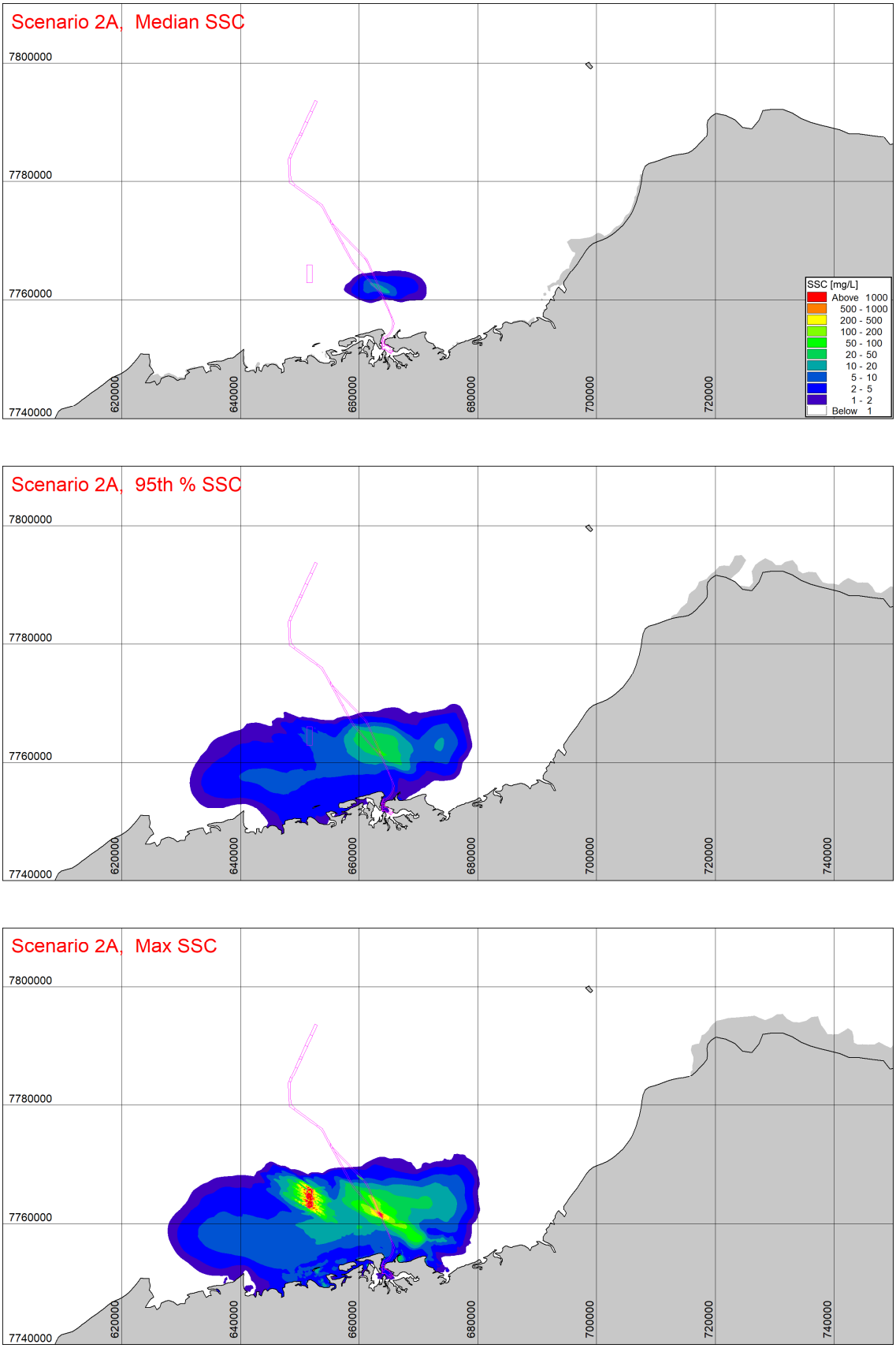

Figure D-4 Statistical SSC fields of sediment plumes from Scenario 2A (CSD/TSHD, neutral residual character). Derived from the depth-maximum total SSC at each output timestep.

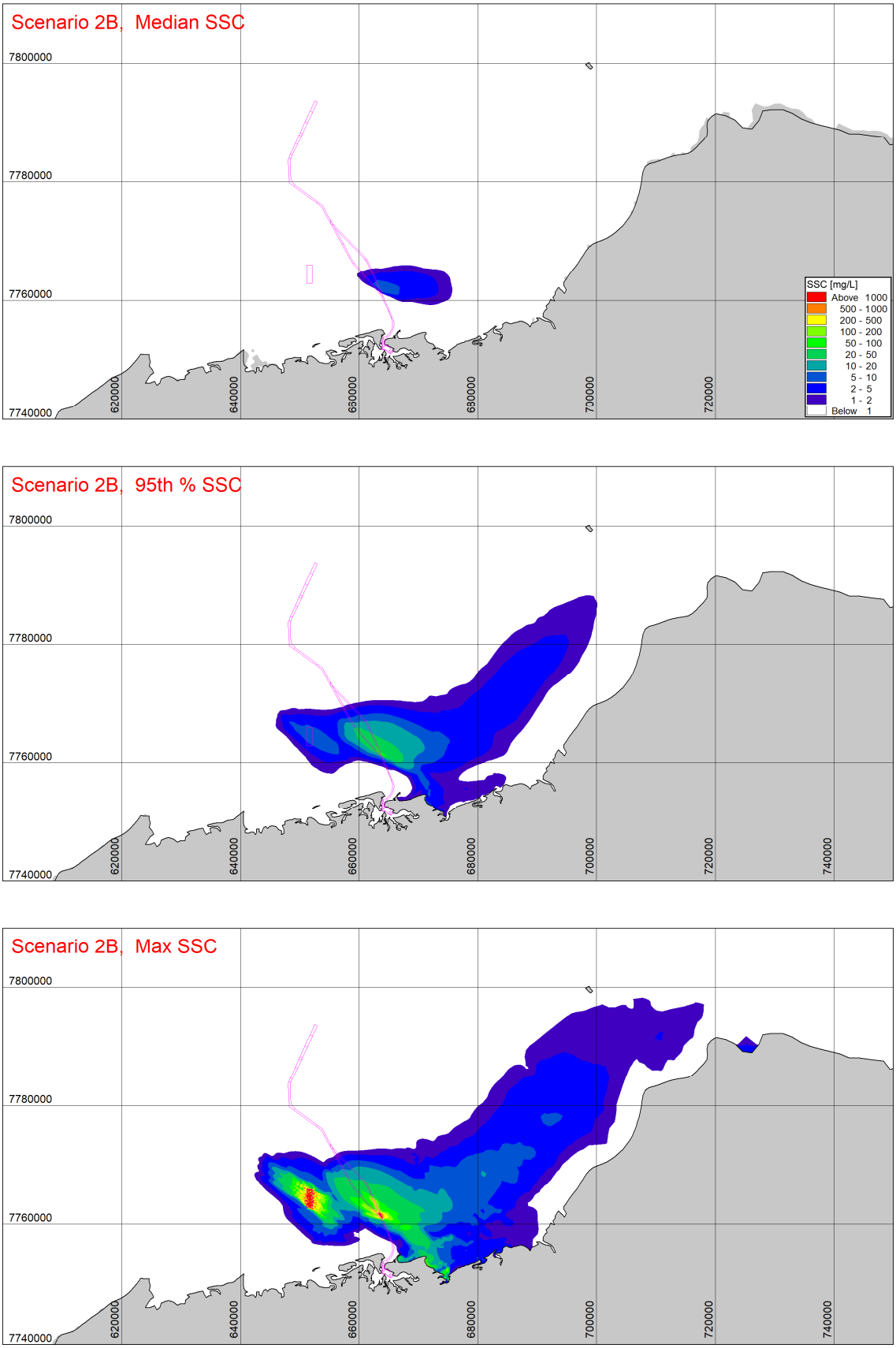

Figure D-5 Statistical SSC fields of sediment plumes from Scenario 2B (CSD/TSHD, eastward residual character). Derived from the depth-maximum total SSC at each output timestep.

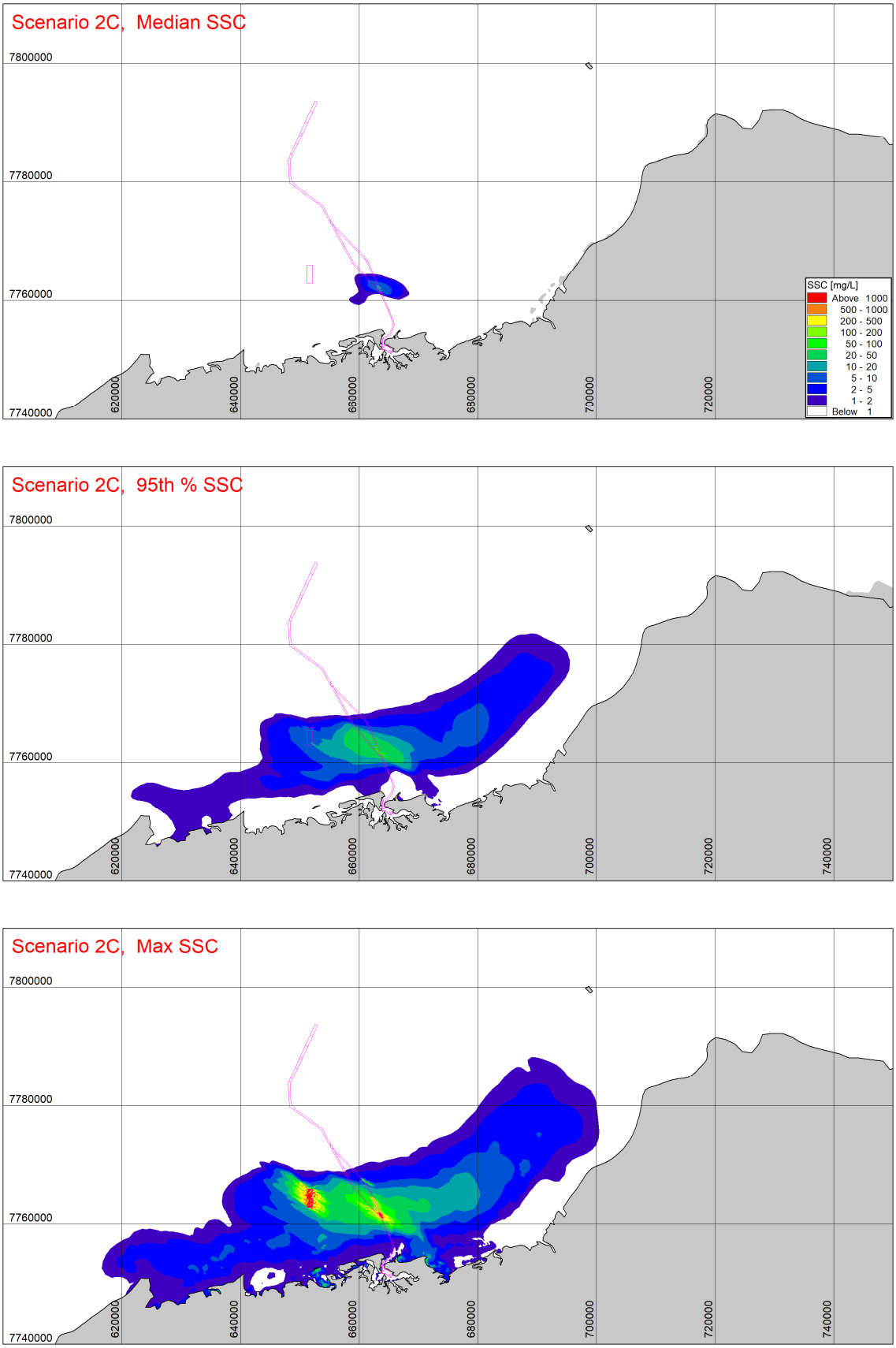

Figure D-6 Statistical SSC fields of sediment plumes from Scenario 2C (CSD/TSHD, westward residual character). Derived from the depth-maximum total SSC at each output timestep.